Dynamic Modeling and Gain Scheduling Control of a Chilled Water Cooling System

Jun, Liu

A thesis in

Department of Building, Civil and Environmental Engineering

Presented in Partial Fulfillment of the Requirements

For the Master of Applied Science (Building Engineering) at

Concordia University

Montreal, Quebec, Canada

July 2013

CONCORDIA UNIVERSITY

SCHOOL OF GRADUATE STUDIES

This is to certify that the thesis prepared

By: **Jun Liu**

Entitled: **Dynamic Modeling and Gain Scheduling Control of a Chilled Water Cooling System**

and submitted in partial fulfillment of the requirements for the degree of

MASTER OF APPLIED SCIENCE (Building Engineering)

complies with the regulations of the University and meets the accepted standards with respect to originality and quality.

Signed by the final examining committee:

_____ Chair

Dr. Z. Chen

_____ External Examiner

Dr. Y. Zeng (to program)

_____ Examiner

Dr. H. Ge

_____ Examiner

Dr. Z. Chen

_____ Thesis Supervisor

Dr. M. Zaheeruddin

Approved by _____

Dr. M. Elektorowicz, Graduate Program Director

Department of Building, Civil and Environmental Engineering

_____

Dr. C. Trueman, Interim Dean

Faculty of Engineering & Computer Science

Date _____

ABSTRACT

Dynamic Modeling and Gain Scheduling Control of a Chilled Water Cooling System

Jun Liu

In this thesis, a dynamic model of a chilled water (ChW) cooling system with a stratified ChW tank was developed. The model-based analysis of the energy consumption and the cost under different control strategies were studied. The dynamic model consists of a zone, a cooling coil, a chiller, a stratified ChW tank, and a cooling tower. Nonlinear differential equations were written to describe and evaluate the performance of the entire chiller plant with the ChW tank.

A PI-based gain scheduling (GS) control was designed and its performance was compared with the constant gain PI control by subjecting to setpoint changes and load disturbances. The simulation results showed that the system with GS control gives good control and has more stable performance.

Five different operation strategies were simulated for comparing the energy consumption and the cost of the ChW cooling system under full load and partial load conditions. The results showed that the operating strategy with optimized chilled water setpoint saved 7.16% energy (21.5% cost) compared to the case with constant setpoint. These savings were more significant (36%) under partial load conditions.

The gain scheduling control with optimal setpoint has great potential for energy savings as demonstrated by the results presented in the thesis.

ACKNOWLEDGEMENTS

I would like to express my deepest appreciation to Dr. M. Zaheer-Uddin for his very patient and circumspective guidance, encouragement, sustained interest, and financial support throughout my whole studies.

I am also truly grateful for my colleagues, Min Ning and Songchun Li, for their suggestions and guidance in my study. Thanks to the staffs in BCEE department who gave me help during my studies at the department.

Very special thanks go to my parents, Fuli Liu, and Yangwei Huang, as well as my sister, Lucheng Liu, for their endless love, understanding and support during my studies.

TABLE OF CONTENTS

LIST OF FIGURES

LIST OF TABLES

NOMENCLATURE

α_s	surface absorptance to the solar radiation (%)
$A_{cr_{tank}}$	cross-section area of the stratified chilled water tank (m^2)
A_{nw_z}	net area of the wall (m^2)
A_{roof}	the area of the roof (m^2)
$A_{it_{ccv}}$	inside heat transfer area of each control volume of the cooling coil (m^2)
$A_{ot_{ccv}}$	total outside heat transfer area of each control volume of the cooling coil (m^2)
c	empirical constant for particular to tower-fill design
c_f	specific heat of the water/glycol mixture flowing through chiller and storage (J/(kg ºC))
cp_a	the specific heat of air (J/(kg ˚C))
cp_{cw}	the specific heat of chilled water (J/(kg ˚C))
C_{a_z}	the zone air thermal capacity in the zone (J/˚C)
C_{br_z}	the heat capacity of the brick walls (J/˚C)
C_{cow}	the thermal mass of the cooled water in the condenser side (J/˚C)
C_{cw}	the thermal mass of the chilled water in the evaperator side (J/˚C)
C_i	*i*th coefficient of multivariate polynomial regression equation, (unitless)
$C_{cw_{tank_{cv}}}$	thermal capacity of the ChW water contained in the control volumes in the tank (J/˚C)
C_{rcd}	the thermal mass of the roof concrete deck (J/˚C)
COP_{evap}	COP of the evaporator, (unitless)
D_{o_c}	the outside diameter of the coil tube (m)
D_{i_c}	the inside diameter of the coil tube (m)
$\varepsilon_{c,max}$	maximum heat transfer effectiveness for charging if all the chilled water/glycol flow passes through the tank – no bypass (%)
FOM	figure-of-merit of the full cycle operation of the tank (%)
G	intensity of solar radiation hitting on building façade (watt/m^2)

$h_{a_{ct_{in}}}$ the enthalpy of the air entering into the cooling tower (kJ/kg)

$h_{a_{ct_{out}}}$ the enthalpy of the air entering leaving the cooling tower (kJ/kg)

h_i conductivity of interior air film (watt/(m^2 ºC))

h_o conductivity of exterior air film (watt/(m^2 ºC))

h_{o_c} heat transfer coefficient of the coil tube wall at airside (watt/(m^2 ºC))

h_i heat transfer coefficient of the coil tube wall at water-side (watt/(m^2 ºC))

$H_{cw_{tank_{cv}}}$ height of chilled water in each control volume of the tank (m)

L_{tb_c} length of the cooling coil (m)

$m_{a_{ct}}$ the mass flow rate of air entering into the cooling tower (kg/s)

m_{a_z} the mass flow rate of air supplied into each zone (kg/s)

$m_{a_{s_c}}$ supply air mass flow rate t to the coil (kg/s)

m_{cw} mass flow rate of chilled water (kg/s)

$m_{cw_{s_c}}$ supply chilled water mass flow rate t to the coil (kg/s)

$m_{cw_{chi}}$ supply chilled water mass flow rate t to the coil (kg/s)

$m_{cow_{cond}}$ mass flow rate of cooled water in the condenser water loop (kg/s)

η cycle thermal efficiency of the stratified chilled water tank (%)

n empirical constant for particular to tower-fill design

NTU number of transfer unit (unitless)

NuD_{a_c} Nusselt number of the cooling coil at airside (unitless)

NuD_{cw_c} Nusselt number of the cooling coil at water-side (unitless)

Pr_{a_c} Prandtl number of the cooling coil at airside (unitless)

$Pr_{a_{cs}}$ Prandtl number of the cooling coil surface at airside (unitless)

Pr_{cw_c} Prandtl number of the cooling coil at water-side (unitless)

Ptg_{tank} tank energy consumption ratio (%)

Q_{c_z} the cooling load supplied by the cooling coil to the zone (watt)

Q_{comp} compressor work input (watt)

$Q_{h_{s_z}}$ the total sensible heat gain of the zone (watt)

$Q_{loss_{tank}}$ the capacity loss of the tank (watt)

Q_{rej} rejected heat out of the cooling tower (watt)

R_{ra} thermal resistance from layer of outdoor air to half layer of the concrete deck (m^2 ˚C)/watt

R_{rz} thermal resistance from the half layer of concrete deck to the indoor air ((m^2 ˚C)/watt)

R_{tank} thermal resistance of the tank wall (watt/(m^2 °C))

R_{wa} thermal resistance from lay of outdoor air to half layer of the brick ((m^2 ˚C)/watt)

R_{wz} thermal resistance from the half layer of brick to the indoor air ((m^2 ˚C)/watt)

ReD_{a_c} Reynolds number of the cooling coil at airside (unitless)

ReD_{cw_c} Reynolds number of the cooling coil at water-side (unitless)

ST_c the transverse distance between coil tubes, (m)

SL_c the longitude distance between coil tubes, (m)

$T_{cw_{s_{chi}}}$ supply chilled water temperatures from chiller (ºC)

$T_{cw_{s_c}}$ supply chilled water temperature to the load (ºC)

T_{sat} solar-air temperature at the building facade surface (ºC)

T_o Outdoor air temperature (ºC)

$T_{o_{tank}}$ stratified chilled water tank surrounding air temperature (ºC)

T_{roof} the temperature of the roof (˚C)

T_{wall} the temperature of the wall (ºC)

$T_{a_{s_c}}$ supply air temperature from coil to the zone (ºC)

$T_{a_{c_{cv}}}$ air temperature after passing through the control volume of the coil (ºC)

$T_{cow_{s_{cond}}}$ cooled water temperature leaving the cooling tower (ºC)

$T_{cow_{r_{cond}}}$ cooled water temperature leaving the condenser (ºC)

$T_{cw_{c_{cv}}}$ chilled water temperature after passing through the control volume of the coil (ºC)

$T_{cw_{s_c}}$ supply chilled water temperature to the coil (ºC)

$T_{cw_{s_{chi}}}$ chilled water temperature leaving the evaporator (ºC)

$T_{cw_{tank_{cv}}}$ chilled water temperature in each control volume of the tank (ºC)

T_{c^*} mass averaged inlet temperature of the tank during previous charge cycle (ºC)

T_{h^*} mass averaged discharge inlet temperature of the tank (ºC)

$T_{tb_{c_{cv}}}$ coil tube wall temperature in the control volume of the coil (ºC)

u_k charging or discharging rate of the storage (watt)

V_c Volume of the cooling coil (m^3)

v_{a_c} Velocity of the air passing through the cooling coil (m/s)

v_{cw_c} Velocity of the chilled water passing through the cooling coil (m/s)

ρ_a density of air (kg/m^3)

ρ_{cw} density of chilled water (kg/m^3)

ABBREVIATE

ACH Air change hour

AHU Air handling unit

ChW Chilled water

CEV Coefficient of variation

CT Cooling tower

CV Control volume

DB Dry – Bulb

ICS Ice-storage

PLR Partial load ratio

RH Relative humidity

RTP Real-time-price

TES Thermal energy storage

TV Throttling valve

VAV Variable air velocity

WB Wet – Bulb

CHAPTER 1 INTRODUCTION

1.1 Introduction

Chilled water cooling systems are widely used for air conditioning of buildings. In majority of cases cool energy is stored in storage tanks for load levelling and to improve energy efficiency. The thermal energy storage (TES) system charges thermal energy within an insulated tank and discharges the stored thermal energy during peak energy demand period in order to reduce the system operation cost when the real-time-price (RTP) utility rate is in effect. The most popular TES systems use chilled water as medium in a stratified chilled water (ChW) tank or as ice-storage (ICS) tank.

Figure 1.1.1 shows a typical operation of a stratified ChW tank with its charge and discharge cycles.

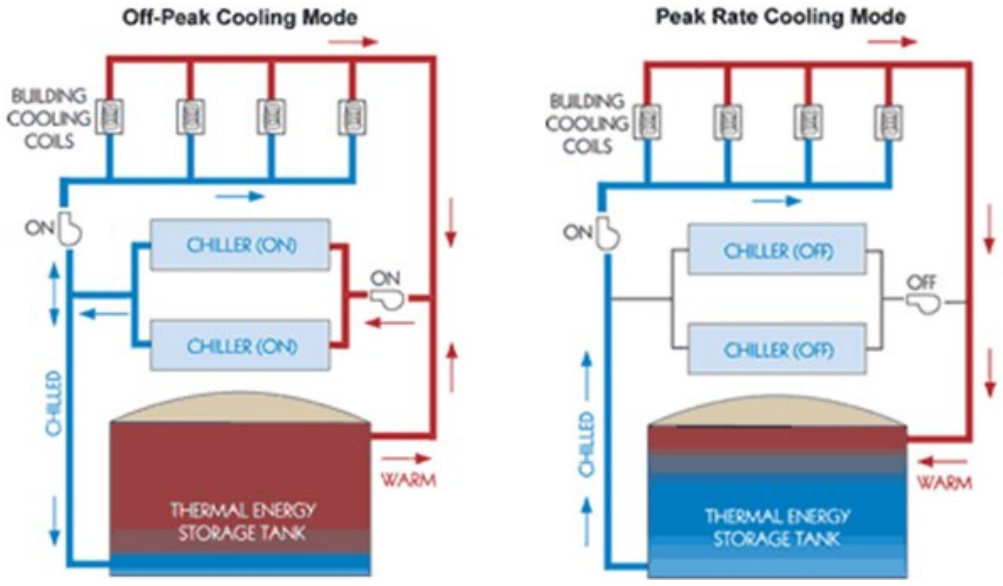

Figure 1.1.1 Schematic diagram of stratified ChW tank operation (Cypress. Ltd)

As shown in the left figure, the stratified ChW tank is charged by the chillers which also supply ChW to the load side to maintain thermal comfort of the zone. The chilled water going through the inlet of the tank located at the button of the tank and warm water returns through the outlet of the tank located at the top is mixed with the return ChW from the load side and back to the chiller. During the discharge cycle of the tank, as shown in the right figure, the ChW is supplied to the load from the stratified tank while the chiller water loop remains closed and the water returns back to the tank without passing through chillers. It is called full-storage-priority operation of the tank in the literature. The size of the ChW tank must be properly chosen for meeting the design day load demand requirement and minimizing the initial cost.

1.2 Scope of the thesis

In this thesis, a chiller plant, consisting of a zone, a cooling coil, a chiller, and a cooling tower, along with a stratified ChW tank, was studied. The ChW tank was designed to cover a partial load ratio (PLR) of 80% of the design day load. The cooling system performance was investigated using different control strategies.

Objectives of the study

The main goals of this study is to develop a dynamic model of a chilled water cooling system with ChW tank, design control strategies and improve energy efficiency of the overall system. To achieve these main goals, the following objectives were defined.

1. Select a physical model of the ChW cooling system with ChW tank and design the system components using steady state design methods.
2. Develop dynamic models of the components and the overall ChW system to simulate the dynamic responses of the system.

3. The overall ChW system consists of several control loops. To improve the control performance of the system, design a gain scheduling PI controller and compare its control performance with conventional fixed gain PI controller.
4. Conduct a detailed study of the performance of the chiller plant and the stratified ChW tank under design day and partial load conditions.
5. Develop a near-optimal algorithm for reducing energy consumption of the chiller plant by increasing the use of cool energy from stratified ChW tank.

Structure of the thesis

There are 6 chapters in this thesis: Chapter 1 introduces the scope and objectives of the thesis; chapter 2 presents the literature review; chapter 3 describes the physical model of the ChW tank and the chiller plant and as well as presents dynamic models and open loop simulation results; control strategies and operation of the ChW cooling system with ChW tank are described in chapter 4; Energy simulations and analysis are presented in chapter 5; the conclusions, contributions and the recommendations for the future research are given in chapter 6.

CHAPTER 2 LITERATURE REVIEW

2.1 Introduction

Thermal energy storage systems are very popular because of their lower initial cost, high efficiency, and flexible operation. Many studies on ChW tank storage system have focused on the laboratory and field experiments and as well as through numerical simulations. The main objectives of the studies include optimized tank size selection, improvement of the energy shift by different operation of the ChW tank, and the cost reduction due to the shift. The literature review in this chapter includes the economic benefits of using ChW tank with the ChW cooling system, tank size selection, simulation models for the ChW cooling system using TES, control strategies, and optimized operation of the ChW tank.

2.2 Studies on using ChW tank

The studies on using TES tank include the economic benefits, field testing, and simulations as described below.

Economic benefits of using ChW tank

Andrepont (2006) showed that the large systems using sensible TES tank supply ChW at lower temperature than the normal supply temperatures. This increases the capital cost ($ per kW or per ton) for the chiller; but significantly reduced the size and capital cost for the water pump in the chiller water loop, piping, and indirectly reduced the size of the air-handling units. However the lower supply temperatures would cause inefficient performance of the TES tank due to more pump work and more heat gain into the TES tank. The study concluded that in spite of the inefficient performance, the TES tank improves the energy efficiency through charging of the

TES tank during the night time and avoiding the use of the chiller and their auxiliaries (fans in the cooling tower and water pumps in the condenser water loop) when low load demand condition occurs.

Bahnfleth and Joyce (1994) reasoned that the ChW tank increased the cooling plant energy consumption, but with a well-designed and operated system plant efficiency could be improved. The authors studied a stratified ChW tank of diameter of 32.6 m with 19.9 m water height integrated with 7 chillers to satisfy the cooling load requirement in a U.S. university. The results of the study showed that there is higher opportunity of avoiding the use of chiller at low load and this contributed to 8% overall efficiency improvement of the system.

Roth & Zogg (2006) studied the economics of TES system involving the utility rate structures, building daily electricity demand profile, and the cost for the space requirement of the system. Buildings with high load factors, high peak to average electric demand ratio, and very high peak demand charges were found to be more desirable for the TES system. The authors recommended that reasonable forecasting of load profile at least half a day ahead of the time of operation is the key to improve the efficiency of the system and reduce the cost of the TES.

Caldwell & Bahnfleth (1998) showed that the stratified ChW tanks, without electric demand charges or time of use differentials and without capital cost rebates, can achieve the first cost saving of 9-17% and a life-cycle savings of 33-36% when compared to the non-TES plant. Another point of their paper is that a change in ΔT from 5.6 ºC – 12.2 ºC significantly decreased heat gains from the piping.

Field and simulation studies of using TES tank

Wildin and Truman (1985) defined that the cycle efficiency of a stratified ChW tank as a ratio of the integrated discharge capacity during the whole discharge cycle to the integrated charge capacity during the whole charge cycle of the tank when the initial and final state of the tank is identical. However it is extremely difficult to obtain the identical initial and final condition in short period cycles. They concluded that it is better to describe the thermal performance of the tank in long term cycles because of the extremely large capacities compared to the difference between the initial and final conditions of the tank. In their study, the capacity loss of the tank due to internal mixing of water was not included.

Tran and Kreider (1989) defined a figure-of-merit (FOM) of TES systems to measure the loss of usable capacity in addition to ambient heat gain. It is a ratio of integrated discharge capacity for a given volume of water to the ideal capacity of that volume of water that could be withdrawn without considering the capacity loss. It is hard to measure FOM in the field because most of the tanks do not operate for more than 24 hours. Therefore Musser and Bahnfleth (1999) presented another indicator known as half-cycle Figure-of-merit which is defined as a ratio of integrated charge or discharge capacity of the tank to its theoretical capacity of one tank volume. The half FOM only measures single charge or discharge cycle of the tank which is much easier to implement during shorter cycles.

2.3 Simulation Studies

In this section, the literature review pertaining to the simulation studies and model development are reviewed. It includes the dynamic models of zone, cooling coil, stratified tank, chiller, and cooling tower.

Zone and AHU models

Zheng and Zaheer-uddin (1997) proposed two different dynamic models, using bottom-up and top-down approaches, for studying the interactions between the components of multizone VAV system and building shell. The zone model was characterized by the density, enthalpy, and humidity ratio of air in the zone. The zone temperature was assumed to be well mixed and was represented by a single node.

Teeter and Chow (1998) developed a single-zone dynamic model based on reduced-order function link neural network to emulate the performance of the HVAC system. The training time and training error of the model are improved by reducing inputs and minimize the complexity of the functional link neural network. The model was characterized by the zone air temperature, fluid temperatures in the heat exchanger, and flow rates, etc. The results showed that the neural networks are capable to tune when disturbance occurs in the plant and accurately depict the performance of the system.

Wang and Jin (1999) developed a simplified physical model to predict the air-conditioning system response. This adaptive finite-time prediction model consists of building, coil, fan, VAVA system, chilled water loops, pump and chiller which are written to predict the energy and the performance of the system. The zone air temperature and humidity can be described by the

differential equations. The supply air flow rate and conditions were assumed to be constant when the time step during the simulation is small. The results showed that the genetic algorithm is a convenient tool for optimization of air-conditioning system performance.

Tashtoush (2004) derived a dynamic model of an HVAC system which consists of the zone, heating coil, cooling and dehumidifying coil, humidifier, ductwork, fan, and mixing box. The zone load model was characterized by three state variables, the zone air temperature, the inner walls temperature, and the humidity ratio. The zone air temperature was assumed well mixed in the zone and the density of the air was kept constant during the simulation. The pressure losses in the zone and during mixing process were neglected. The heating/cooling coil models were developed to study their transient behavior and responses. The air and water temperatures and humidity ratio are analyzed. Since the humidifier and dehumidifier are not considered in the thesis, the humidity ratio is not included in the zone load model.

Chiller models

There are numbers of studies on vapor compression refrigeration (VCR) system. The developed models are distinguished into detailed deterministic models or simplified curve-fitting models. The characteristics of the deterministic models are the demand of uncertain and unavailable inputs and thermodynamic-law-based analysis of the thermal performance of each components of the chiller system. The curve-fitting model representing the chiller is a simplified and empirically-based way of using a polynomial function to fit with the data from manufacture's catalogues.

Bryan (2000) developed dynamic models to predict the performance of a VCR system for multivariable control design purposes. Sub-models of compressor, condenser, expansion valve, and evaporator together to form a unique type of a vapor compression cycle which was referred to as the transcritical cycle. The phase change of the fluid through evaporator and condenser is considered by applying moving boundary and lumped parameter approach. The results showed that these nonlinear models are adequate to predict the dominant system dynamics.

Guan and Zaheer-uddin (2005) proposed a dynamic model of VCR system, consisted of sub-model of thermostat expansion valve, evaporator, compressor motor, and condenser, to evaluate the time response characteristics of each component and performance of multiple chiller systems under varying cooling load. The results showed that the COP decreased when the anticipated load increased in a single chiller system; and the COP can be maximized by tracking the maximum COP curve for multiple chiller operation. The dynamic chiller model is relatively accurate and was used for control analysis and design.

Li (2009) developed a dynamic model for evaluating the performance of the VCR system during shut-down and start-up operations. The advanced switch heat exchanger models were developed as combinations of different sub-zone models representing the stage of the refrigerant in the heat exchangers, subcooled, two-phase, and superheated, etc. The whole dynamic model consists of a compressor, an electronic expansion valve, an evaporator, a condenser, and pipe models which are interacted with each other during the simulation. The validation of the results is achieved by comparing the results from experimental system. The results showed that the agreement between the results from switched heat exchanger models and from the experimental system are quite good. In other words, the advance switched heat exchanger models are capable of predicting the VCR system performance.

Mark Hydeman (2002) developed a regression-based electric chiller model. This modified DOE-2 model has three basic functions: one is to present the capacity of the chiller as function of the evaporator and condenser temperatures; another function is to describe the energy input ratio as function of the evaporator and condenser temperatures; the last basic function is the energy input ratio as function of part-load ratio which represents the part-load efficiency as function of part load. In the modified DOE-2 model, the last basic function also includes the condenser temperature in the regression equation. The study showed that the modified DOE-2 model improved the performance of the chiller with variable-speed drives and variable condenser water flow applications. However the existing DOE-2 model, properly calibrated, gave nearly the same results for fixed-speed chillers with no variations in condenser water flow. It was stated that the modified DOE-2 model can be extrapolated beyond the range of calibration data once calibrated.

Derk (2002) presented a comprehensive comparison of the vapor-compression liquid chillers using empirically based model under steady-state working conditions. Four types of regression models were studied and compared: 1) a simple linear regression, 2) a bi-quadratic regression, 3) a multivariate polynomial regression, and 4) a physically based fundamental thermodynamic model. All the models were applied to a single-circuited centrifugal and a more complex twin-circuited twin-screw chiller systems to study their COP. Also, two models based on artificial neural networks were also compared with the regression models. The results of the study showed that the neural network models have higher level of difficulty but higher accuracy abilities than the regression models.

Lee and Lu (2010) presented an empirically-based regression model for predicting energy performance of vapor-compression water chillers. In the multivariate polynomial (MP) model to describe the COP of the chiller, the chiller cooling capacity, inlet water temperature to

evaporator, and water temperature inlet to condenser were considered as independent variables and 10 regression parameters were selected in the MP model. The coefficient of variation (CEV) of root-mean-square error of the MP model was about 2.25% of the prediction accuracy.

The curve-fitting models are more robust compared to detailed deterministic models because of significantly less computation time and less complexity of the model.

Cooling tower models

Khan and Zubair (2001) developed an improved steady state model of the counter flow wet cooling tower. They used number of transfer unit (NTU) and efficiency as performance indicators. The effect of water evaporation, the resistance of heat transfer in the water film and the non-unity Lewis number were considered in the model. The results showed that the differences in the cooling tower efficiencies could be as much as 15% when considering the effect of air-water interface temperature. They concluded that and the magnitude of the errors in calculating the thermal performance of the tower is strongly depend on the ratio between the heat and mass transfer coefficients.

Khan, Qureshi, and Zubair (2004) presented a study on the fouling of cooling tower fills by using a steady state model. In the cooling tower model, they assumed that the heat and mass-transfer occurs in the direction normal to the flows only; the heat and mass transfer through the walls and from the tower fans to air or water streams were neglected. Also the Lewis number throughout the tower, water and dry air specific heats were held constant. The calculated NTU was compared with the empirical value of NTU which showed close agreement.

Long (2013) presented a steady state model to predict the performance of cooling tower used in air conditioning applications under variable operating conditions. The cooling tower was modeled as a heat exchanger. Three cooling towers were simulated and results were compared with the data from the manufacturers catalogues. The errors between the simulation values of the cooling capacity of the cooling tower and the data were in the range of 0.12 % – 0.15%.

Stratified Tank models

Homan (1996) stated that the flow dynamics are orders of magnitude more important than other factors in modeling of stratified tanks. For instance, the heat transfer through the tank walls was shown to be less than 2% of the capacity of the reasonable sized, underground, or well-insulated above-ground tank. An unsteady one-dimensional energy equation was used to analyze the performance of the tank. The results of the model showed that there are three non-dimensional significant parameters: effective Peclet number, the Nusselt number, and the ratio of tank height to hydraulic diameter of tank. The heat transfer through the tank wall was negligible when charging flow rate reaches up to a typical value. The predicted tank efficiency was over 90% when one-dimensional thermal conduction phenomenon in the tank was considered.

Nelson (1997) used a one dimensional conjugate heat conduction model to analyze the stratification decay in a vertical thermal stratified chilled water storage tank. The study showed that the degree of thermal stratification is depended on the ratio of length to diameter of the tank, ratio of tank wall thickness to length, insulation, the thermo-physical properties of the material of the ChW tank, and the admission system for both of the cold and warm water. The water column in the tank was divided into several equal volume of water in the longitudinal direction and the

initial temperature in each element was set as a known condition. The differential equations based on one-dimensional transient conduction and the energy balance were written. Several boundary conditions were set-up for more accurate description of the performance of the tank. It was concluded that by increasing the length and decreasing the thickness of the wall of the storage tank could help in better thermal degradation. An aspect ratio of 3.0 was suggested in order to improve the stratification of the tank.

Li (2002) showed that the storage temperature distribution in a stratified tank significantly affects the overall system performance. As an example the predictions from a solar heating or cooling storage tank were found to be more accurate when considering the stratification within the tank. He developed a one-dimensional multi-node approach by considering the axial heat conduction between each node to analyze the temperature stratification in a thermal storage tank. The stratified tank was divided into several equal volumes and energy balances were written for each node in the tank. Heat loss to surroundings, heat gain due to the solar collectors, and energy utilized by the load were taken into account. The temperature of each node was solved as function of time. The study showed that the accuracy of the simulation depends on the number of equal elements in the tank and the volume of each element must be greater than the amount of water flowing into the tank. The paper also showed the results of the effect of parameters on the performance of the tank, for example the collector flow rate, tank size, time step of simulation, etc.

Control Studies

In this section the controller selection and design method will be reviewed. It is well known that the PID and PI controls are very popular in HVAC applications.

Henze and Dodiet (1997) developed a predictive optimal controller for the TES operation with RTP structures. The logic of the controller is to predict an optimal way of the control trajectory for each time step, and implementing it during the operation. The model of the plant, storage tank and predicted cooling load are required to simulate the system. The efficiency of the cooling plant was assumed to be constant.

Massie (2002) developed a neural network-based optimal controller for a commercial ICSS to minimize the cost for the energy consumption. He concluded that the model's ability to learn patterns allows it to self-calibrate for any given price utility rate structure, building load and equipment operations is the major advantage of the neural network controller.

Henze and Schoenmanm (2003) developed a model-free reinforcement learning controller for the purpose of optimizing the operation of the TES system. The controller was trained to operate the TES system to charge and discharge based on the feedback from its previous control actions. The results of the simulation showed that the controller was capable of learning the difficult task of operating the TES system with good performance. However, cost savings were less compared to a predictive optimal controller.

Bai and Zhang (2006) proposed an adaptive PI controller for HVAC system. This adaptive controller can make continues adjustment throughout its life time compared with traditional PI control method which generates control outputs based on fixed proportional and integral gains.

The study showed that the adaptive PI controller is better in limiting overshoots and minimizing oscillation compared to PI controller.

Sedaghati (2006) developed a gain-scheduling scheme of a PI controller for improving the performance of a synchronous generator. The controller allows its proportional and integral gains to be varied within a predetermined range. The maximum and minimum values of the proportional gain were predetermined and a constant "α" was selected for determining the rate of variation between the maximum and minimum values of the proportional gain of the controller. Results from simulation showed that the gain-scheduling controller keeps the system more stable than the conventional PI controller does.

Zaky and Ismaeil (2008) presented a gain scheduling adaptive PI controller for hybrid stepper motor drives. It was shown that the controller improves the performance of the hybrid stepper motor within a predicted range of gain and eliminated the problem of continuous tuning of conventional PI controllers.

2.4 Optimization of TES system

The ways of optimizing the operation of the TES are reviewed in this section. Most of the studies are on the ICSS. However review shows the optimization techniques used in the literature.

Braun (1992) compared the control strategies for a partial ICSS in an office building located in Milwaukee, Wisconsin. The results showed that the load-limiting strategy applied a near-optimal control method to lower the demand cost with considering all environmental conditions.

Krarti and Brandemuehl (1995) studied the chiller-priority and storage-priority control strategies for an ICSS with consideration of wide range of systems, PRT utility rate structures, and operation conditions. The load-limiting, storage-priority control gave near-optimal performance when significant differentials between on-peak and off-peak energy and demand charges occurred. The chiller-priority gave good performance for the days when the peak demand power was less than the monthly peak without consideration about the Time-of-Use energy charges.

Yoshida and Gotou (1999) developed an algorithm for the optimum operation of ChW tank by using MATLAB/SUMULINK. The optimal operation algorithms procedure consisted of four steps: predict the cooling load, determination of required heat storage, system simulation, and optimal system operation control. The optimum setpoint temperature of the ChW to the coil remained as 10.9 ºC, 13.7 ºC, and 16.9 ºC under heavy, medium, and light load condition, respectively; and the energy consumption reduced by 8.6%, 17.0%, and 26.8%, respectively compared to the case which has the chiller operated at maximum capacity until power consumption falls down to 20% of rated performance.

Yoshida and Yamaguti (2001) presented an improved the methodology by applying the optimum algorithm to a real building. The results showed that the reduction of the energy consumption compared with non-optimized operation can be about up to 30% if the air-conditioning load is perfectly predicted. However monitoring results showed that the system encountered 11 days of unsatisfied air-conditioning or insufficient energy storage in the tank if the prediction error level reached up to 5%. For the partial load operation conditions, chillers were operated for 10 hours both in the nighttime and the daytime; and the tank was charged during the nighttime period. It was shown that the nighttime storage operation at 9 ºC followed by the daytime operation could

help in reducing the energy consumption, cost and CO_2 emission by 15%, 9%, and 14%, respectively.

Braun (2007a) presented a near-optimal control method for charging and discharging an ICSS when RTP utility rate structure is available. The different combinations of cooling plants, storage sizes, building locations, and RTP rates are studied in the paper. The ChW supply temperature setpoint (T_{chws}) depended on the stage operation of the ice-tank (charging or discharging), the setpoint of supply ChW to the load (T_{coil}), and the storage charging or discharging rate. The T_{chws} for regulating the discharge rate of the ice-tank during discharging cycle were expressed by using following equation:

$$T_{chws} = T_{coil} - \frac{u_k}{\dot{m}_{chw} c_f} \tag{2.4.1}$$

The T_{coil} is assumed to be constant at 4.4 ºC for all cases in this study.

The T_{coil}, during charging model, is set below the T_{chws} and the storage temperature (T_s) in order to make the control valve deliver all of the flow through the ice-tank. The calculation for T_{chws} is shown below:

$$T_{chws} = T_s - \frac{u_k}{\varepsilon_{c,max} \dot{m}_{chw} c_f} \tag{2.4.2}$$

where u_k = the storage charging or discharging rate;

$\varepsilon_{c,max}$ = maximum heat transfer effectiveness for charging if all the chilled water/glycol flow passes through the tank (no bypass).

c_f= specific heat of the water/glycol mixture flowing through chiller and storage;

$\dot{m}_{chw}$ = mass flow rate of water/glycol mixture flowing through chiller.

The results of the study showed that the near-optimal algorithm applied to all cases in the study worked well and provided annual costs within approximately 2% of the minimum possible costs when using the optimal control.

Braun (2007b) also studied on the savings and the operating cost based on previous study (Braun – 2007a) by applying a near-optimal algorithm to an ICSS comparing with other chiller-priority operation. The savings with the near-optimal control method compared with chiller-priority control were as high as 60% with typical savings in the range from 25% to 30%. The results showed that the savings would be more significant when RTP utility rate structure is applied to the cold storage system. It is possible that the TES system operating under chiller-priority control would have higher costs than the system without using TES system. Therefore chiller-priority control was not suggested as a good option for the case with RTP utility rate structure is employed for the TES system.

Henze and Biffar (2008) applied a ChW TES system to a group of large buildings in pharmaceutical industry in south Germany to study the economic and qualitative benefits of using the TES system. Three types of chiller systems were studied: a steam-driven centrifugal chiller, an electrically driven centrifugal chiller, and a two-stage absorption chiller. The results of the study revealed that the operating costs savings when comparing with the chiller plant without using TES system were about 8% of the annual cooling by using very economical steam-driven centrifugal chiller instead of the more expensive absorption chillers.

Zhang (2010) did a comprehensive study on finding an optimal operating strategy for a chilled water storage system. The optimal strategy method is based on historical data which includes the

profiles of loop cooling load and weather condition; rate model based on utility rate structure and system information, plant model, TES model, and chiller model. Different control strategies were applied to the ChW plant to determine the monthly operating strategies of the system and optimized setpoints. The ChW tank operated under full-storage cycle condition during the simulation for determining the optimal control strategy and setpoints in both summer and winter. The results of the study showed that larger size tank can shift more electricity load from peak demand period to off-peak demand period which lead to higher annual total billing cost savings. The on-peak demand reduction in summer reached up to 45.9% of the total summer demand.

From the above literature review the following points are noted.

a) Most of the studies in the literature are geared towards TES systems and discuss energy storage strategies.
b) Energy storage systems integrated with air handling units, and cooling towers and their dynamic modelling is lacking.
c) Also, majority of the studies addressed the operation strategies. Not much work is done on the design and performance of controllers for chilled water systems.

To this end, the major objectives of this thesis is to model an integrated cooling water system with a chilled water tank, and design an improved PI controller for regulating the performance of the whole system. Also to develop an optimal algorithm for improved energy efficiency and cost savings.

CHAPTER 3 PHYSICAL MODEL OF THE ChW COOLING SYSTEM

3.1 Introduction

To simulate the dynamic processes of the ChW cooling system, dynamic models of each component and the whole chiller plant with the TES system are needed to be developed. Therefore first the physical model of the whole system would be described and then component models of the system including the zone and coil dynamic model, chiller model, cooling tower dynamic model, and ChW tank model will be developed.

3.2 Physical model of the chilled water cooling system

The physical configuration of the system is shown in figure 3.2.1. The system was designed by using steady state design method. The design parameters are given in Appendix A. The operation of the whole ChW system is divided into two stages: one is the charge cycle of the ChW tank; and the other one is the discharge cycle of the tank. The charge cycle of the tank starts from 20:00 to 7:00 and the discharge cycle is activated during the occupant period which is from 7:00 to 20:00 for this building. In other words, the ChW tank is operated under its discharge cycle during the whole occupant period of the building. Figure 3.2.1 shows the whole system of the chiller plant with the ChW tank.

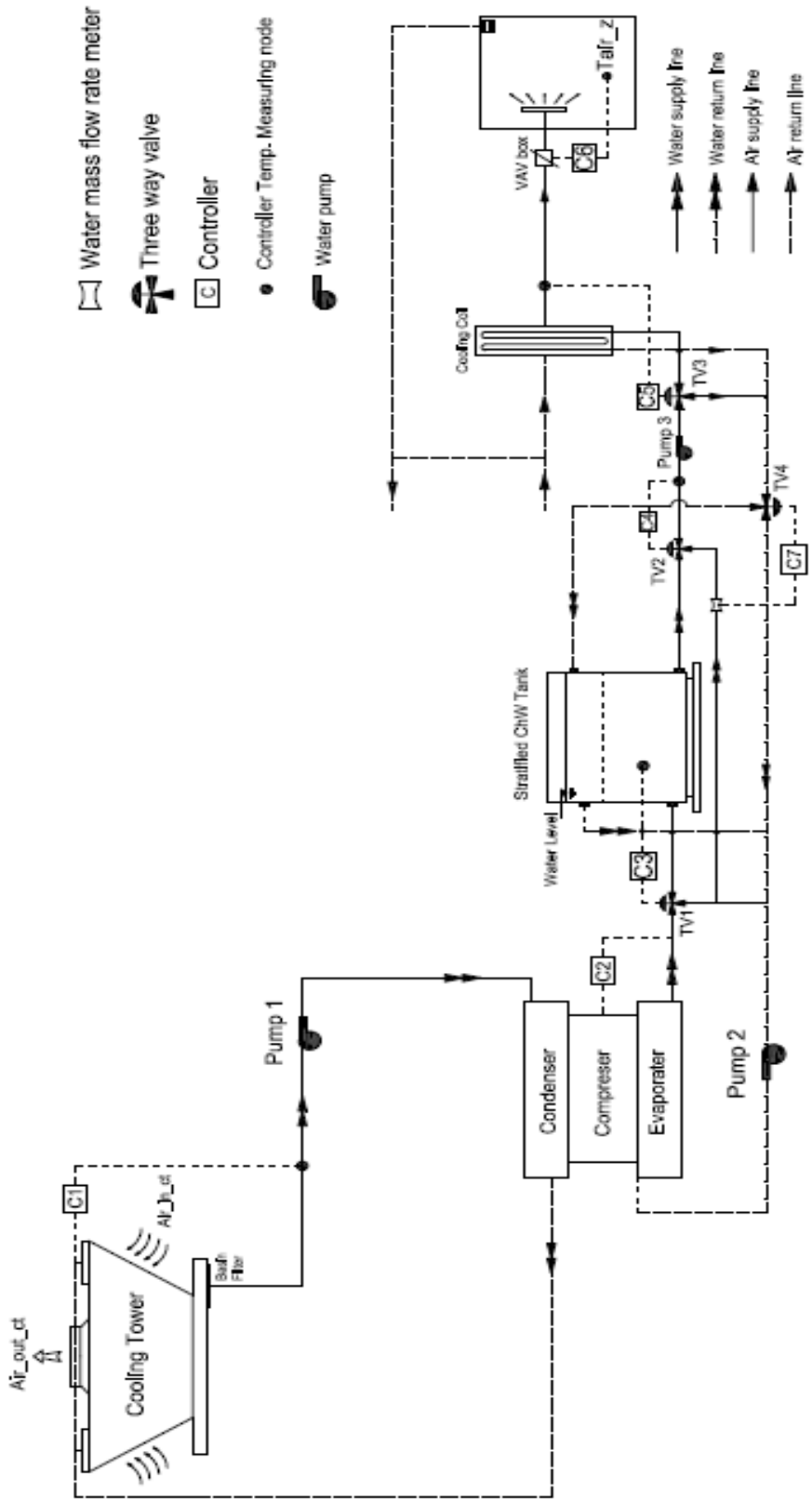

Figure 3.2.1 Whole chiller plant with TES system.

As it shown in figure 3.2.1, there are 7 controllers in the ChW cooling system. The functions of the controllers are described in the following:

VAV box control loop

The controller C6 is used to control the supply mass flow rate of the air into the zone in order to maintain the zone air temperature as its setpoint.

Coil control loop

The supply air temperature to the zone is controlled by the controller C5 which by-passes the mixed supply ChW from both of the tank and the chiller.

ChW tank charge and discharge control loop

During the discharge cycle of the tank, the controller C4 adjusts the opening of the throttling valve (TV) TV2 which determines the mass flow rate of ChW from both of the tank and chiller by maintaining the temperature of the mixed supply ChW to the coil.

When the ChW tank is operated under its charge cycle, the controller C3 controls the three-way throttling valve 1 by supplying the ChW from the chiller to the bottom of the tank; and the rest ChW would be by-passed and supplied to the coil for controlling the supply air temperature to the zone.

It is very important to remember that the discharge and charge cycle of the tank are not operating simultaneously, therefore the controller 4 regulating the TV2 would not interact with controller 3.

Chiller control loop

The controller C2 maintains the supply ChW temperature in the evaporator water loop. The water mass flow rate in the evaporator water loop is held constant.

Cooling tower control loop

The controller C1 maintains the cooled water temperature leaving the cooling tower by adjusting the fan speed in the cooling tower.

ChW tank discharge/charge water mass flow rate balancing control loop

The controller C7, is a mass flow rate controller, allows the same amount of ChW returning back to the chiller as it is supplying to the coil. Therefore the rest of the ChW would return to the tank in order to maintain constant water level in the ChW tank.

3.3 Zone dynamic model

In this section, the zone dynamic simulation model will be developed. The cooling load is predicted by solving set of differential equations describing the zone.

Building configuration

A single story single zone building is considered in this study. The dimension of the building is 80*50*3 m^3. The window area is 30 percent of each wall area. The air change rate (ACH) of 0.25 was assumed which means the air in the building would exchange one quarter of the building volume in an hour.

Wall and roof configuration

The following figure shows the construction detail of the wall and roof, and the table below indicates the thermal properties of each material. The overall thermal resistance of the wall and roof are 3.36 RSI and 5.34 RSI, respectively.

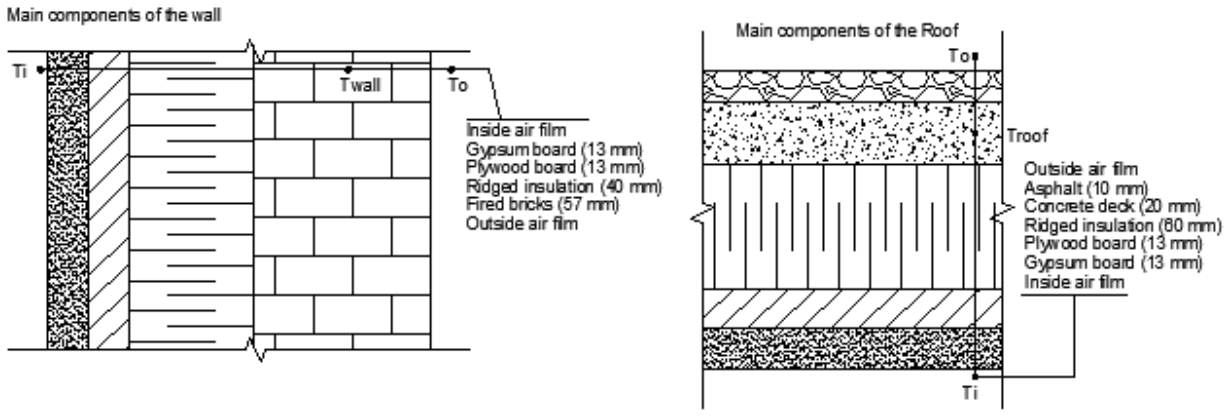

Figure 3.3.3 Construction detail of the wall and roof in the building.

The thermal properties of the materials, the conductance for both of the external and internal air film are shown in the following table:

Table 3.3.1. Materials' properties of the wall and roof.

Materials	Conductivity watt/(m K)	Thermal capacity J/(kg ˚C)	Density kg/m^3
Fired bricks	1.5	900	1700
Asphalt	1.26		
Ridged insulation	0.033	840	120
Plywood board	0.13	2510	700
Concrete deck	1.7	800	2200
Gypsum board	0.18	270	910
Interior surface film conductance: h_i = 8.3 (watt/(m^2 ˚C))			

External surface film conductance: h_o = 22 (watt/(m^2 ˚C))

Dynamic equations for the zone model

By using this dynamic model, the wall, roof, and the zone air temperatures were simulated under predicted cooling load conditions. The wall construction details are shown in figure 3.3.3. The dynamic equation for the wall temperature which is based on the energy conservation law is shown as below.

$$\frac{dT_{wall_s}}{dt} = \frac{\frac{A_{nw_s}}{R_{wa}}(T_{sat_s} - T_{wall_s}) - \frac{A_{nw_s}}{R_{wz}}(T_{wall_s} - T_{a_z})}{C_{br_{sw}}} \quad (3.3.1)$$

$$\frac{dT_{wall_w}}{dt} = \frac{\frac{A_{nw_w}}{R_{wa}}(T_{sat_w} - T_{wall_w}) - \frac{A_{nw_w}}{R_{wz}}(T_{wall_w} - T_{a_z})}{C_{br_{ww}}} \quad (3.3.2)$$

$$\frac{dT_{wall_n}}{dt} = \frac{\frac{A_{nw_n}}{R_{wa}}(T_{sat_n} - T_{wall_n}) - \frac{A_{nw_n}}{R_{wz}}(T_{wall_n} - T_{a_z})}{C_{br_{nw}}} \quad (3.3.3)$$

$$\frac{dT_{wall_e}}{dt} = \frac{\frac{A_{nw_e}}{R_{wa}}(T_{sat_e} - T_{wall_e}) - \frac{A_{nw_e}}{R_{wz}}(T_{wall_e} - T_{a_z})}{C_{br_{ew}}} \quad (3.3.4)$$

where T_{wall} = the temperature of the wall, ˚C

$T_{sat} = T_o + \frac{G\alpha_s}{h_o}$ = solar air temperature, ˚C

G = intensity of solar radiation hitting on building facade, watt/m^2

α = surface absorption ratio, %

A_{nw} = net area of the wall, m^2

R_{wa} = thermal resistance from layer of OA to half layer of the brick, (m^2 ˚C)/watt

R_{wz} = thermal resistance from the half layer of brick to the indoor air, (m^2 ˚C)/watt

C_{br} = the heat capacity of the bricks, J/˚C

The subscripts s, w, n, and e are representing the direction of its facing which are south, west, north, and east, respectively.

The dynamic equation for the zone air temperature is shown below:

$$\frac{dT_{a_z}}{dt} = \left(Q_{h_{s_{cond}}} + Q_{h_{s_{solar}}} + Q_{h_{s_{opt}}} + Q_{h_{s_{inf}}} + Q_{h_{s_{light}}} + Q_{h_{s_{eqp}}} - Q_{c_z}\right)/Ca_z \quad (3.3.5)$$

where Q_{h_s}= the total sensible heat gain of the zone due to heat conduction, solar radiation, occupants, air infiltration, light, and equipment, watt

Q_{c_z} = the cooling supplied by the cooling coil to the zone, watt

Ca_z = the zone air thermal capacity in the zone, J/˚C

The equation for calculating Q_{c_z} can be written as below:

$$Q_{c_z} = m_{a_z} cp_a \left(T_{a_z} - T_{a_{s_c}}\right) \quad (3.3.6)$$

where m_{a_z} = the mass flow rate of air supplied into each zone, kg/s;

cp_a = the specific heat of air at 13 ˚C which is 1011.27 J/(kg ˚C)

$T_{a_{s_c}}$ = the supply cooled air temperature from the cooling coil, ˚C;

Figure 3.3.3 also shows a typical roof cross-section details. The dynamic equation for the roof temperature which is similar to the equation for the wall temperature is shown below:

$$\frac{dT_{roof}}{dt} = \frac{\frac{A_{roof}}{R_{ra}}(T_{sat_r} - T_{roof}) - \frac{A_{roof}}{R_{rz}}(T_{roof} - T_{a_z})}{C_{rcd}} \quad (3.3.7)$$

where T_{roof} = the temperature of the roof, ˚C

A_{roof} = the area of the roof, m^2

R_{ra} = thermal resistance from layer of OA to half layer of concrete deck, (m^2 ˚C)/watt

R_{rz} = thermal resistance from the half layer of concrete deck to the zone air, (m^2 ˚C)/watt

C_{rcd} = the thermal mass of the roof concrete deck, J/˚C

3.4 Cooling coil model

The design of cooling coil is described in detail in reference (McQuiston, 2005). The CLTD method was used to estimate peak cooling load of the building on design day. The Montreal design day conditions were chosen in the calculation. The estimated design coil cooling load was found to be 282 kW. To this end, a four row cross-flow type cooling coil was selected. The coil configuration is described below.

Coil configuration

The figure below shows the sizing of the coil and the tube information.

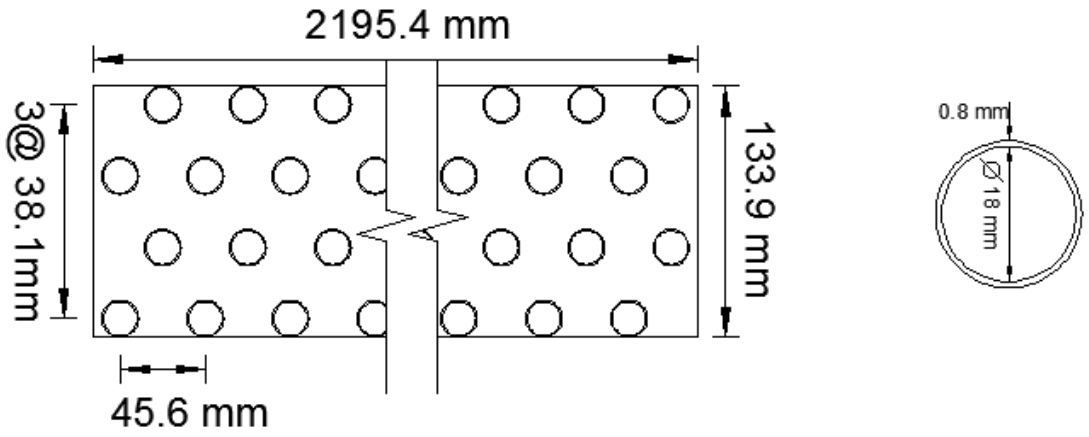

Figure 3.4.1. Cooling coil configuration.

The main parameters of the coil is shown in the following table.

Table 3.4.1 Main parameters of the coil.

Symbols	Meaning	Magnitude	Unit
L_{tb_c}	length of the coil (tube)	3.179	m
H_c	coil height	2.195	m
W_c	coil width	0.134	m
V_c	volume of the coil	0.935	m^3
N_{row_c}	Number of rows in the coil	4	
N_{tb_c}	number of tubes per row	48	
D_{o_c}	the outside diameter of the tube	0.0196	m
D_{i_c}	inside diameter of the tube	0.018	m
ST_c	the transverse distance between tubes	0.0456	m
SL_c	the longitude distance between tubes	0.0381	m
A_{dt_c}	coil face area	6.978	m^2
A_{ot_c}	total outside heat transfer area of the tubes	966.331	m^2

Coil dynamic model

The coil is divided into four control volumes (CV) which have one row of tubes in each control volume. It is assumed that the air temperature, chilled water temperature, and tube wall temperature in each control volume are uniformly distributed. The direction of air flow and chilled water flow rates are shown in the following figure.

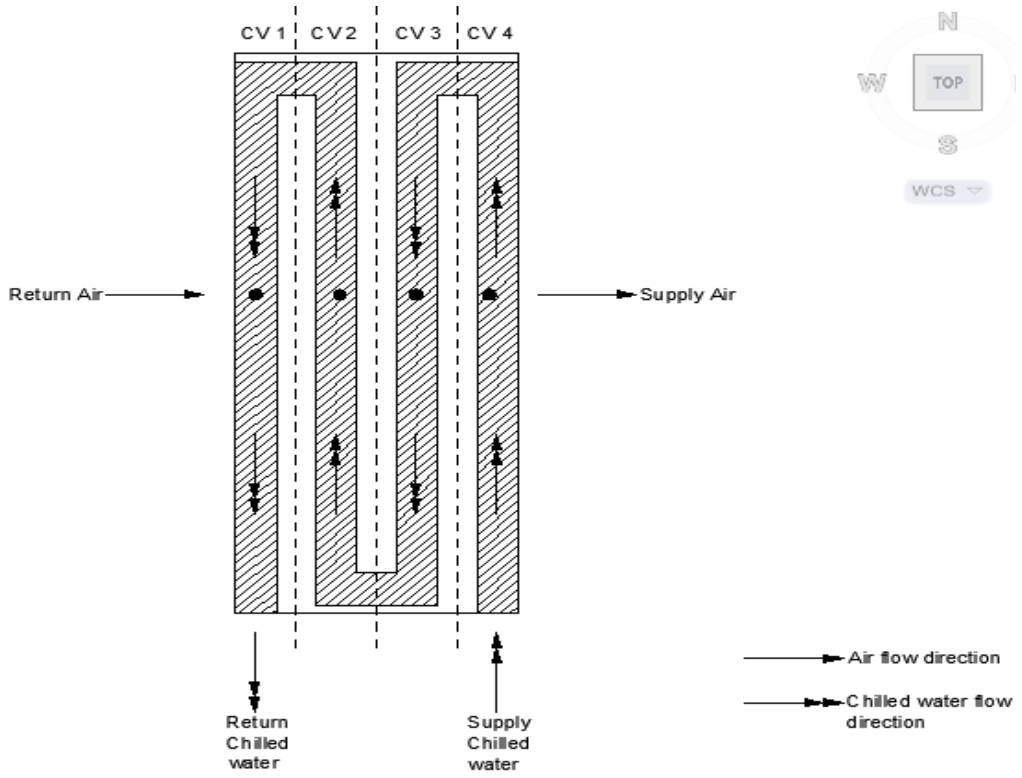

Figure 3.4.2 Air and chilled flow in the cooling coil.

The figure below shows a typical section of the tube in the coil which is the side view to coil.

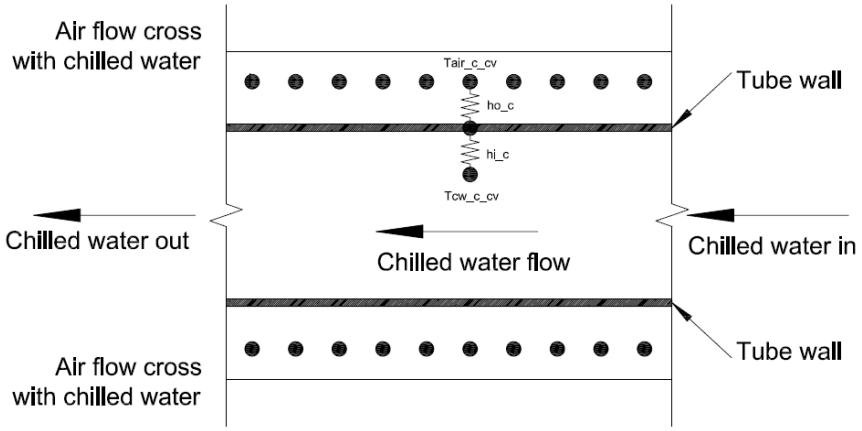

Figure 3.4.3 A typical section of the tube in the cooling coil (cross-section view).

The energy is transferred from air to the flowing chilled water through the tube wall. Therefore the energy released from air is negative; and the chilled water which absorbs energy from the tube wall is considered positive. The h_{o_c} and h_{i_c} are the heat transfer coefficients on the airside and waterside of the tube, respectively.

Dynamic equations for the coil

The modal equations corresponding to the node depicted in figure 3.4.2 were written:

For the air temperature in each control volume

$$\frac{dT_{a_{s_c}}}{dt} = \frac{m_{a_{s_c}} cp_a\left(T_{a_{c_{cv3}}} - T_{a_{s_c}}\right) + h_{o_c} A_{ot_{ccv4}}\left(T_{tb_{c_{cv4}}} - \frac{T_{a_{s_c}} + T_{a_{c_{cv3}}}}{2}\right)}{C_{a_{c_{cv4}}}} \tag{3.4.1}$$

$$\frac{dT_{a_{c_{cv1}}}}{dt} = \frac{m_{a_{s_c}} cp_a\left(T_{a_{r_c}} - T_{a_{c_{cv1}}}\right) + h_{o_c} A_{ot_{ccv1}}\left(T_{tb_{c_{cv1}}} - \frac{T_{a_{c_{cv1}}} + T_{a_{r_c}}}{2}\right)}{C_{a_{c_{cv1}}}} \tag{3.4.2}$$

$$\frac{dT_{a_{c_{cv2}}}}{dt} = \frac{m_{a_{s_c}} cp_a\left(T_{a_{c_{cv1}}} - T_{a_{c_{cv2}}}\right) + h_{o_c} A_{ot_{ccv2}}\left(T_{tb_{c_{cv2}}} - \frac{T_{a_{c_{cv1}}} + T_{a_{c_{cv2}}}}{2}\right)}{C_{a_{c_{cv2}}}} \tag{3.4.3}$$

$$\frac{dT_{a_{c_{cv3}}}}{dt} = \frac{m_{a_{s_c}} cp_a\left(T_{a_{c_{cv2}}} - T_{a_{c_{cv3}}}\right) + h_{o_c} A_{ot_{ccv3}}\left(T_{tb_{c_{cv3}}} - \frac{T_{a_{c_{cv2}}} + T_{a_{c_{cv3}}}}{2}\right)}{C_{a_{c_{cv3}}}} \quad (3.4.4)$$

For the tube wall temperature in each control volume

$$\frac{dT_{tb_{c_{cv1}}}}{dt} = \frac{h_{o_c} A_{ot_{ccv1}}\left(\frac{T_{a_{c_{cv1}}} + T_{a_{r_c}}}{2} - T_{tb_{c_{cv1}}}\right) + h_{i_c} A_{it_{ccv1}}\left(\frac{T_{cw_{r_c}} + T_{cw_{c_{cv2}}}}{2} - T_{tb_{c_{cv1}}}\right)}{C_{cop_{c_{cv1}}}} \quad (3.4.5)$$

$$\frac{dT_{tb_{c_{cv2}}}}{dt} = \frac{h_{o_c} A_{ot_{ccv2}}\left(\frac{T_{a_{c_{cv1}}} + T_{a_{c_{cv2}}}}{2} - T_{tb_{c_{cv2}}}\right) + h_{i_c} A_{it_{ccv2}}\left(\frac{T_{cw_{c_{cv3}}} + T_{cw_{c_{cv2}}}}{2} - T_{tb_{c_{cv2}}}\right)}{C_{cop_{c_{cv2}}}} \quad (3.4.6)$$

$$\frac{dT_{tb_{c_{cv3}}}}{dt} = \frac{h_{o_c} A_{ot_{ccv3}}\left(\frac{T_{a_{c_{cv2}}} + T_{a_{c_{cv3}}}}{2} - T_{tb_{c_{cv3}}}\right) + h_{i_c} A_{it_{ccv3}}\left(\frac{T_{cw_{c_{cv3}}} + T_{cw_{c_{cv4}}}}{2} - T_{tb_{c_{cv3}}}\right)}{C_{cop_{c_{cv3}}}} \quad (3.4.7)$$

$$\frac{dT_{tb_{c_{cv4}}}}{dt} = \frac{h_{o_c} A_{ot_{ccv4}}\left(\frac{T_{a_{s_c}} + T_{a_{c_{cv3}}}}{2} - T_{tb_{c_{cv4}}}\right) + h_{i_c} A_{it_{ccv4}}\left(T_{cw_{c_{cv4}}} - T_{tb_{c_{cv4}}}\right)}{C_{cop_{c_{cv4}}}} \quad (3.4.8)$$

For the chilled water temperature in each control volume

$$\frac{dT_{cw_{c_{cv4}}}}{dt} = \frac{m_{cw_{s_c}} cp_{cw}\left(T_{cw_{s_c}} - T_{cw_{c_{cv4}}}\right) + h_{i_c} A_{it_{cv1}}\left(T_{tb_{c_{cv1}}} - \frac{T_{cw_{s_c}} + T_{cw_{c_{cv4}}}}{2}\right)}{C_{cw_{c_{cv4}}}} \quad (3.4.9)$$

$$\frac{dT_{cw_{c_{cv2}}}}{dt} = \frac{m_{cw_{s_c}} cp_{cw}\left(T_{cw_{c_{cv3}}} - T_{cw_{c_{cv2}}}\right) + h_{i_c} A_{it_{cv2}}\left(T_{tb_{c_{cv2}}} - \frac{T_{cw_{c_{cv3}}} + T_{cw_{c_{cv2}}}}{2}\right)}{C_{cw_{c_{cv2}}}} \quad (3.4.10)$$

$$\frac{dT_{cw_{c_{cv3}}}}{dt} = \frac{m_{cw_{s_c}} cp_{cw}\left(T_{cw_{c_{cv4}}} - T_{cw_{c_{cv3}}}\right) + h_{i_c} A_{it_{cv3}}\left(T_{tb_{c_{cv3}}} - \frac{\left(T_{cw_{c_{cv4}}} - T_{cw_{c_{cv3}}}\right)}{2}\right)}{C_{cw_{c_{cv3}}}} \quad (3.4.11)$$

$$\frac{dT_{cw_{r_c}}}{dt} = \frac{m_{cw_{s_c}} cp_{cw}\left(T_{cw_{c_{cv2}}} - T_{cw_{r_c}}\right) + h_{i_c} A_{it_{cv4}}\left(T_{tb_{c_{cv4}}} - \frac{T_{cw_{c_{cv2}}} - T_{cw_{r_c}}}{2}\right)}{C_{cw_{c_{cv1}}}} \quad (3.4.12)$$

The following table shows the meaning of the symbols and their magnitude and units.

Table 3.4.2 Details of the main parameters in the coil model.

Symbols	Meaning	magnitude	Unit
$m_{a_{s_c}}$	Air mass flow rate in the coil	As function of time	kg/s
$m_{cw_{s_c}}$	Chilled water mass flow rate in the coil	As function of time	kg/s
$A_{ot_{c_{cv}}}$	The outside heat transfer area of the tube at airside	241.58	m^2
$A_{it_{c_{cv}}}$	Inside heat transfer area of the tube at waterside	8.629	m^2
$T_{a_{s_c}}$	Supply air temperature after passing through the coil	As function of time	˚C
$T_{a_{r_c}}$	Mixed air temperature with return and fresh air	As function of time	˚C
$T_{a_{c_{cv}}}$	air temperature in each control volume of the coil	As function of time	˚C
$T_{tb_{c_{cv}}}$	Tube wall temperature in each CV of the coil	As function of time	˚C
$T_{cw_{c_{cv}}}$	Chilled water temperature in each CV of the coil	As function of time	˚C
$T_{cw_{s_c}}$	Supply ChW temperature to the coil	As function of time	˚C
$T_{cw_{r_c}}$	Return ChW temperature leaving the coil	As function of time	˚C
$C_{a_{c_{cv}}}$	the thermal capacity of air in each CV	-	J/˚C
$C_{cop_{c_{cv}}}$	The thermal capacity of the tube wall in each CV	-	J/˚C
$C_{cw_{c_{cv}}}$	The thermal capacity of the chilled water in each CV	-	J/˚C

The equations for heat transfer coefficients hi and ho were obtained from the reference (Kreith, 2001). These are given below:

Calculation of h_{o_c}

As the Reynolds number of the air is less than 10000 and the ratio of transverse distance to the longitude distance is 1.2 which is less than 2, the applicable equation to calculate the airside Nusselt number is shown below:

$$NuD_c = 0.35\left(\frac{ST_c}{SL_c}\right)^{0.2} ReD_{a_c}{}^{0.6} Pr_c^{0.36}\left(\frac{Pr_c}{Pr_{cs}}\right)^{0.25} \quad (3.4.13)$$

And the heat transfer coefficient for the airside of the tube is calculated by using following equation:

$$h_{o_c} = NuD_c \frac{k_a}{D_{o_c}} \quad (3.4.14)$$

The heat transfer coefficient of the tube at airside is 58.1 watt/(m^2 ˚C) under peak load condition.

Calculation of h_{i_c}

The Reynolds number of the chilled water is 13813 which is higher than 10000. According to the reference ASHREA fundamental handbook (2009), the Nusselt number of the water is determined by using the following equation:

$$NuD_{cw_c} = 0.023 ReD_{cw_c}{}^{0.8} Pr_{cw_c}{}^{0.3} \quad (3.4.15)$$

By using the Nusselt number of chilled water, the waterside heat transfer coefficient is obtained from the equation below:

$$h_{i_c} = NuD_{cw_c} \frac{k_{cw}}{D_{i_c}} \quad (3.4.16)$$

3.5 Chiller model

To describe the behaviour of the chiller selected for the building, a multivariate polynomial regression (MPR) model was developed. Data from the manufacturer's catalogue (Napps, Application Manual) were used to develop the regression model. The coefficients of the MPR model were determined using MATLAB. There are four parameters in the MPR model to predict the COP of the chiller: mass flow rate of ChW in the evaporator water loop, mass flow rate of the cooled water in the condenser water loop, the ChW temperature in the evaporator water loop, and the cooled water temperature in the condenser water loop. The MPR equation for calculating the COP of the evaporator is shown as below.

$$COP_{evap} = C_0 + C_1 T_{cow_{s_{cond}}} + C_2 \mathrm{T_{cw_{s_{chi}}}} + C_3 m_{cow_{cond}} + C_4 \mathrm{m_{cw_{s_{chi}}}} + C_5 \mathrm{T_{cow_{s_{cond}}}}^2 + C_6 \mathrm{T_{cw_{s_{chi}}}}^2 + C_7 \mathrm{m_{cow_{cond}}}^2 + C_8 \mathrm{m_{cw_{s_{chi}}}}^2 + C_9 \mathrm{T_{cow_{s_{cond}}}} \mathrm{T_{cw_{s_{chi}}}} + C_{10} \mathrm{m_{cow_{cond}}} \mathrm{m_{cw_{s_{chi}}}} \quad (3.5.1)$$

where $T_{cow_{s_{cond}}}$=cooled water temperature leaving the cooling tower, ˚C;

$\mathrm{T_{cw_{s_{chi}}}}$ = chilled water temperature leaving the evaporator, ˚C;

$m_{cw_{cond}}$= cooled water mass flow rate in the condenser water loop, kg/s;

$\mathrm{m_{cw_{s_{chi}}}}$ = chilled water mass flow rate in the evaporator water loop, kg/s;

The following table shows the coefficient of C.

Table 3.5.1 Regressive coefficients for calculating the COP of the evaporator.

C_0	-116.7134	C_1	-0.1748
C_2	0.2191	C_3	-6.0588
C4	-7.7558	C_5	0.0012
C_6	0.0018	C_7	0.5767
C_8	0.3487	C_9	-0.0039
C_{10}	0.4749		

Dynamic equation for the water temperature

The supply ChW temperature leaving the evaporator and the cooled water temperature leaving the condenser were modeled. The dynamic differential equations are written as below:

$$\frac{dT_{cow_{r_{cond}}}}{dt} = \frac{\mathrm{m_{cow_{cond}}cp_{cow}}\left(\mathrm{T_{cow_{s_{cond}}}} - T_{cow_{r_{cond}}}\right) + \mathrm{Q_{comp}}\left(\mathrm{COP_{evap}}+1\right)}{C_{cow}} \tag{3.5.2}$$

$$\frac{dT_{cw_{s_{chi}}}}{dt} = \frac{\mathrm{m_{cw_{s_{chi}}}cp_{cw}}\left(\mathrm{T_{cw_{r_{chi}}}} - T_{cw_{s_{chi}}}\right) - \mathrm{Q_{comp}COP_{evap}}}{C_{cw}} \tag{3.5.3}$$

Where $\mathrm{cp_{cow}}$ = specific heat of cooled water, J/(kg ˚C);

$\mathrm{Q_{comp}}$ = compressor power input, watt;

$\mathrm{COP_{evap}}$ = COP of the evaporator, unit less;

C_{cow} = thermal capacity of the cooled water in the condenser side, J/˚C;

C_{cw} = thermal capacity of the chilled water in the evaporator side, J/˚C;

3.6 Cooling Tower model

The air mass flow rate into the cooling tower

According to energy conservation principle, the heat rejected by air should be equal to the energy removed by the cooling water. Therefore the following equation was used to calculate the mass flow rate of air entering to the cooling tower:

$$m_{a_{ct_{in}}}\left(h_{a_{ct_{out}}} - h_{a_{ct_{in}}}\right) = m_{cow_{cond_{in}}} cp_{cow}\left(T_{cow_{cond_{out}}} - T_{cow_{cond_{in}}}\right) \qquad (3.6.1)$$

Where $m_{a_{ct_{in}}}$ = mass flow rate of air entering into the cooling tower, kg/s

$h_{a_{ct_{in}}}$ = the enthalpy of the outdoor air entering into the CT, kJ/kg

$h_{a_{ct_{out}}}$ = the enthalpy of the saturated outdoor air leaving the CT, kJ/kg;

$m_{cow_{cond_{in}}}$ = cooled water mass flow rate in the condenser, kg/s;

cp_{cow} = specific heat of cooled water, J/(kg ˚C)

$T_{cow_{cond_{out}}}$ = cooled water leaving the condenser, ˚C;

$T_{cow_{cond_{in}}}$ = cooled water entering into the condenser, ˚C;

ε - NTU method analysis

Thomas H. Kuehn (1998) presented a ε - NTU method. The following figure shows the energy transfer between the water and air in the cooling tower.

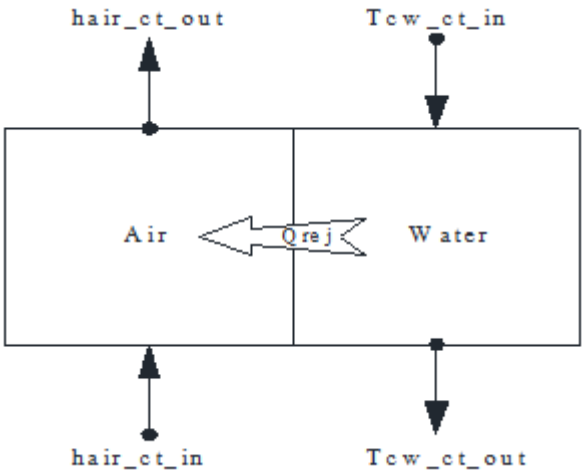

Figure 3.6.1 Thermal interaction between the air and water in the cooling tower.

The performance of the cooling tower was described by using NTU method:

$$\frac{h_D A_V V}{\dot{m}_w} = NTU = c\left(\frac{\dot{m}_w}{\dot{m}_a}\right)^{-n} \tag{3.6.2}$$

where h_D= mass – transfer coefficient, $kg_w/(sec\ m^2)$;

A_V= surface area of water droplets, m^2/m^3;

V = contact volume between air and water, m^3;

NTU = the number of transfer unit;

$\dot{m}_a$ = mass flow rate of air, kg/s;

$\dot{m}_w$ = mass flow rate of water, kg/s;

c & n = empirical constant for particular tower-fill design.

As recommended by *ASHRAE HVAC system s and Equipment Handbook 2005*, c and n are 1.3 and 0.6, respectively. When m_w is less than m_a,

$$NTU = 1.3(\frac{\dot{m}_w}{\dot{m}_a})^{-0.6} \tag{3.6.3}$$

And if $\dot{m}_a$ is less than or equal to $\dot{m}_w$,

$$NTU = 1.3(\frac{\dot{m}_w}{\dot{m}_a})^{1-0.6} \tag{3.6.4}$$

The ratio of the capacity rates could be calculated by using following equation:

$$C = \frac{m_{min}}{m_{max}} \tag{3.6.5}$$

where m_{min}= m_a and m_{max}= m_w or vice versa.

The effectiveness of the cooling tower therefore can be determined as below:

$$\varepsilon = \frac{1-\exp[-NTU(1-C)]}{1-C\ \exp[-NTU(1-C)]} \tag{3.6.6}$$

Then the energy rejected by the cooling tower could be obtained from

$$Q_{rej} = \varepsilon m_a \left(h_{a_{ct_{out}}} - h_{a_{ct_{in}}}\right) \tag{3.6.7}$$

The steady state equation for the energy transfer by the condenser water is given by:

$$m_{cow_{ct_{in}}} T_{cow_{ct_{in}}} cp_{cow} - Q_{rej} = m_{cow_{ct_{out}}} T_{cow_{ct_{out}}} cp_{cow} \tag{3.6.8}$$

where $m_{cow_{ct_{in}}}$ = cooled water mass flow rate entering into the cooling tower, kg/s;

$T_{cow_{ct_{in}}}$ = cooled water temperature when entering into the cooling water, ˚C;

cp_{cow} = specific heat of cooled water, J/(kg ˚C);

$m_{cow_{ct_{out}}}$ = mass flow rate of cooled water at outlet of the cooling tower, kg/s;

$T_{cow_{ct_{out}}}$ = cooled water temperature when leaving the cooling tower, ˚C;

3.7 Stratified Tank model

The stratified tank, with its inside diameter of 8 meters and its height of 4.2 meter, is used as thermal energy storage system integrated with the cooling tower, chiller, and cooling coil in the ChW system. As shown in the following figure, the supply tubes from both of the evaporator and cooling tower are located at the bottom of the tank, and the return pipe located at the top of the tank; this is because that the thermocline separates the chilled water into two parts in the tank – one is the warmer chilled water at the top and the cooler chilled water at the bottom of the tank. The chilled water in the tank is divided into two control volumes; and the simulation will cover both of the charge and discharge cycles in the tank. The chilled water temperature in each control volume is effected by the outside ambient air temperature, chilled water temperature in the adjacent control volume, and the fluid temperature in the cooling tower loop, evaporator loop, and the coil loop.

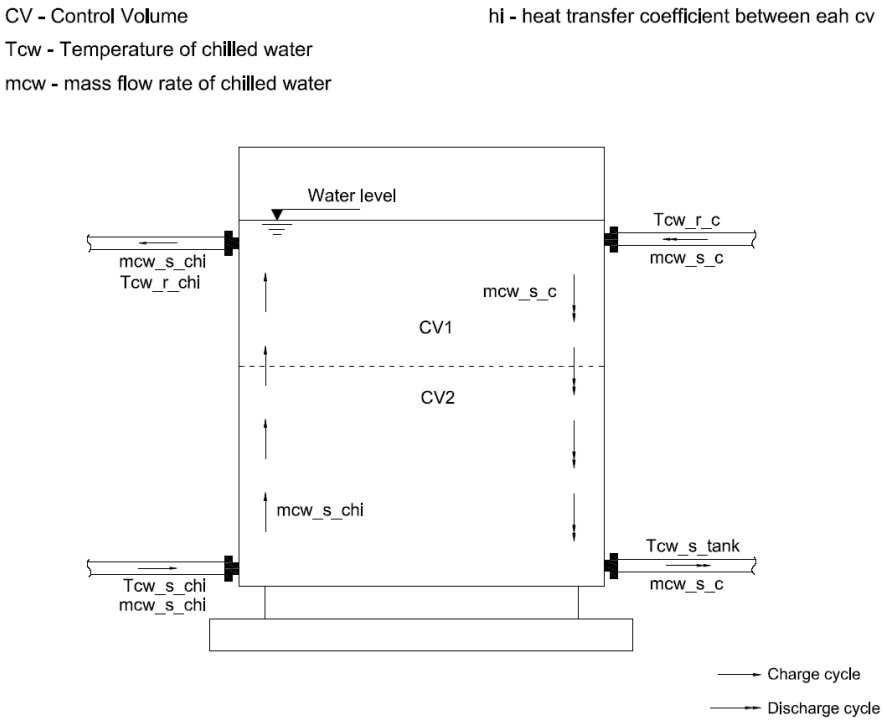

Figure 3.7.1 Schematic diagram of the stratified tank (charge or discharge cycle).

Tank sizing test

The ChW tank is designed based on the objective of covering 80% heat gain of the building on the design day from 9:00 to 14:00. Therefore the ChW tank must be capable of satisfying the load requirement without failing to maintain the thermal comfort in the building. In this case, the zone air temperature in excess of 23.5 ºC would be considered as lost thermal comfort in the building. The tank sizing test model only involves the zone – load model, cooling coil model, and stratified water tank model. Three PI controllers will be used for controlling the zone air temperature, supply air temperature to the zone, and the mass flow rate of the ChW supply to the coil.

Dynamic equations of the stratified tank

The tank was divided into two control volumes. The dynamic equations for each node of the control volume of the stratified tank during the charge cycle are shown in following:

$$\frac{dT_{cw_{tank_{cv1}}}}{dt} = \frac{m_{cw_{s_{chi}}} cp_{cw}\left(T_{cw_{tank_{cv2}}} - T_{cw_{tank_{cv1}}}\right) + \frac{A_{w_{tank_{cv1}}}}{R_{tank}}\left(T_{o_{tank}} - T_{cw_{tank_{cv1}}}\right)}{C_{cw_{tank_{cv1}}}} \tag{3.7.1}$$

$$\frac{dT_{cw_{tank_{cv2}}}}{dt} = \frac{m_{cw_{s_{chi}}} cp_{cw}(T_{cw_{s_{chi}}} - T_{cw_{tank_{cv2}}}) + \frac{A_{w_{tank_{cv2}}}}{R_{tank}}(T_{o_{tank}} - T_{cw_{tank_{cv2}}})}{C_{cw_{tank_{cv2}}}} \tag{3.7.2}$$

where $A_{cr_{tank}}$ = cross section area of the tank, m^2;

R_{tank} = thermal resistance of the tank wall, watt/(m^2 °C);

$T_{o_{tank}}$ = outside ambient air temperature of the tank, °C;

$T_{cw_{s_{chi}}}$ = supply chilled water temperature from the evaporator, °C;

$T_{cw_{tank_{cv}}}$ = chilled water temperature in each CV of the tank, °C;

The dynamic equations for the discharge cycle of the stratified tank are shown as below:

$$\frac{dT_{cw_{tank_{cv1}}}}{dt} = \frac{m_{cw_{s_{tank}}} cp_{cw}(T_{cw_{r_c}} - T_{cw_{tank_{cv1}}}) + \frac{A_{w_{tank_{cv1}}}}{R_{tank}}(T_{o_{tank}} - T_{cw_{tank_{cv1}}})}{C_{cw_{tank_{cv1}}}} \tag{3.7.3}$$

$$\frac{dT_{cw_{tank_{cv2}}}}{dt} = \frac{m_{cw_{s_{tank}}} cp_{cw}\left(T_{cw_{tank_{cv1}}} - T_{cw_{tank_{cv2}}}\right) + \frac{A_{w_{tank_{cv2}}}}{R_{tank}}\left(T_{o_{tank}} - T_{cw_{tank_{cv2}}}\right)}{C_{cw_{tank_{cv2}}}} \tag{3.7.4}$$

where $m_{cw_{s_{tank}}}$ = mass flow rate of chilled water from the tank to coil, kg/s;

3.8 Open loop test for the whole ChW system

The component model equations described above were integrated to develop the overall model and the system equations were solved by using MATLAB. It should be noted that the model equations describe the thermal behavior of the system. Open loop tests (OLT) were conducted to simulate the responses of the system under constant cooling load conditions. Since the ChW system with and without tank are included in this thesis, the OLT would cover the ChW system with and without ChW tank. The predicted cooling load is kept constant which corresponds to the design day load at 14:00 during discharge cycle; and the predicted cooling load for the charge cycle corresponds to the load at 2:00 am.

OLT results for the ChW system without the ChW tank

The results for the OLT for the ChW system without the ChW tank are shown in the following figures:

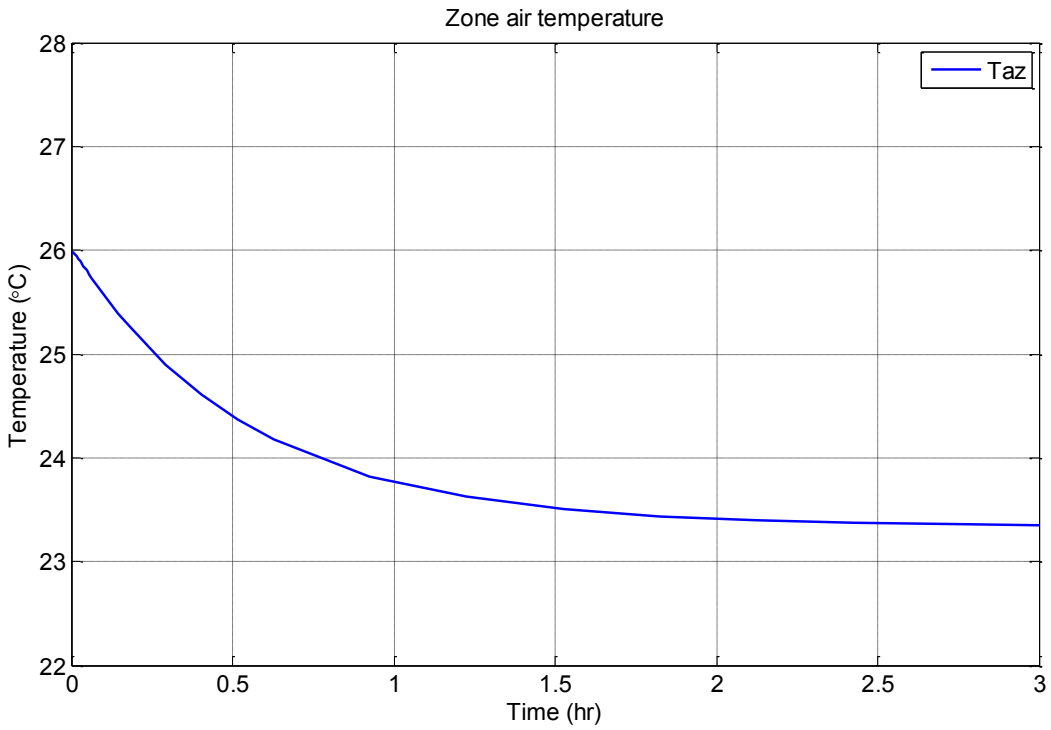

Figure 3.8.1 Zone air temperature of the OLT (No ChW tank).

Figure 3.8.1 shows the zone temperature response for the ChW system without the ChW tank. For this OLT, the VAV box opening was set at 0.85. The Sensible load of the zone was 240 kW. As shown in figure 3.8.1, the zone air temperature reaches steady state value of 23.4 ºC in about 2 hours.

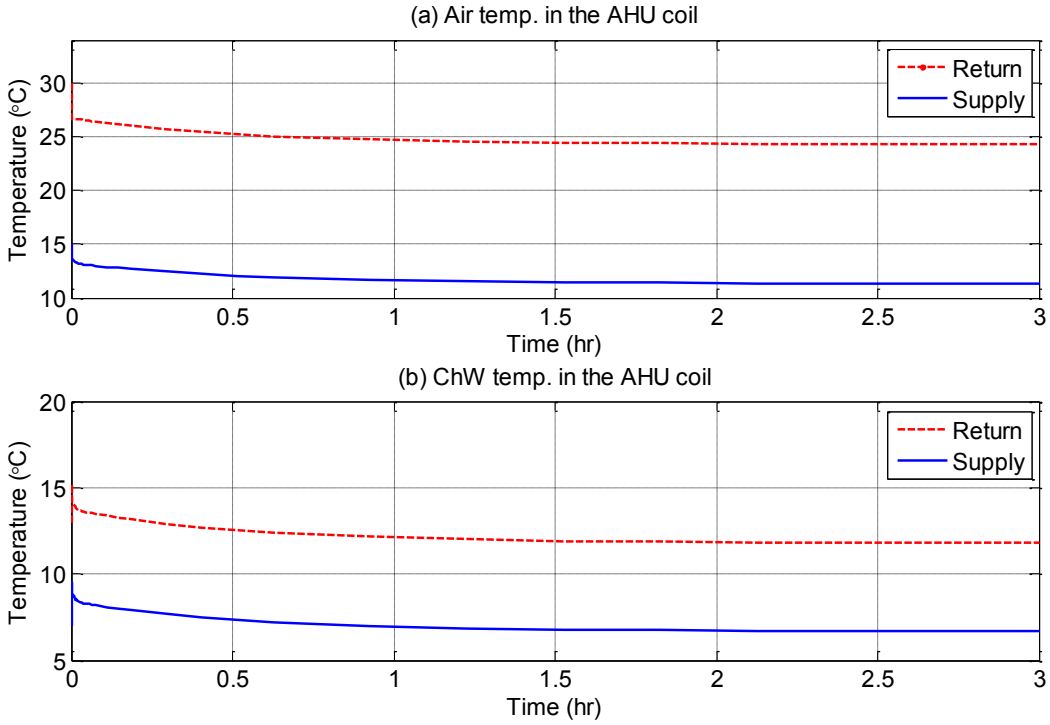

Figure 3.8.2 Coil model responses (No ChW tank).

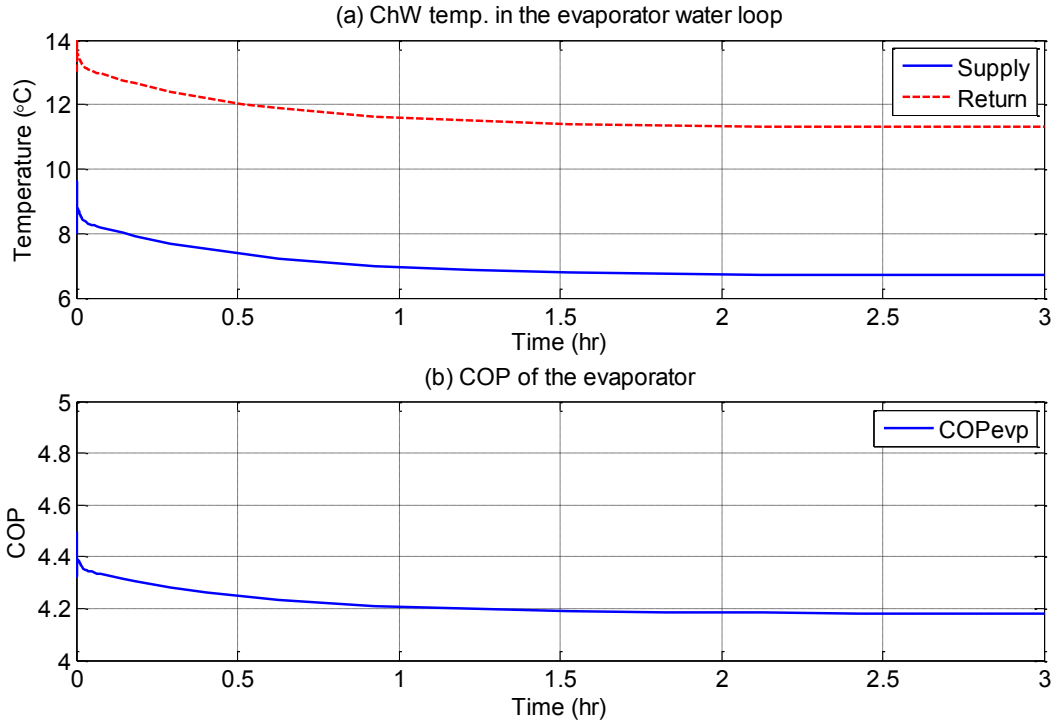

Figure 3.8.3 Chiller model responses (No ChW tank).

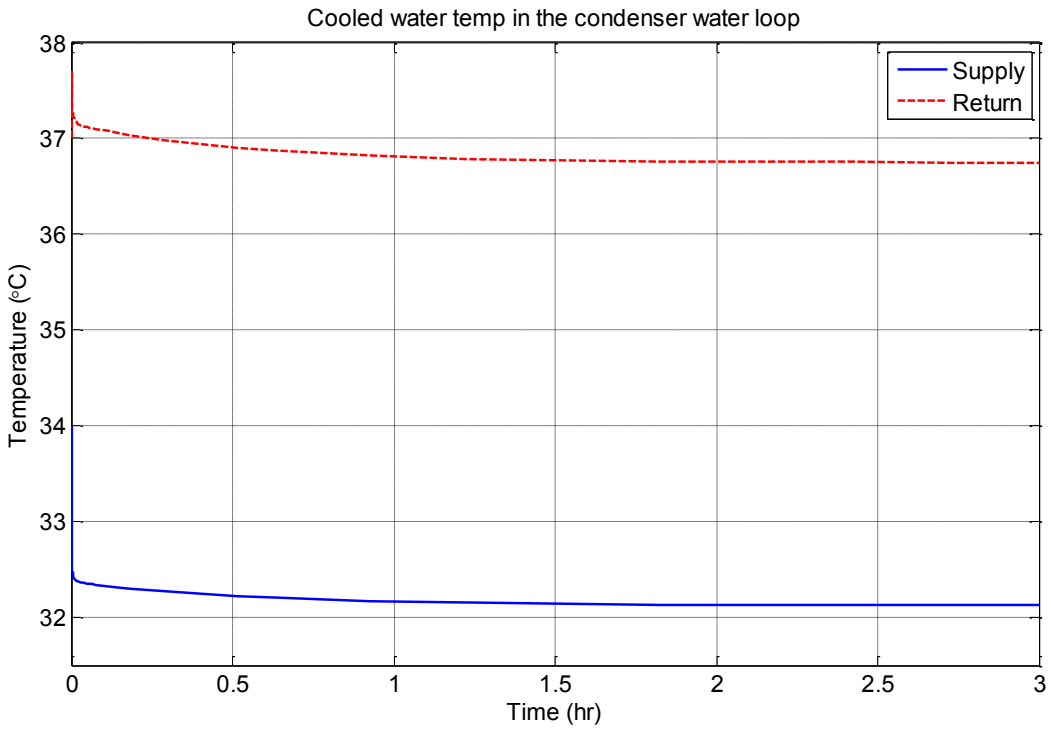

Figure 3.8.4 Cooled water temperature responses (No ChW tank).

Figure 3.8.2 depicts the supply air and chilled water temperature responses. The supply air temperature takes one and half hour to settle at 11.34 ºC and the return mixed air temperature settles around 24.32 ºC. The supply ChW temperature to the coil and the return ChW temperature reach steady state values of 6.7 and 11.81 ºC, respectively. The mass flow rate of the ChW supply to the coil was kept a constant at 12.1 kg/s during this open loop test.

Figure 3.8.3 depicts the temperature responses from the evaporator and condenser loops. The compressor capacity was set at 0.98. It can be seen from figure 3.8.3 (b) that the COP of the system follows the temperature response and reaches steady state value of 4.18.

Figure 3.8.4 shows the cooled water temperature response in the condenser water loop. The fan in the cooling tower was operated at 0.65 of its maximum capacity. The cooled water temperature leaving the cooling tower reaches steady state value of 32.13 ºC and the return

cooled water temperature reached 36.75 ºC. The effectiveness of the cooling tower corresponding to the above results was found to be 62.5 %.

OLT results for the ChW system with using the ChW tank – charge cycle

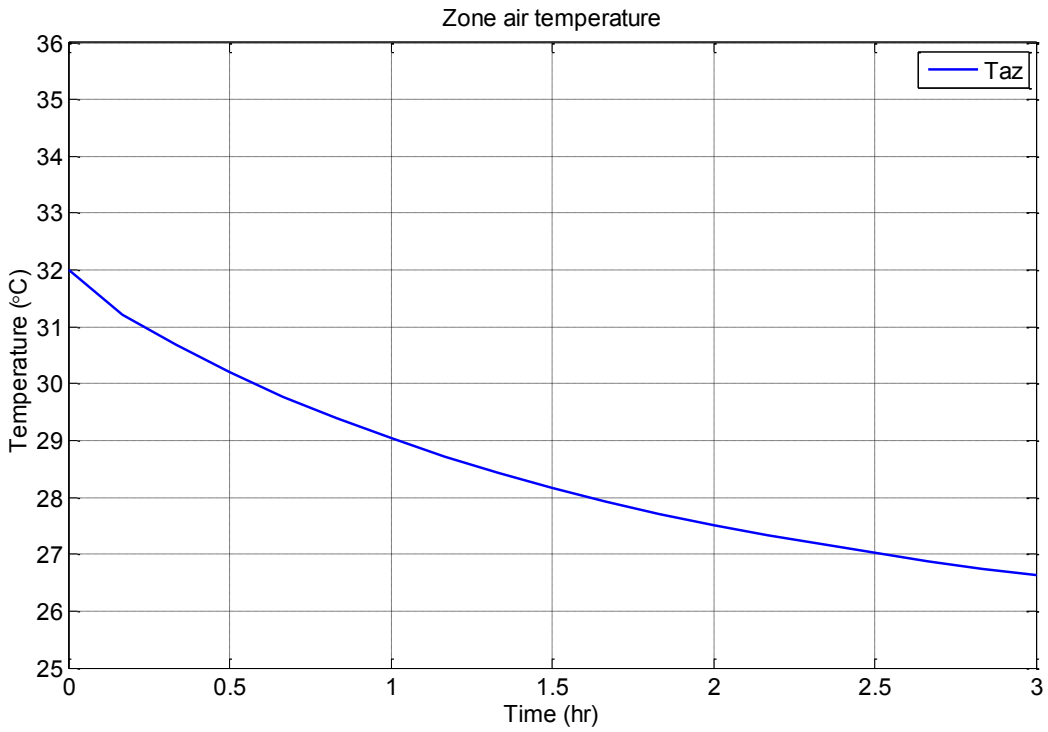

Figure 3.8.5 Zone air temperature OLT results (With ChW tank - charge cycle).

The zone temperature response during the charge cycle is depicted in figure 3.8.5. As can be seen the temperature drops from 32 to 26.6 ºC in about 3 hours. The zone load during the charge cycle was very low (27.5 kW) as such the VAV box opening of 15% was sufficient to provide cooling.

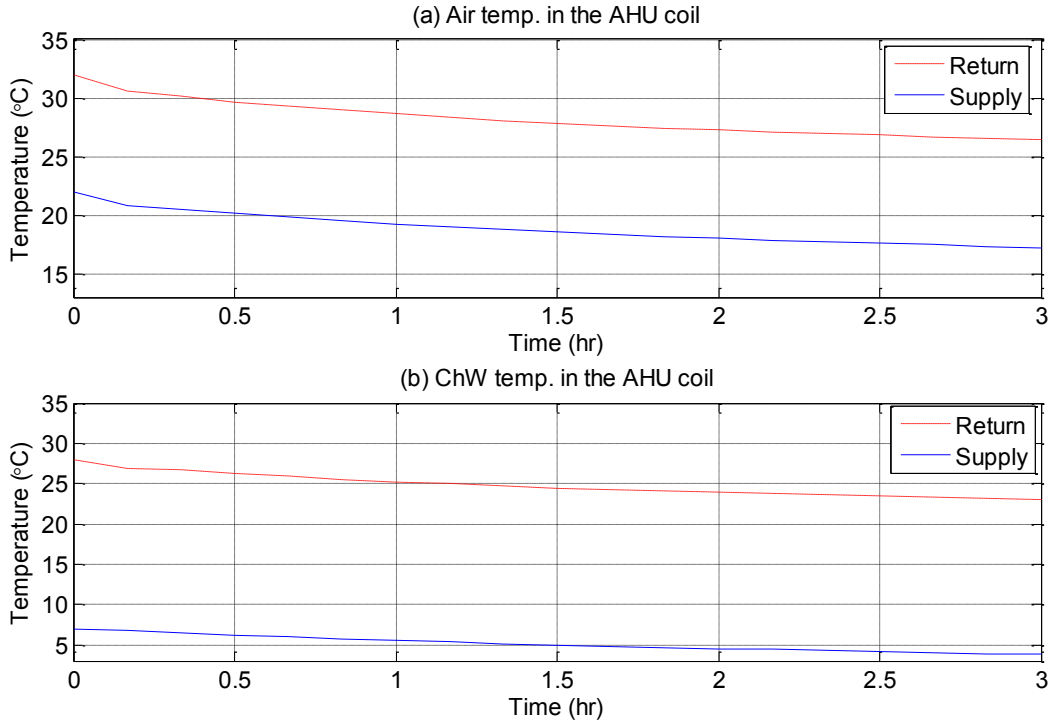

Figure 3.8.6 Coil model results for the ChW system (with tank – charge cycle).

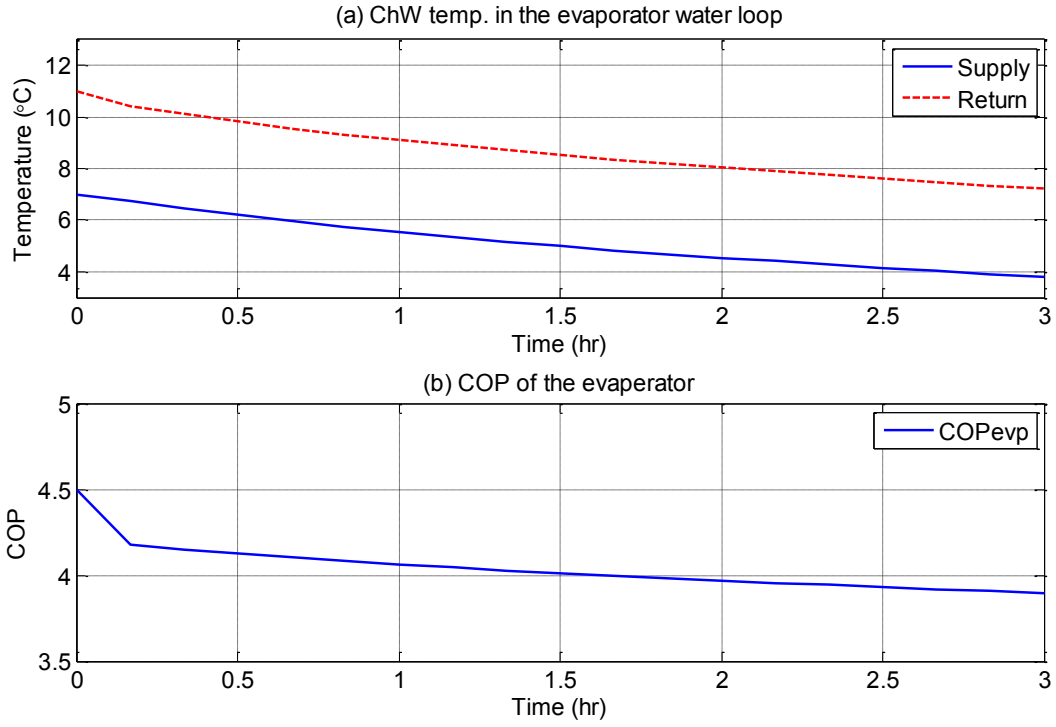

Figure 3.8.7 Chiller model results for the ChW system (with tank – charge cycle).

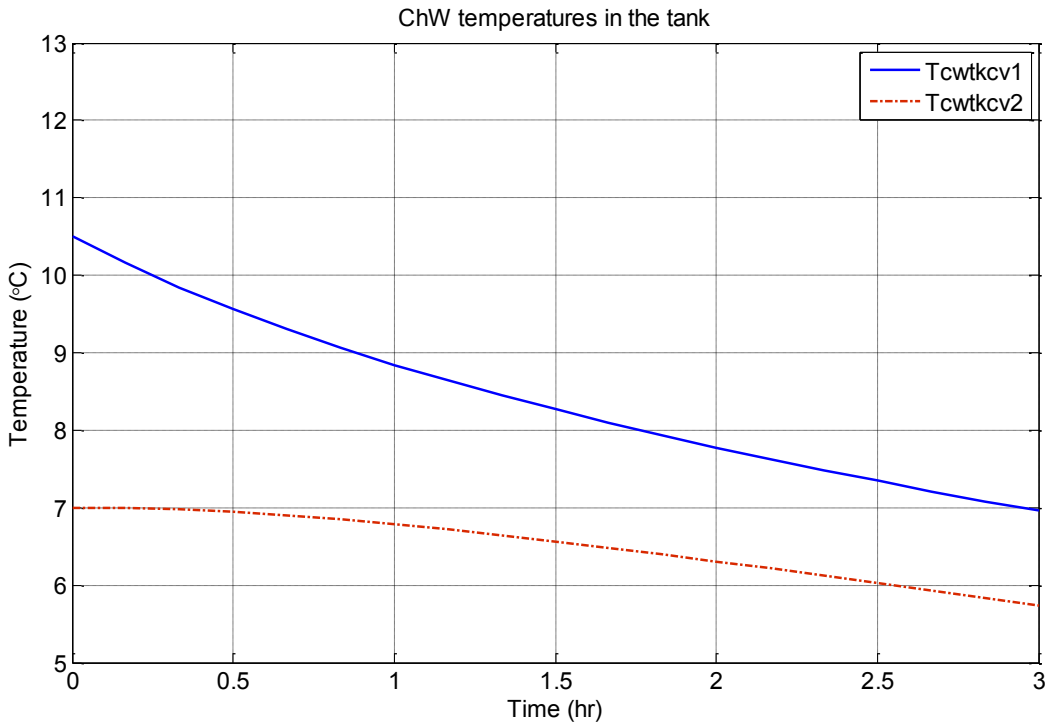

Figure 3.8.8 ChW temp. in the tank for the ChW system (with tank – charge cycle).

The supply air and ChW supply and return temperature responses are depicted in figure 3.8.6. As can be noted, the supply ChW temperature drops to 4 ºC and the supply air temperature remains high at 17.4 ºC due to low load condition acting on the zone. The COP of the chiller (Figure 3.8.7) during the charge cycle remained close to 4 during the simulation period.

Figure 3.8.8 presents the ChW temperatures in the tank. The water temperature in the tank decreased from 7 ºC to 5.8 ºC. The mass flow rate of the ChW to the tank was 12.1 kg/s.

OLT results for the ChW system with using the ChW tank – discharge cycle

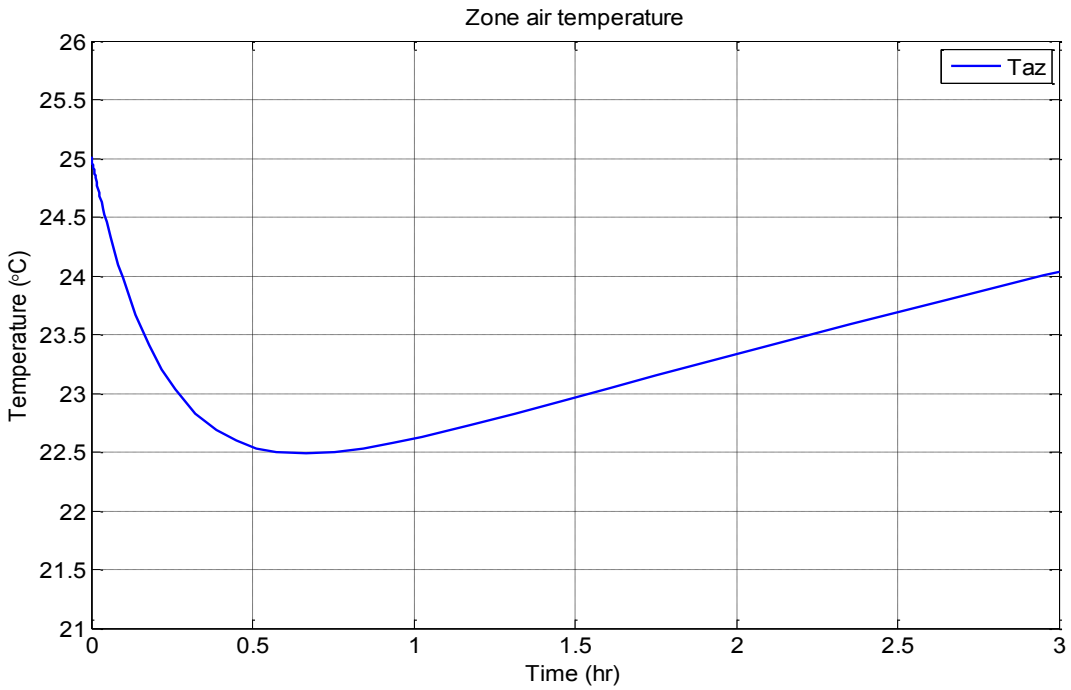

Figure 3.8.9 Zone air temperature results of the OLT (with tank – discharge cycle).

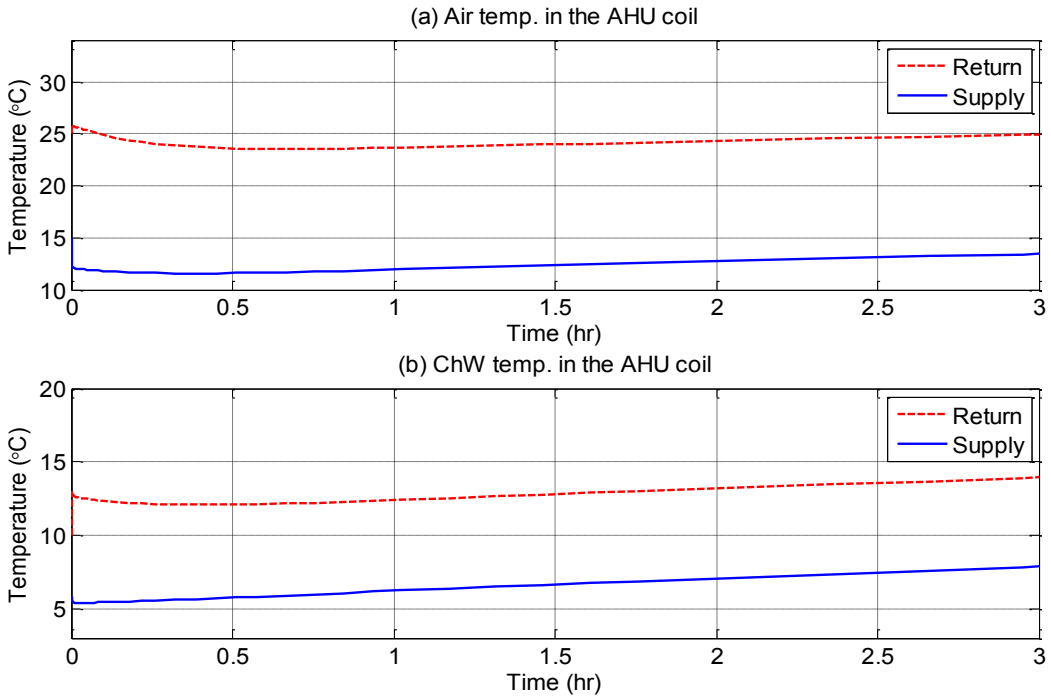

Figure 3.8.10 Coil model results for the ChW system (with tank – discharge cycle).

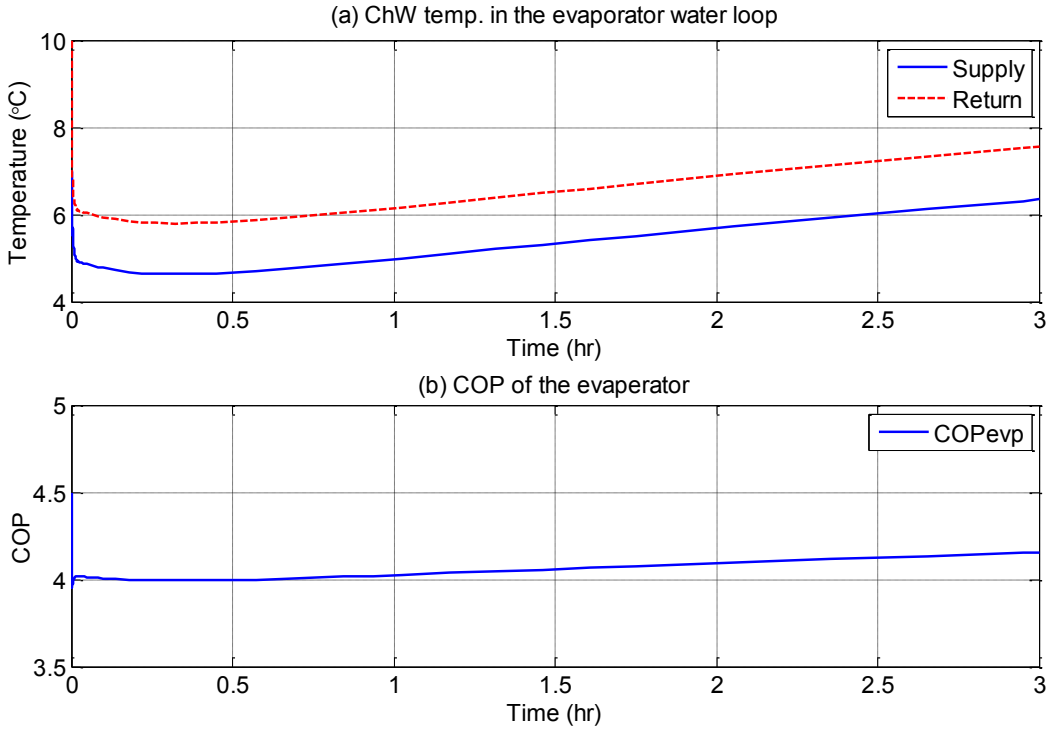

Figure 3.8.11 Chiller model results for the ChW system (with tank – discharge cycle).

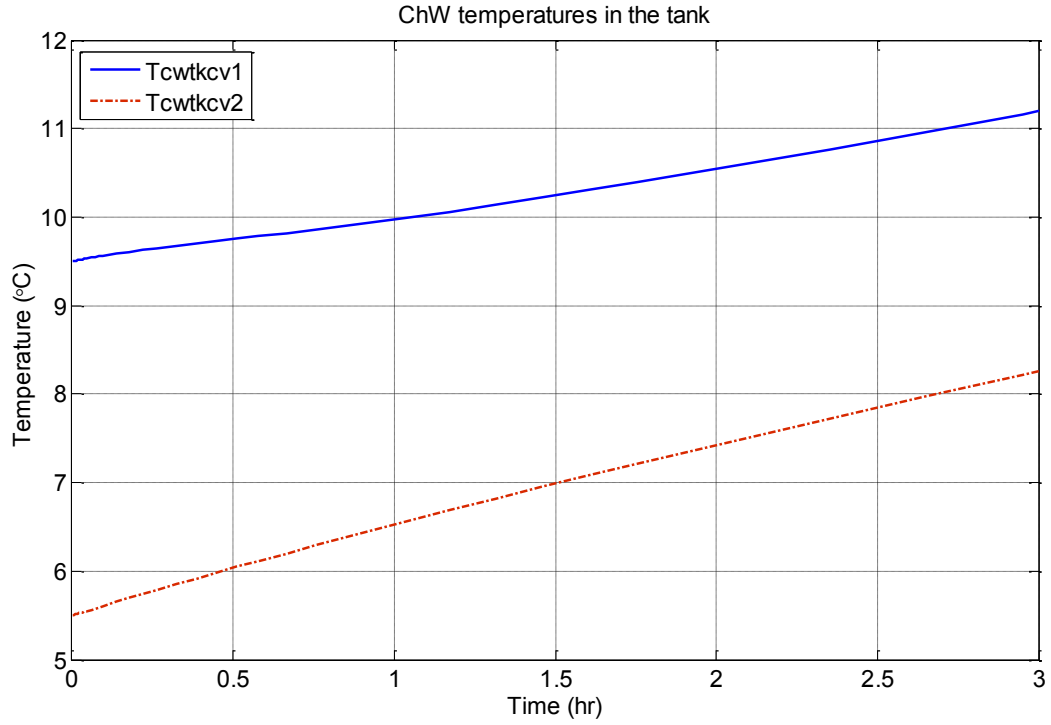

Figure 3.8.12 ChW temperatures in the tank for the ChW system (with tank – discharge cycle).

Sets of responses showing the OLT results during the discharge cycle are depicted in figures 3.8.9 through 3.8.12.

As shown in figure 3.8.9, the zone temperature initially drops to 22.5 ºC and gradually rises to 24 ºC as the chilled water temperature increases from 5.4 ºC to 7.9 ºC (Figure 3.8.10). Similarly the ChW temperature in the tank increased from 5.5 ºC to 8.3 ºC in about 3 hours.

It is noted that the addition of chilled water tank increased the steady state time to more than 5 hours. Also it was noted that the chilled water temperature increased at the rate of 1ºC/hour during the discharge cycle.

CHAPTER 4 GAIN-SCHEDULING CONTROL OF CHILLED WATER COOLING SYSTEM

4.1 Introduction

To maintain thermal comfort in the zone, good controllers for regulating the heating, ventilating and air conditioning (HVAC) system have to be designed. The conventional PI controller is one of the most popular controllers in HVAC control. It can provide temperature regulation fairly well in an efficient way. However the balance between the proportional gain and integral gain of a well-tuned PI controller would be difficult to maintain when the ChW cooling system encounters a sudden change in cooling loads. Therefore a gain scheduling (GS) controller is proposed and its performance will be compared with the conventional PI controller. In this section, there are two cases are presented: In the first case, the ChW cooling system experiences a change from low cooling load condition to higher load condition; and the second case deals with change from high to low load condition.

4.2 Control Loops in the ChW Cooling System

As discussed in chapter 3, the overall system consists of seven control loops interconnected as shown in figure 3.2.1. The functions of control loops were described in section 3.2.

4.3 Load Disturbances

The load disturbances acting on the ChW cooling system are the outdoor air temperature, the incident or transmitted solar radiation into the zone, and the heat gains due to occupants which include the lighting, sensible and latent heat gain due to human activity, and the operation of miscellaneous equipments. All the disturbances may occur simultaneously or in several combinations. In general, the ChW cooling system works under partial load conditions most of

the time. Therefore proper design and selection of the controller is important to improve the system performance.

Both conventional PI control and GS control strategies will be studied under two different cases:

Case 1: The ChW cooling system is simulated to undergo a change from low demand for cooling to higher demand for cooling. In the lower cooling load condition, the outdoor air temperature remained at 30 ºC which is 2 ºC lower than the higher demand case. The heat gain due to the solar radiation and the occupants were reduced to 60% of their peak values.

Case 2: The ChW cooling system experiences a change in load from higher cooling load to lower cooling load.

4.4 Performance of the Conventional Constant gain PI controller

The conventional PI controller diagram is shown in figure 4.4.1. This feedback control system consists of input, output, actuator, and sensor elements as shown in the block diagram.

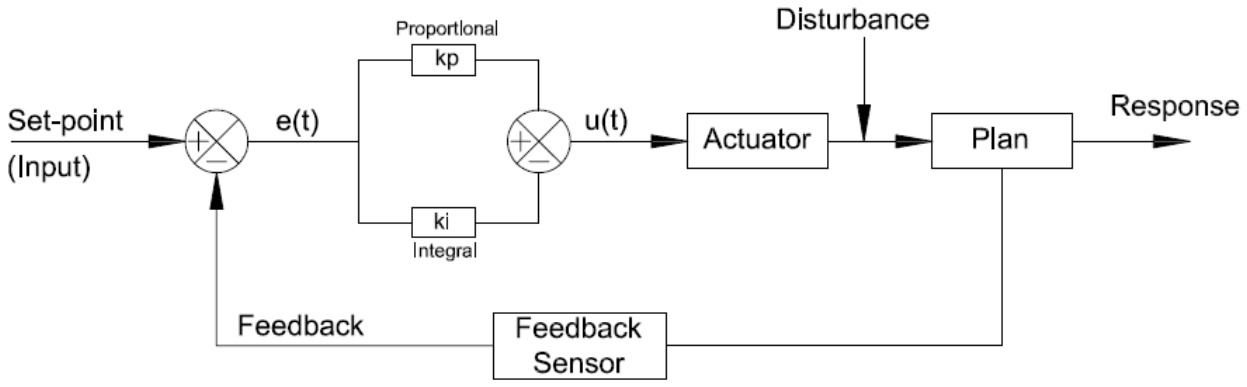

Figure 4.4.1 PI Controller block diagram.

The e(t) stands for the error between the feedback signal and the setpoint as function of time. The u(t) is the controller output signal generated by the control law based on Proportional and integral gains of the controller. The algorithm of the conventional PI controller could be represented by the following equation:

$$u(t) = K_p e(t) + K_i \int e(t)dt \qquad (4.4.1)$$

For the simulation, two different values of kp were chosen to establish an upper and lower bound. The purpose of doing so was to check the tuning ability of the controller. These values of the PI controller parameters are shown in table 4.4.1. The upper and lower bound of the kp values are shown in table 4.5.1.

Table 4.4.1 Parameters of the PI controllers in the ChW cooling system.

Controller #	k_p value	K_i value	Setpoint of lower demand case	Setpoint of higher demand case
1	0.56	0.05	32	32
2	0.56	0.05	5.0	5.0
4	0.56	0.05	6.0	6.0
5	0.56	0.05	18	13
6	0.56	0.1	28	23

Simulation results – PI control (case 1)

The performance of the conventional PI controller with lower kp values is shown in the following figures 4.4.1 – 4.4.4:

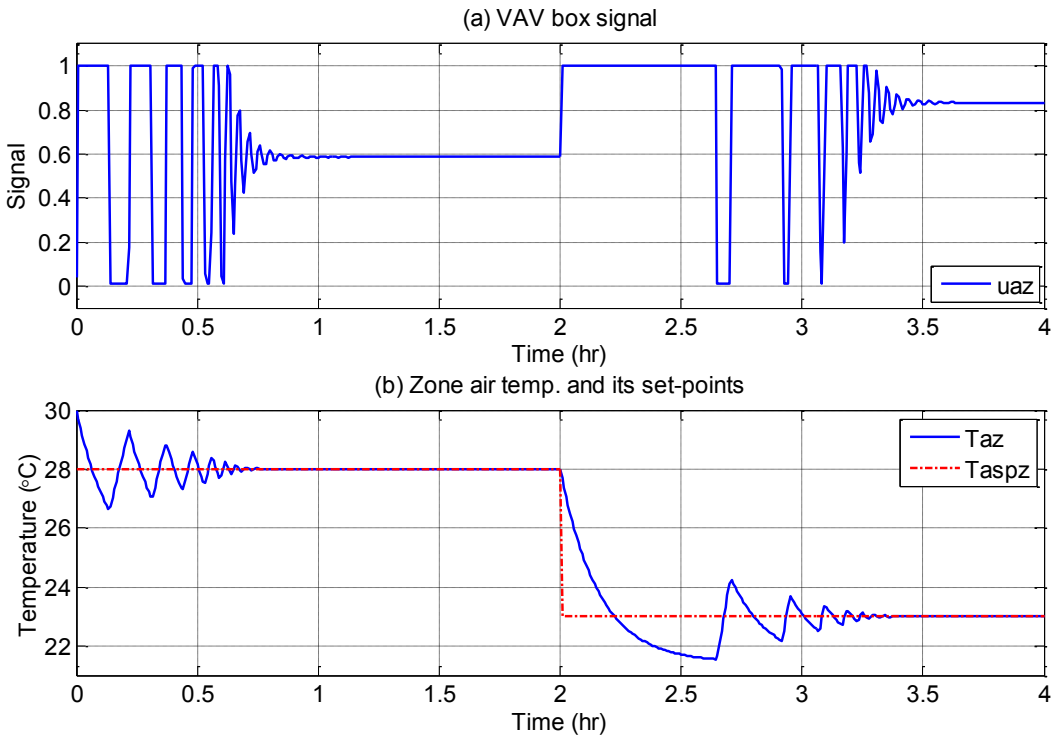

Figure 4.4.2 Simulation results of the PI controller for the VAV box in case 1.

Figure 4.4.2 shows the results for the zone control loop. Following the setpoint change from 28 ºC to 23 ºC, the VAV box signal fluctuating and settling in the first 45 minutes, In other words, it takes 1 hour for the zone air temperature to reach steady state condition when a 5 ºC setpoint change is imposed. The zone air temperature reaches up to 28.5 ºC in the first overshoot.

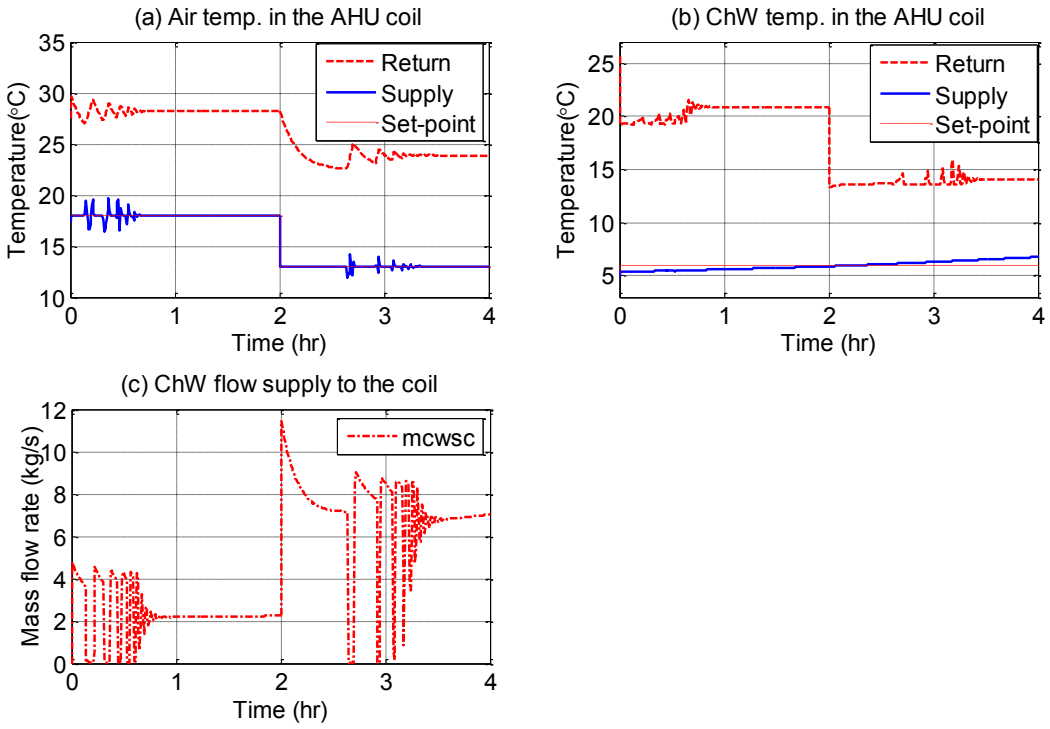

Figure 4.4.3 Simulation results of the PI controller for the cooling coil in case 1.

The supply air temperature fluctuates in the range of ±1.6 ºC from its setpoint at the beginning of the low cooling load condition; and lower range of ± 1.2 ºC during the higher load demand condition as shown in figure 4.4.3 (a). The supply ChW mass flow rate is less stable in high load demand condition. This can be noted by comparing with the amplitude of the fluctuation during low load demand condition as it shown in figure 4.4.3 (c).

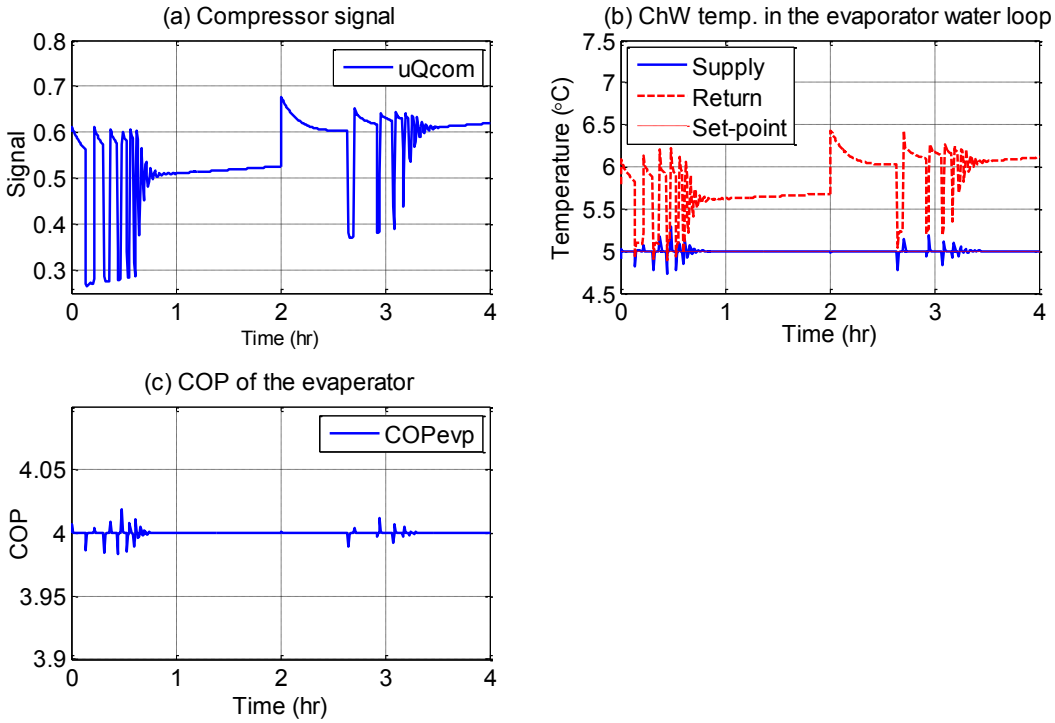

Figure 4.4.4 Simulation results of the PI controller for the chiller in case 1.

The compressor control signal shows the same trend as the VAV box signal but has smaller range of amplitude of the fluctuation because of the higher thermal capacity of the water loop. The COP of the chiller is stable around of 4 over the entire simulation period.

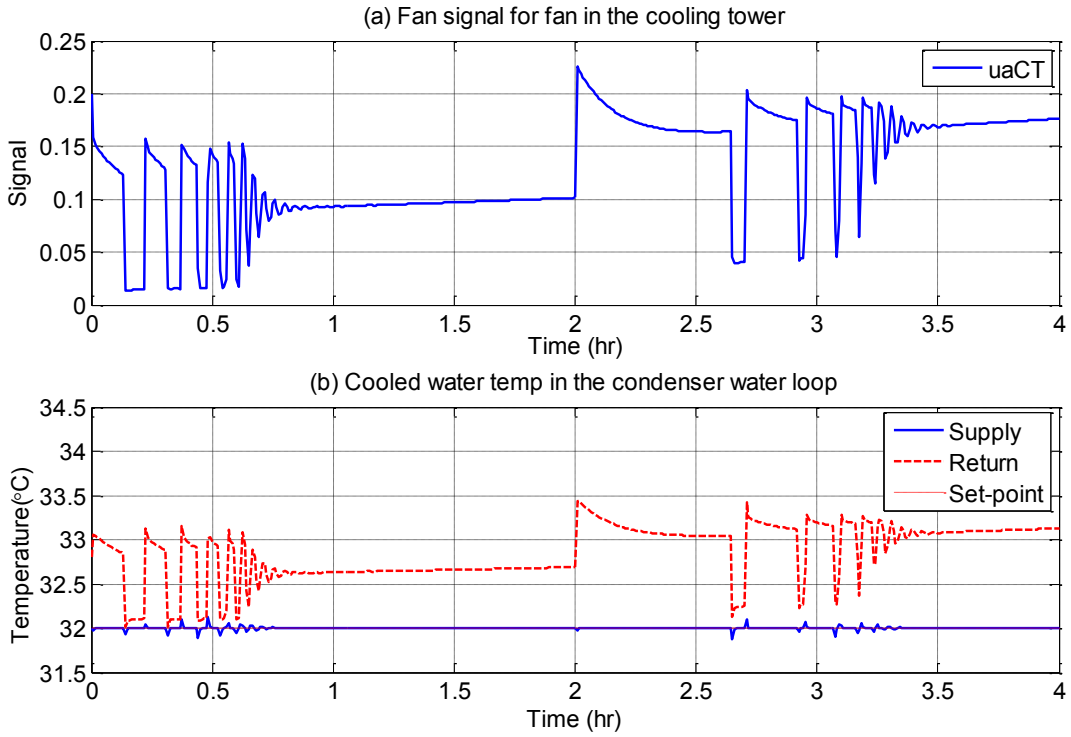

Figure 4.4.5 Simulation results of the PI controller for the cooling tower in case 1.

The cooling tower control loop exhibits similar trends as the compressor control loops. The cooled water temperature follows the same pattern as the ChW temperatures in the evaporator water loop.

Simulation results – PI control (case 2)

The performance of the conventional PI controller undergoing a change in load from higher to lower level (case 2) is depicted in figures 4.4.5 – 4.4.8:

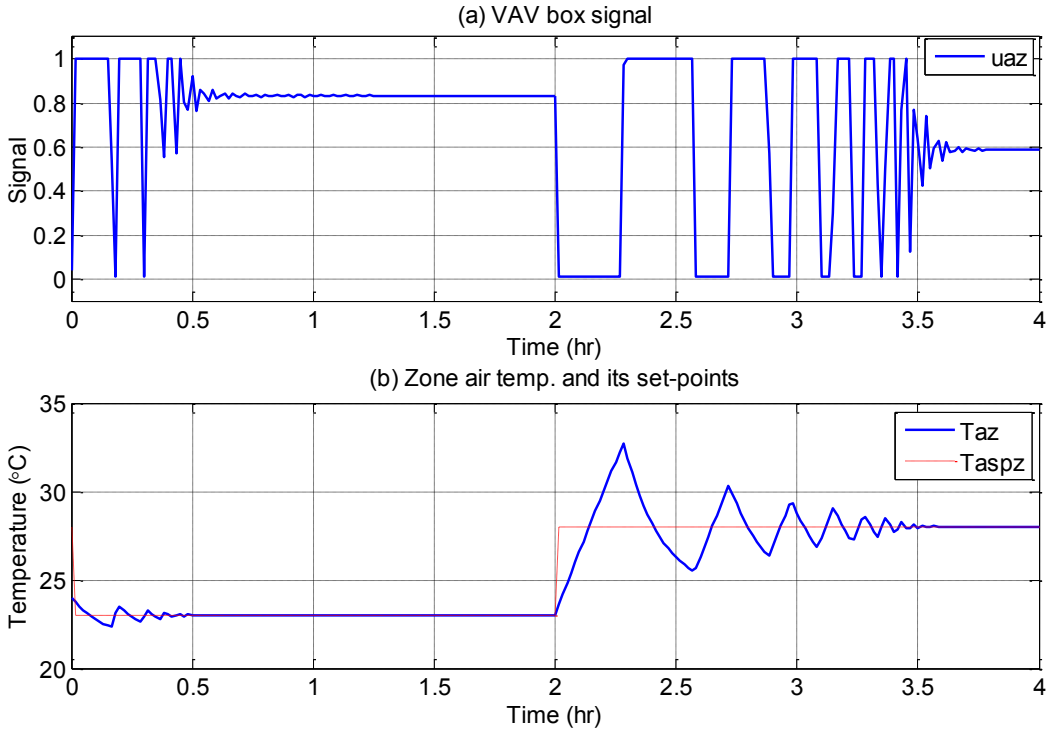

Figure 4.4.6 Simulation results of the PI controller for the VAV box in case 2.

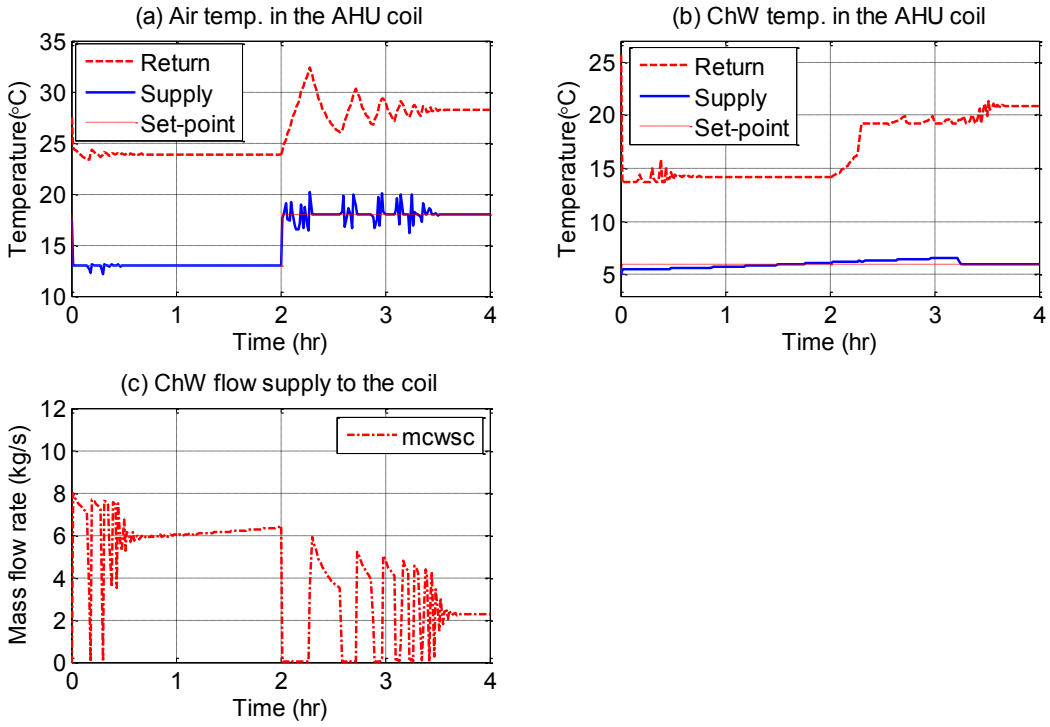

Figure 4.4.7 Simulation results of the PI controller for cooling coil in case 2.

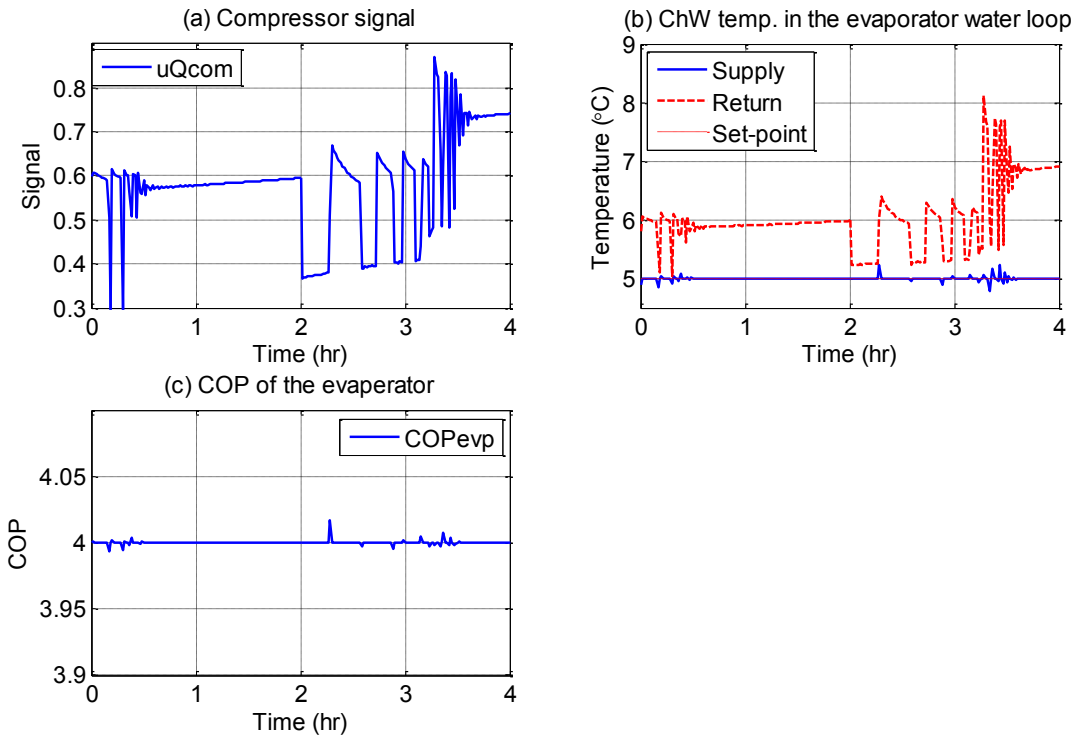

Figure 4.4.8 Simulation results of the PI controller for the chiller in case 2.

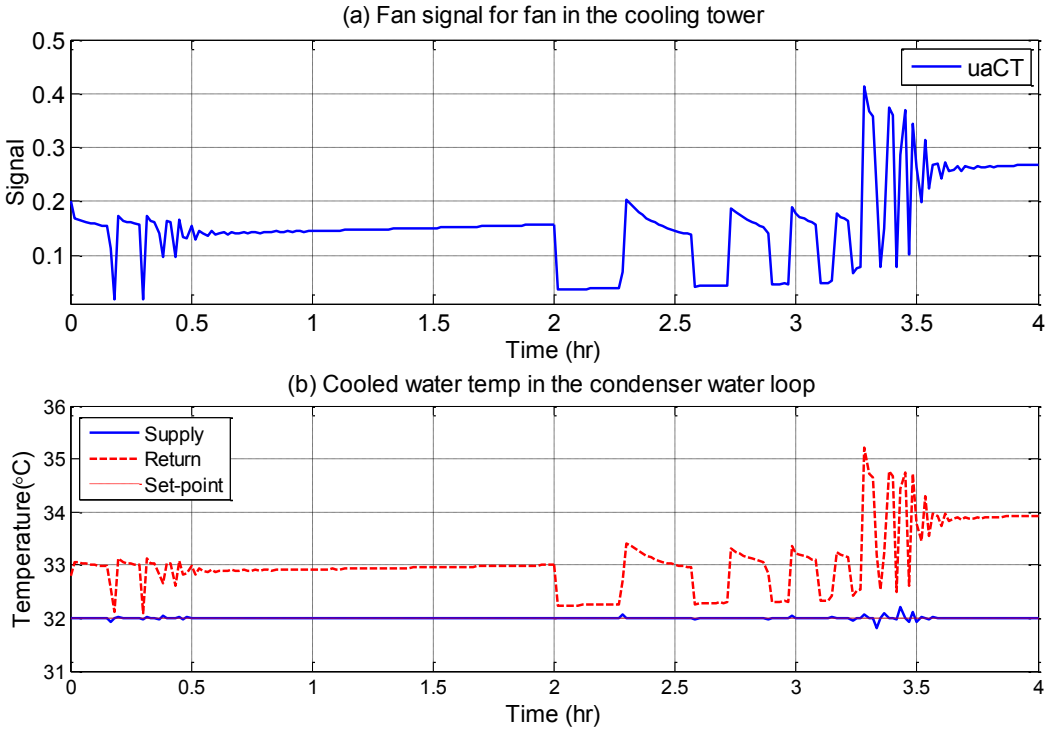

Figure 4.4.9 Simulation results of the PI controller for the cooling tower in case 2.

By comparing the results between case 1 and case 2 responses the following observations were noted. With the same controller gain, the responses in case 2 were more oscillatory compared to case 1. Furthermore the compressor and cooling tower fan control signals show rapid changes. This means the same set of controller gains are not suitable when the cooling load demand changes from higher to lower levels and vice versa. To deal with these issues, a Gain Scheduling control is proposed as discussed in the following section 4.5.

4.5 Gain Scheduling Control of the ChW Cooling System

The gain scheduling scheme has flexibility of adjusting controller gains unlike the constant gain PI controller. As shown in previous studies, constant gain PI controllers need frequent tuning when setpoint or large disturbances occur. Therefore a GS PI controller scheme is introduced in this section for the temperature control in the ChW cooling system.

Controller structure

Several GS control structures are reported as mentioned in Chapter 2. The basic concept is to adjust the proportional gain and integer gain as a function of error. Following the method proposed by Sedaghati (Sedaghati, 2006), the proportional gain could be expressed mathematically as follows:

$$k_p(t) = k_{p(\max)} - (k_{p(\max)} - k_{p(\min)})e^{-(k_1 e(t))} \qquad (4.5.1)$$

$k_{p(max)}$ and $k_{p(min)}$ are the maximum and minimum values of proportional gain, respectively. The k_1 is a constant that is predetermined when designing the controller. Therefore when the e(t) is

increasing, the exponential term approaches to 0 which leads the $k_p(t)$ equals to k_{pmax}, and vice versa to k_{pmin}. The integral gain of the GS controller was calculated as below:

$$k_i(t) = k_{i(\max)}(1 - \tanh(k_2|e(t)|)) \quad (4.5.2)$$

The $ki_{(max)}$ is the maximum integer gain of the controller. The following table shows the gains of the GS controller used in the simulation runs:

Table 4.5.1 kp and ki values of the GS controllers.

Controller #	$k_{p(max)}$	$k_{p(min)}$	$k_{i(max)}$	k_1	k_2
2	4.56	0.56	0.001	10	2.0
5	2.56	0.56	0.001	10	2.0
6	5.56	0.56	0.001	10	2.0

The GS control was implemented on the same control loops described in the previous section under similar load conditions. This facilitated comparison of results from the PI and GS control schemes. The GS control responses are shown in figure 4.5.1 – 4.5.7 (case 1) and figure 4.5.8 – 4.5.14 (case 2).

Simulation results for the GS controllers (case 1- Low load demand to high load demand)

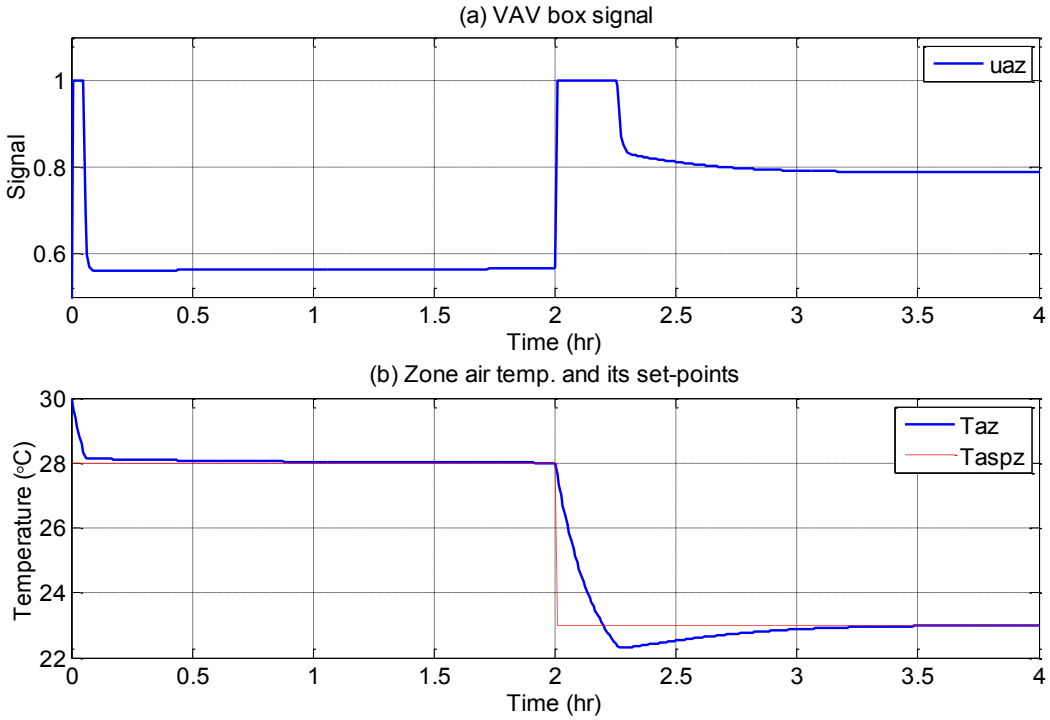

Figure 4.5.1 Simulation results of the GS controller for the VAV box (case 1).

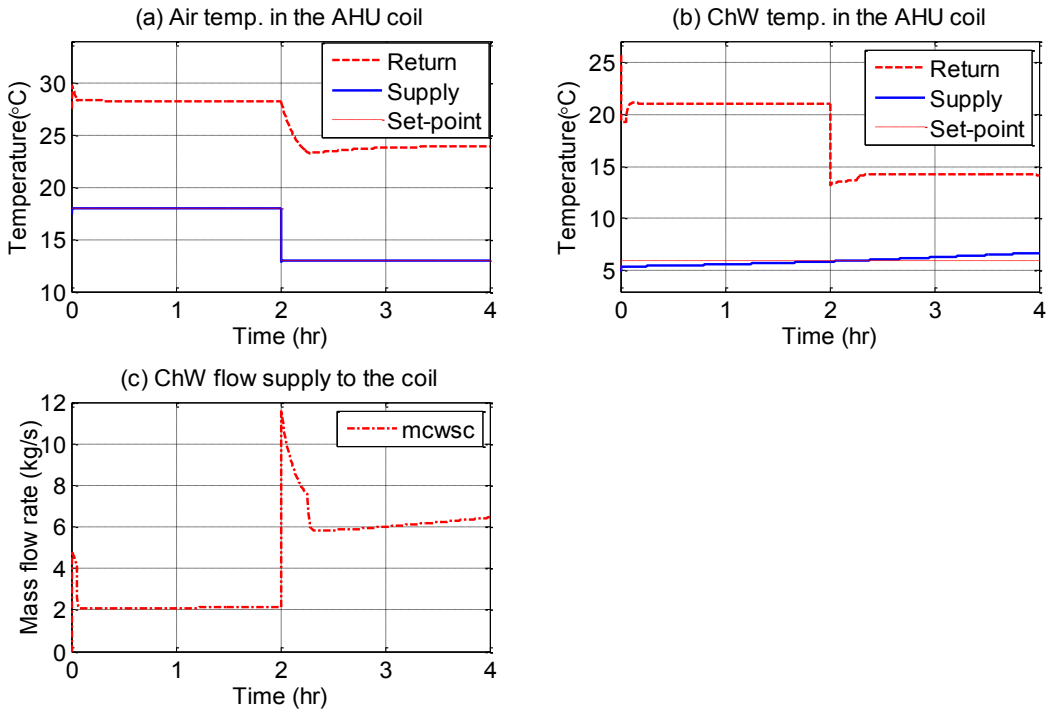

Figure 4.5.2 Simulation results of the GS controller for the cooling coil (case 1).

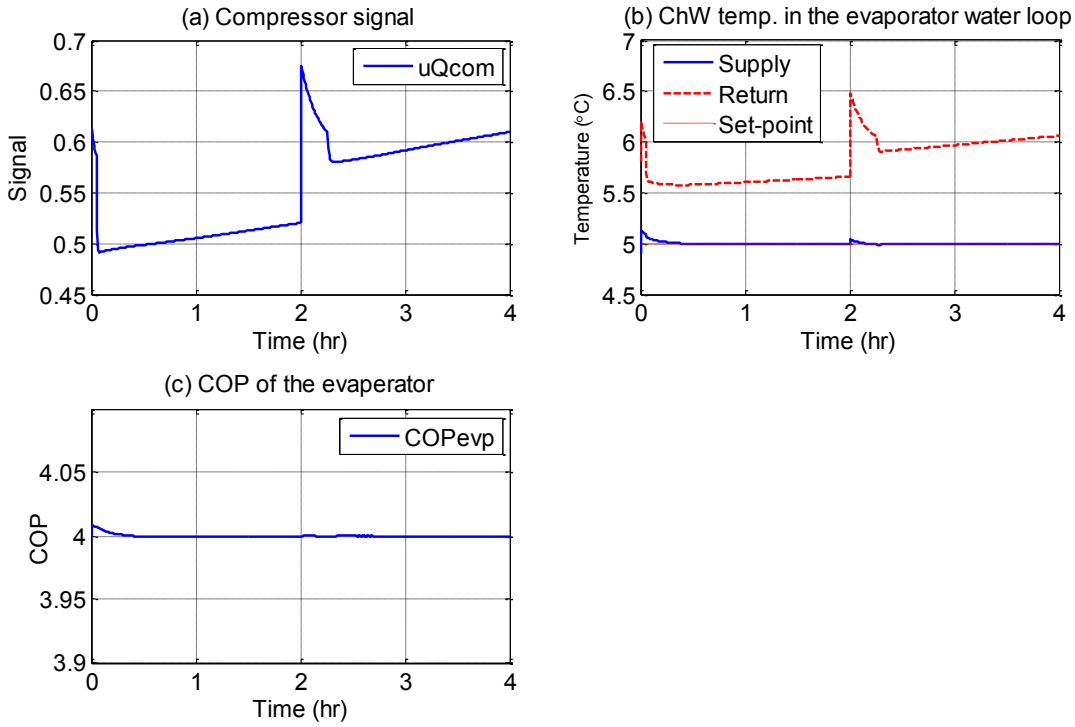

Figure 4.5.3 Simulation results of the GS controller for the chiller (case 1).

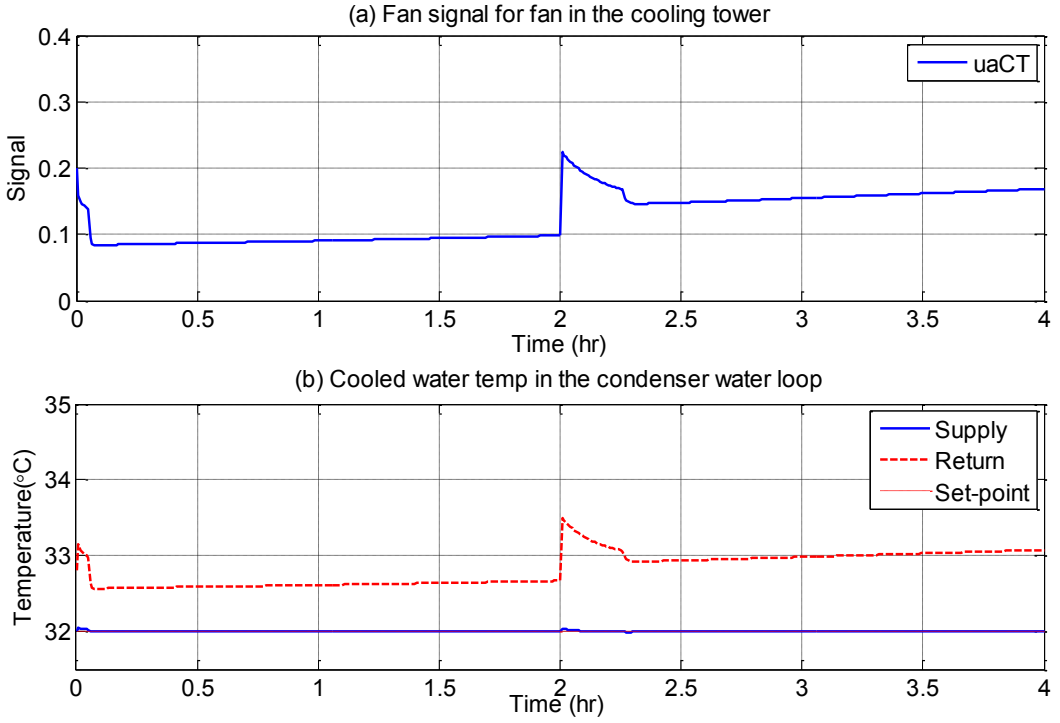

Figure 4.5.4 Simulation results of the GS controller for the cooling tower (case 1).

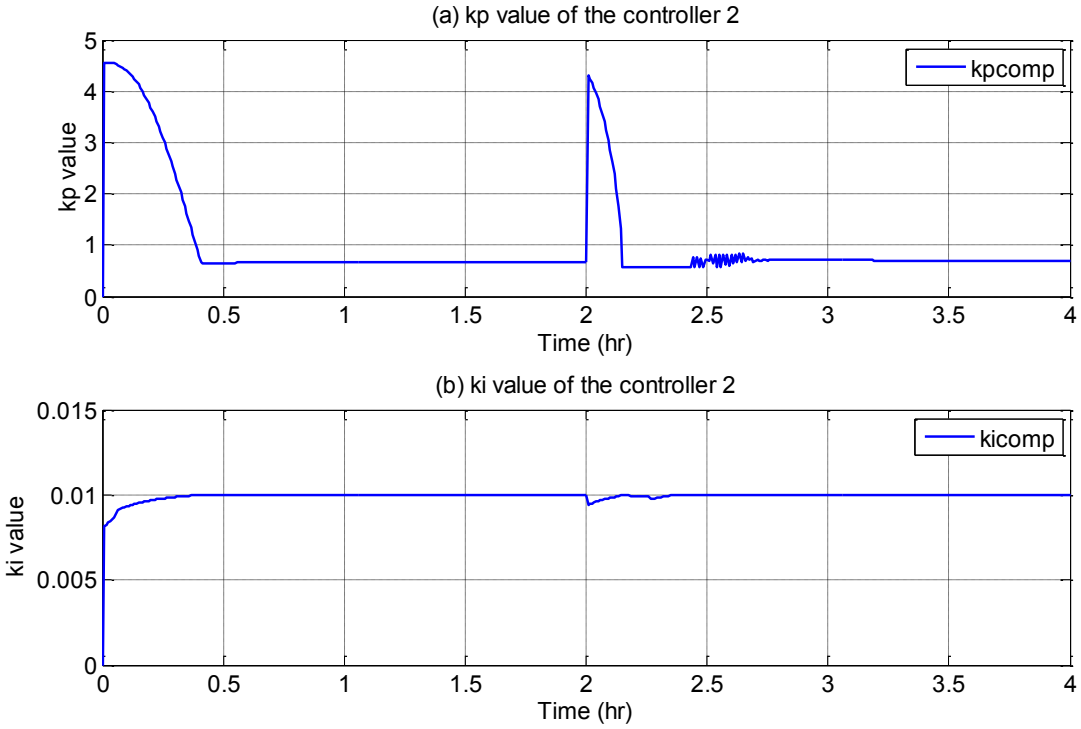

Figure 4.5.5 The k_p and k_i values of the controller 2 for the compressor (case 1).

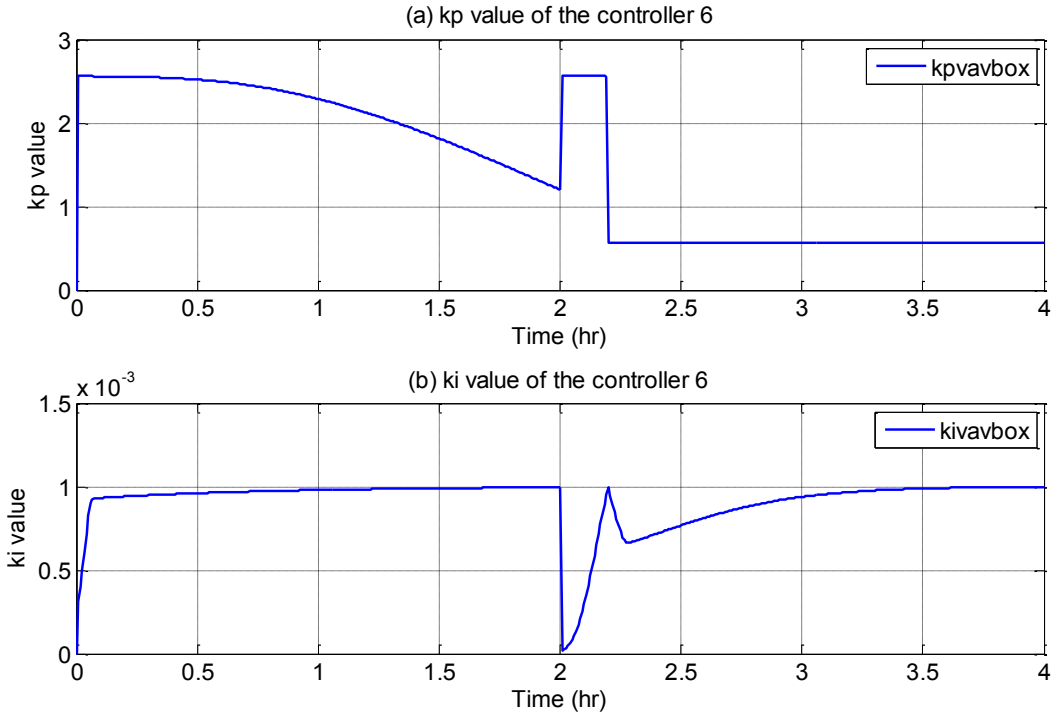

Figure4.5.6 The k_p and k_i values of the controller 6 for the VAV box (case 1).

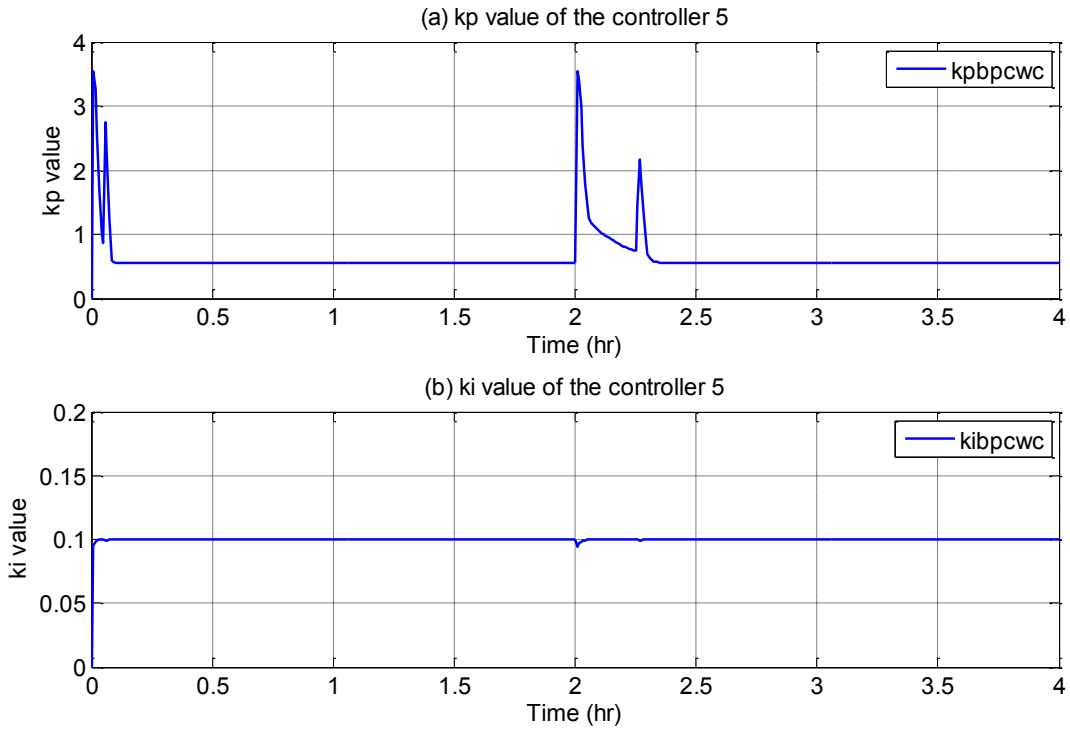

Figure 4.5.7 The k_p and k_i values of the controller 5 for the cooling coil (case 1).

By comparing the responses from PI control and GS control, it can be noted that the GS control responses are much smoother and control signals are lot more stable to give good setpoint tracking performance. This observation is applied to the zone control loop, cooling coil, compressor and cooling tower control loops. Also to note is the fact that the controller gains are continuously adjusted as shown in figure 4.5.5 – 4.5.7 to give smooth and stable responses.

Likewise, when the cooling load changes from high to low load, the GS control provides smooth and stable temperature control responses (figure 4.5.8 – 4.5.11) as compared to the corresponding responses from the PI control (figure 4.4.6 – 4.4.8).

Simulation results for the GS controllers (case 2 – high load demand to lower load demand)

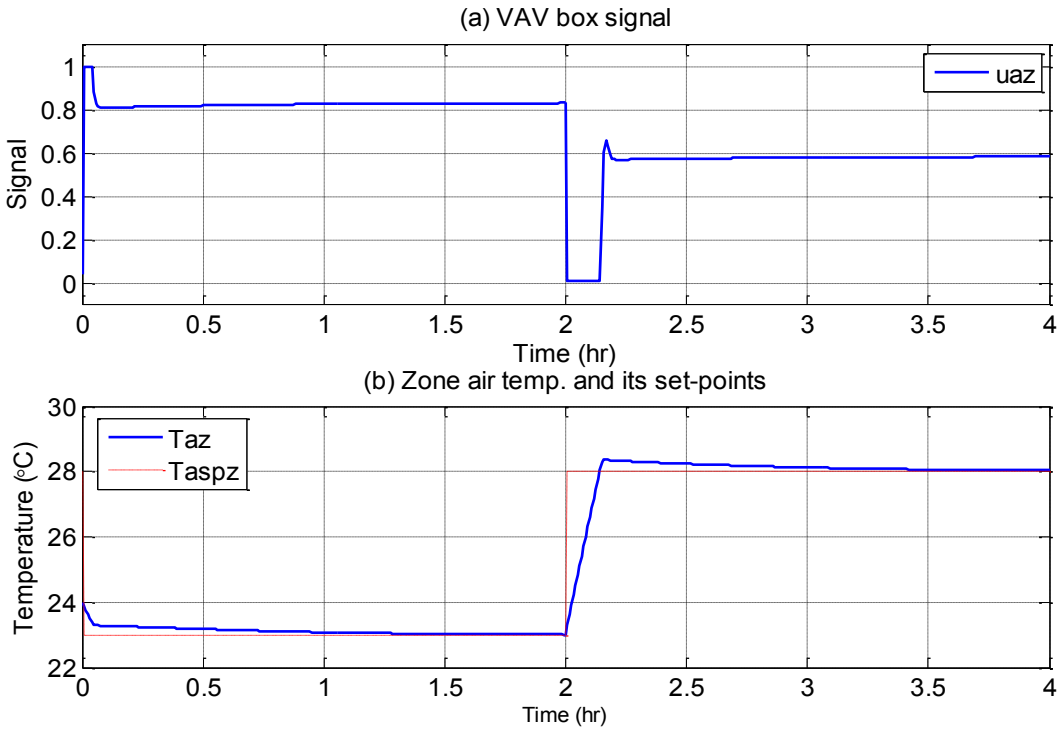

Figure 4.5.8 Simulation results of the GS controller for the VAV box (case 2).

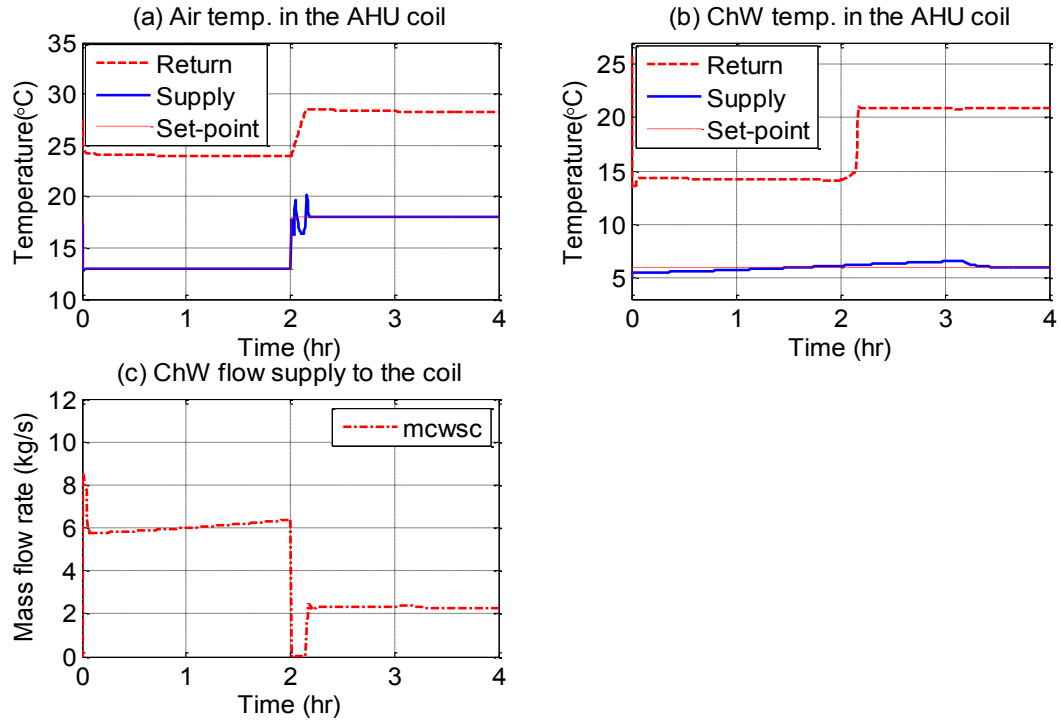

Figure 4.5.9 Simulation results of the GS controller for the cooling coil (case 2).

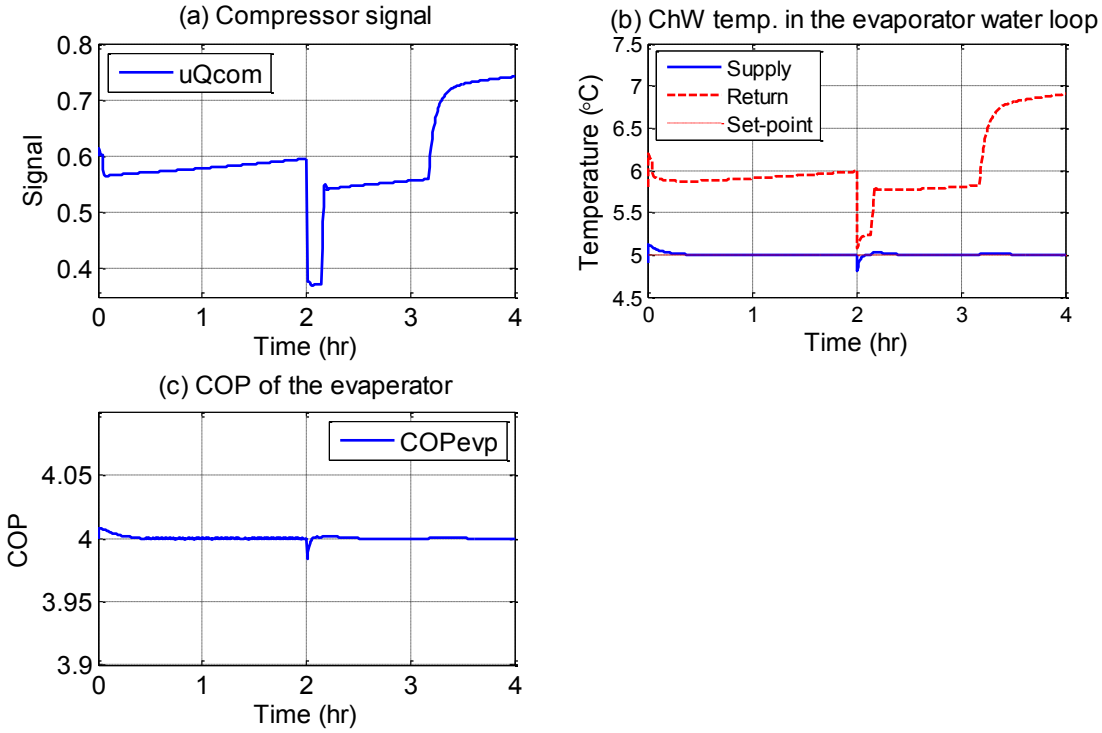

Figure 4.5.10 Simulation results of the GS controller for the chiller (case 2).

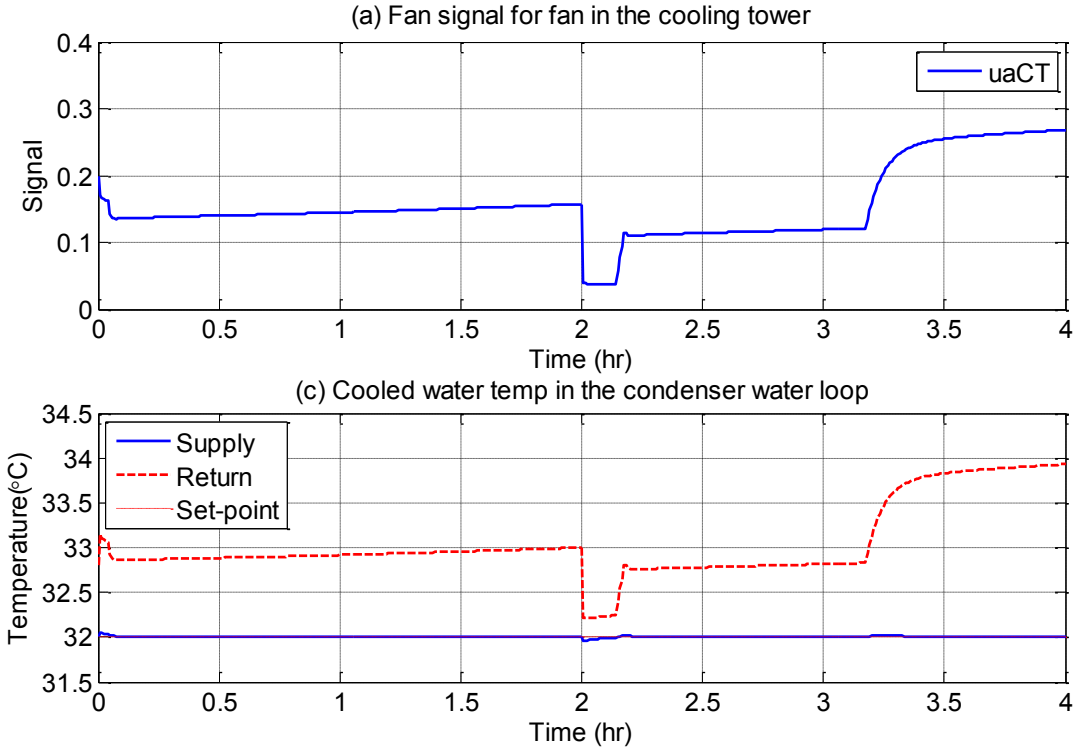

Figure 4.5.11 Simulation results of the GS controller for the cooling tower (case 2).

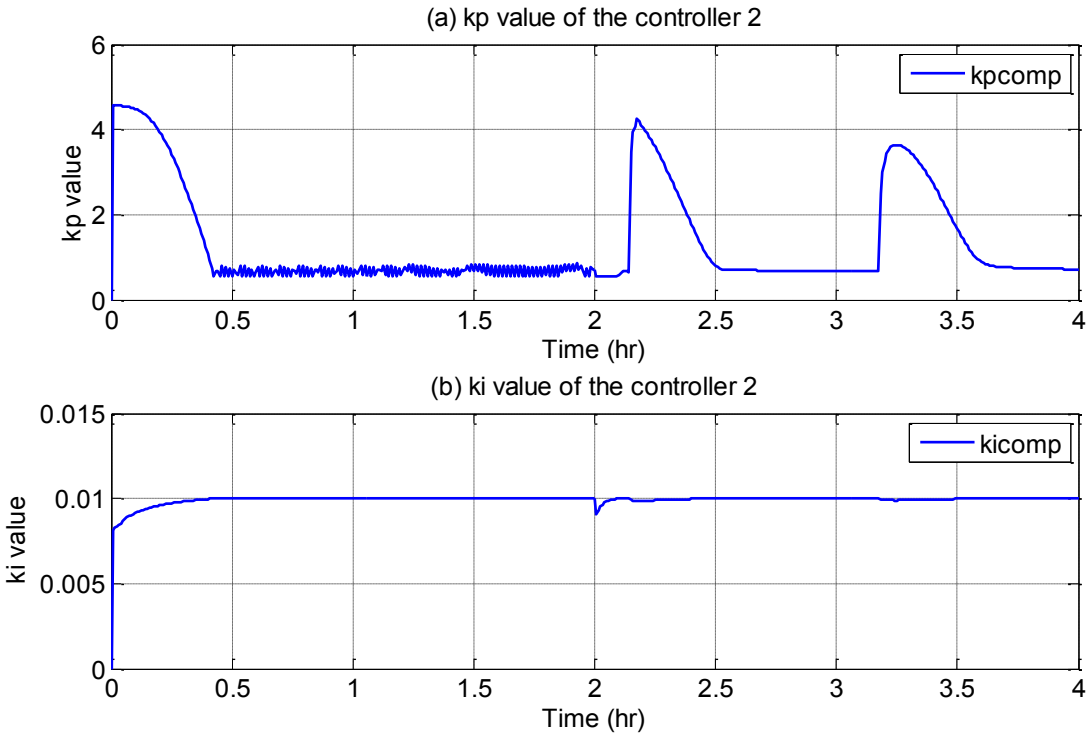

Figure 4.5.12 The k_p and k_i values of the controller 2 for the compressor (case 2).

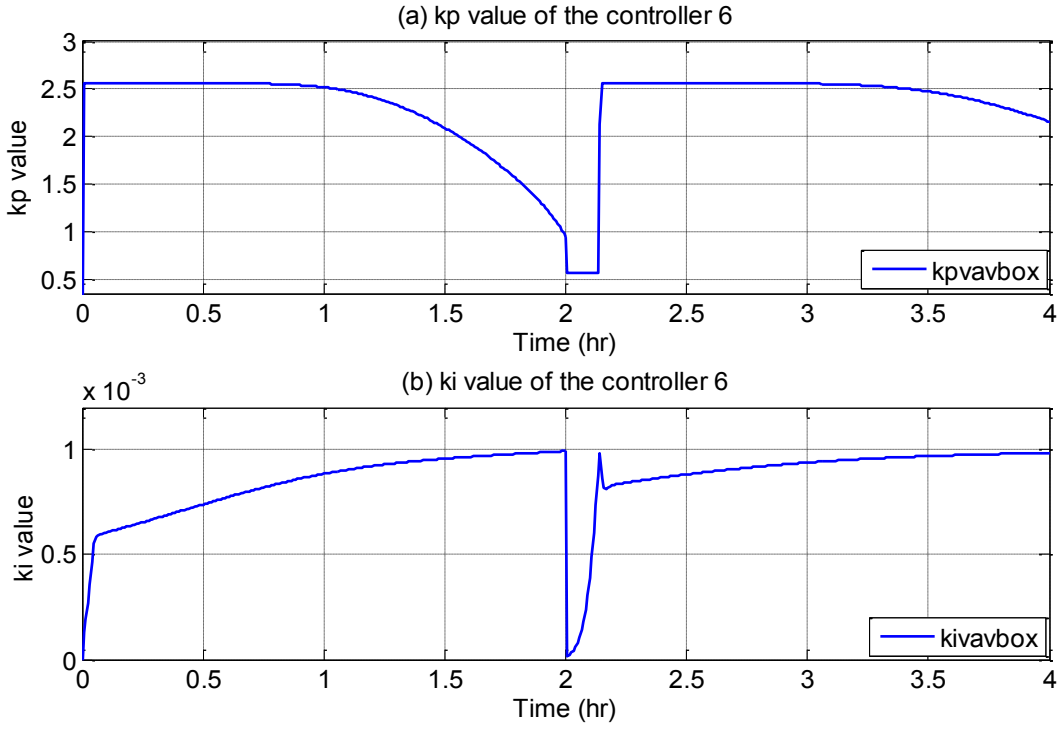

Figure 4.5.13 The k_p and k_i values of the controller 6 for the VAV box (case 2).

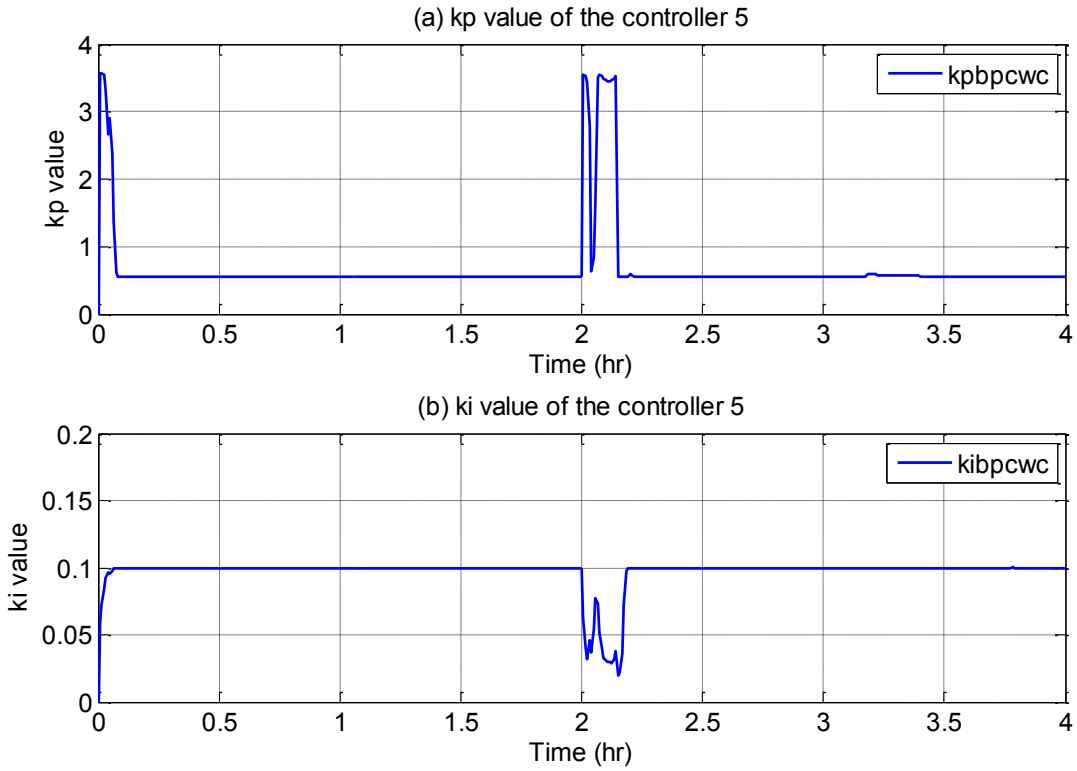

Figure 4.5.14 The k_p and k_i values of the controller 5 for the coil (case 2).

4.6 Typical day simulation results from the conventional PI control and GS control

In this section, the performance of the conventional PI controller and the GS controller are compared by implementing both of the controllers on the ChW cooling system. A typical day operation of the system under design day and partial load (50% of design day load) conditions was simulated. An important difference in the simulation results in this section is that the chilled water cooling system would go through both the charge and discharge cycle of the ChW tank. Therefore, the disturbances in this case will be more severe for the controllers to achieve good control performance.

Weather conditions

The outdoor air temperature for the design day condition was chosen as the hottest day in Montreal in July, 2012. The outdoor air temperatures and relative humidity (RH) ratios are taken from the weather forecast website (Network, Montreal). The temperature and relative humidity profiles are shown below (Figure 4.6.1).

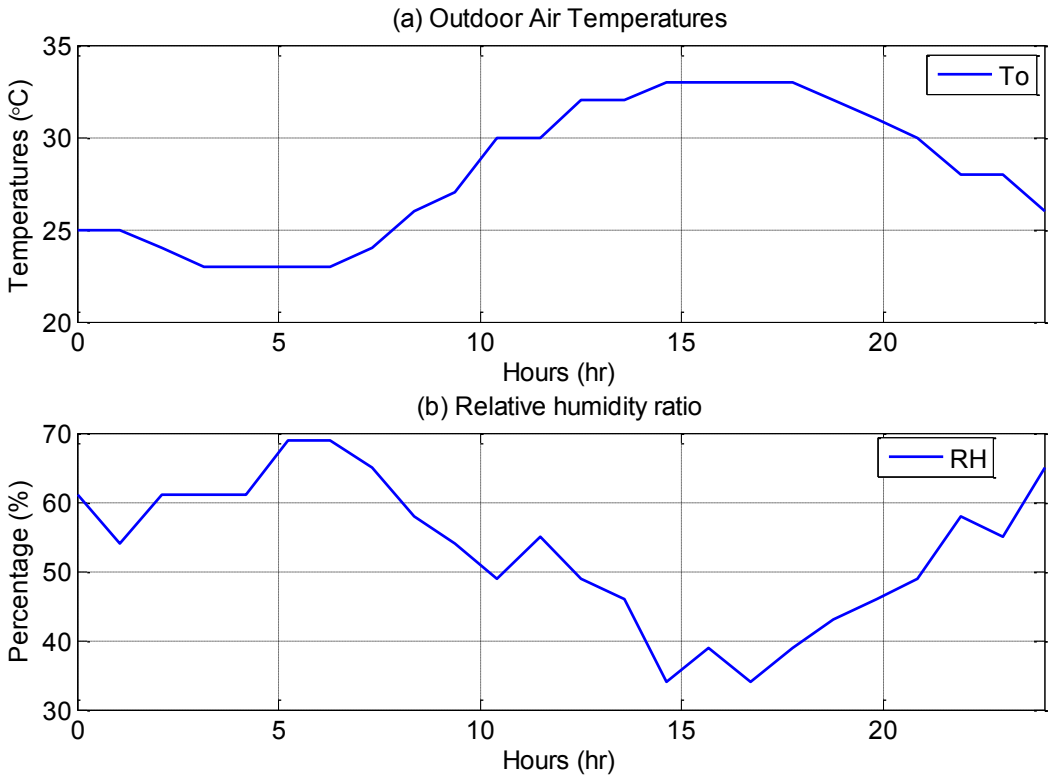

Figure 4.6.1 Weather conditions of the design day for the cooling system.

Solar radiation

The solar radiation is calculated by using the Hottel model (Antienitis, 2002). The solar radiation beam hitting on the facade is calculated and the transmitted solar radiation is also calculated based on the window area of the building and the shading factor of the building. Figure 4.6.2

shows the solar radiation profile. G represents the intensity of the solar beam and subscripts – s, e, n, w, r stand for the South, East, North, West walls and roof, respectively.

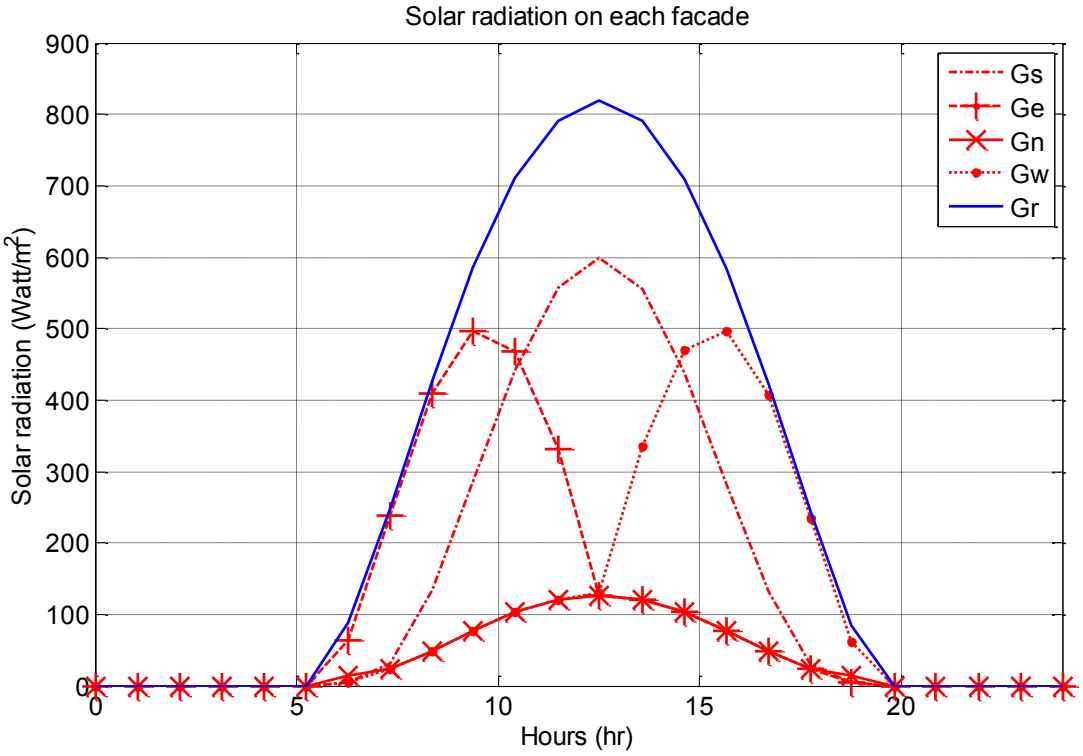

Figure 4.6.2 Solar radiation hitting on the building facade.

Controller parameters

The parameters of the PI controller are the same as those given in table 4.4.1; and the parameters of the GS controllers are also kept as the one shown in table 4.5.1.

Simulation results for the conventional PI controller (Design day load - PLR 100)

The simulation results of the overall system with conventional PI control are shown in the figures 4.6.3 – 4.6.6.

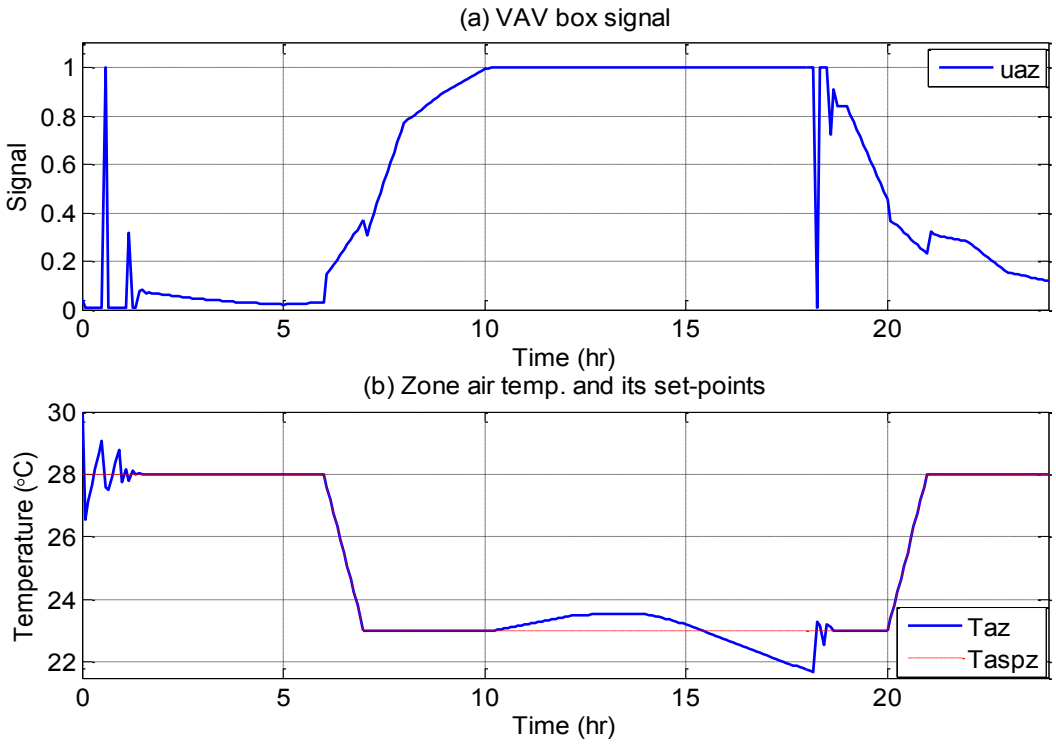

Figure 4.6.3 Simulation results of using PI controller for the VAV box (PLR100).

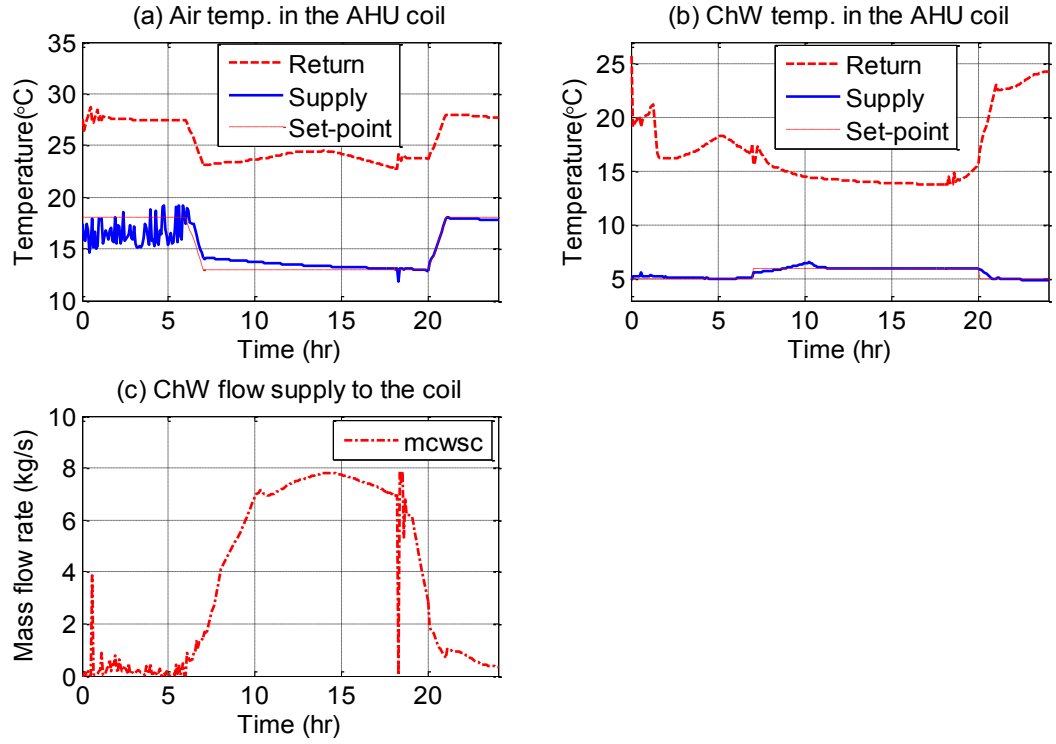

Figure 4.6.4 results of using PI controller for the cooling coil (PLR100).

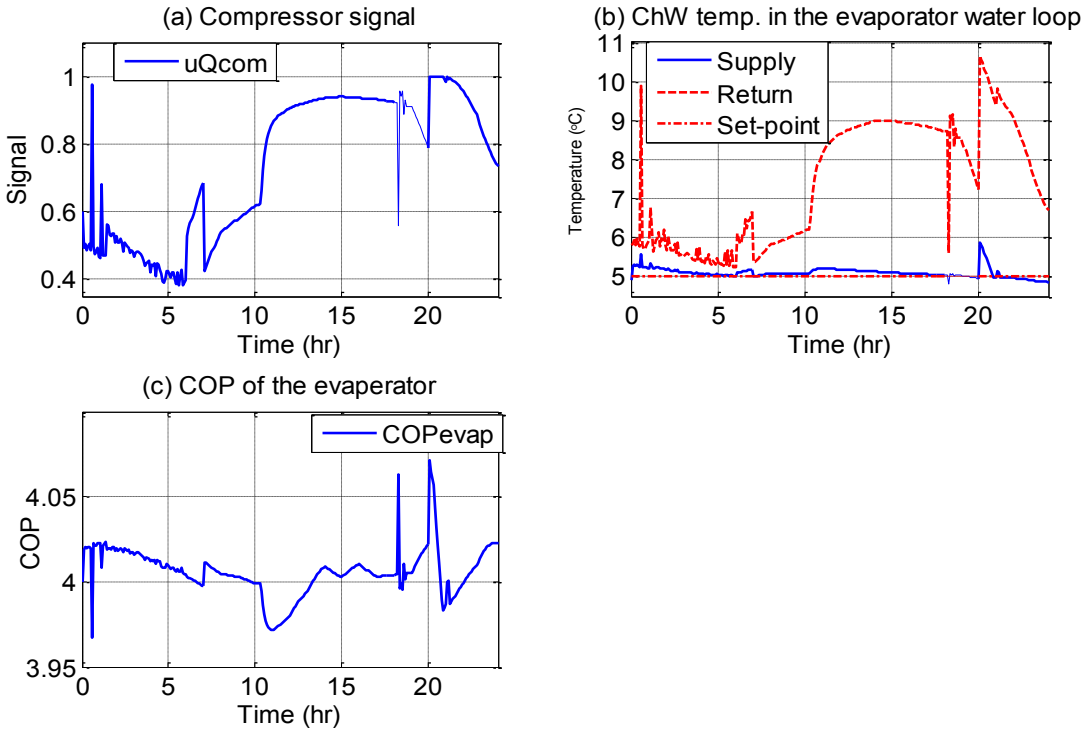

Figure 4.6.5 results of using PI controller for the chiller (PLR100).

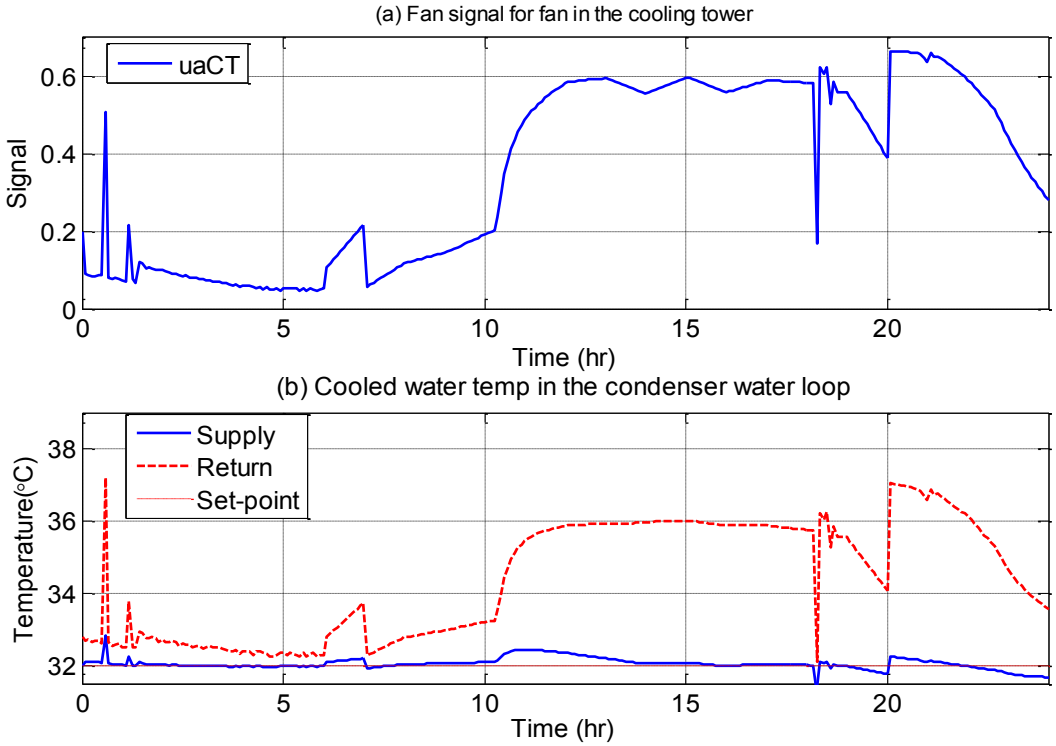

Figure 4.6.6 results of using PI controller for the cooling tower (PLR100).

Figure 4.6.3 shows the evolution of control input and zone temperature over the entire day. The zone air temperature oscillated at the beginning of the first one and half hours and undergoes overshoot during the peak load period due to constant controller gains. The VAV box signal also does not go to zero when the zone air temperature reaches below its setpoint of 23 ºC. This is due to thermal lag effect and inability of the constant gain controller to rapidly adjust to load changes.

Figure 4.6.4 shows the results of the cooling coil loop. The supply air temperature to the zone is not stable and fluctuated rapidly and reached way below the setpoint of 18 ºC; and it does not reach to its setpoint of 23 ºC until 17:00 hours during the occupancy period.

Figure 4.6.5 represents the chiller control loop results. The compressor signal varies in the range of 0.4 and 0.94. It is reaches up to 1 at the beginning of the charge cycle of the tank. The supply ChW temperature is controlled well at its setpoint of 5 ºC in both the charge and discharge cycle of the tank. However the return ChW temperature fluctuates in the beginning of the day. The COP of the chiller remained near 4 throughout the day.

Simulation results for the GS controller (Design day load – PLR 100)

The typical day simulation results from the GS control are depicted in figure 4.6.7 – 4.6.13. By comparing these responses with the corresponding responses from the PI control, it can be stated that GS control significantly improved setpoint tracking performance, overshoot is kept at minimum levels, and control input signals remained smooth throughout the day. The evolutions of controller gains are depicted in figure 4.6.11 – 4.6.13. It can be seen that both kp and ki gains are continuously changed in responses to changes in load acting on the system.

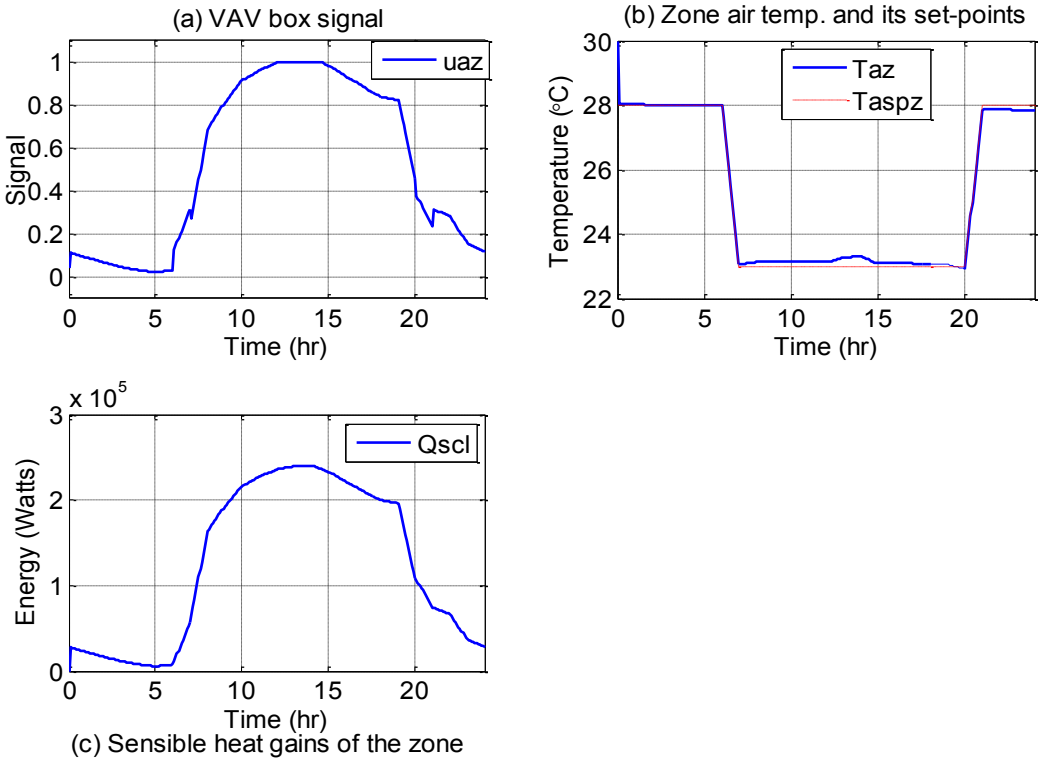

Figure 4.6.7 Simulation results of using the GS controller for the VAV box (PLR 100).

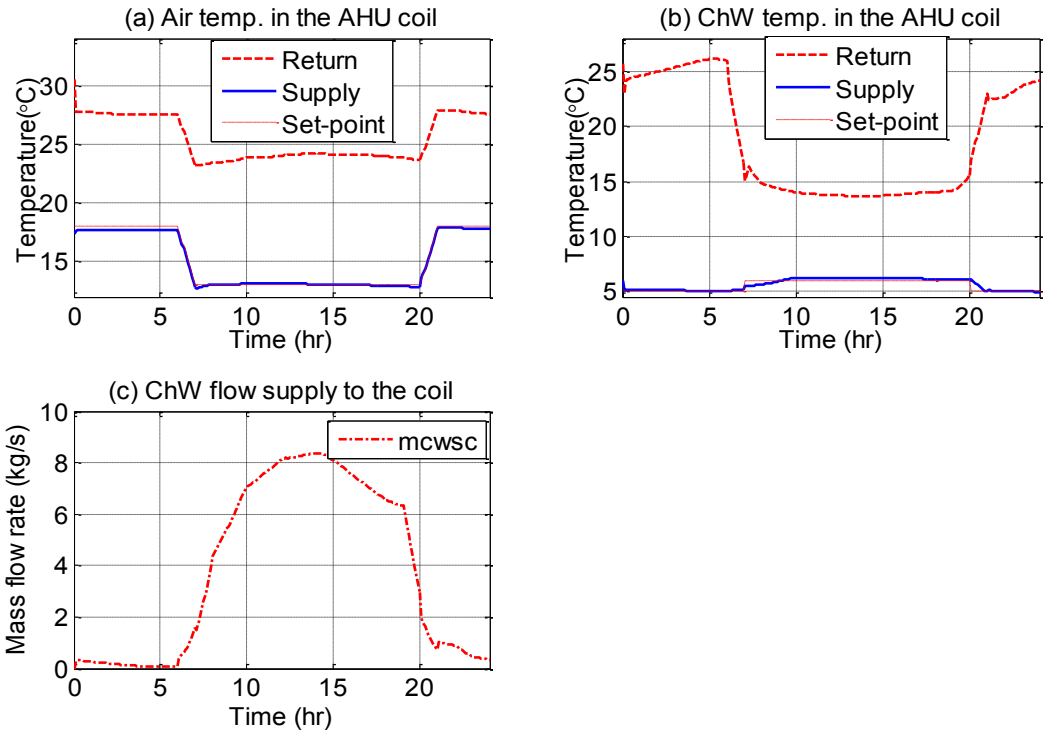

Figure 4.6.8 Simulation results of using the GS controller for the cooling coil (PLR 100).

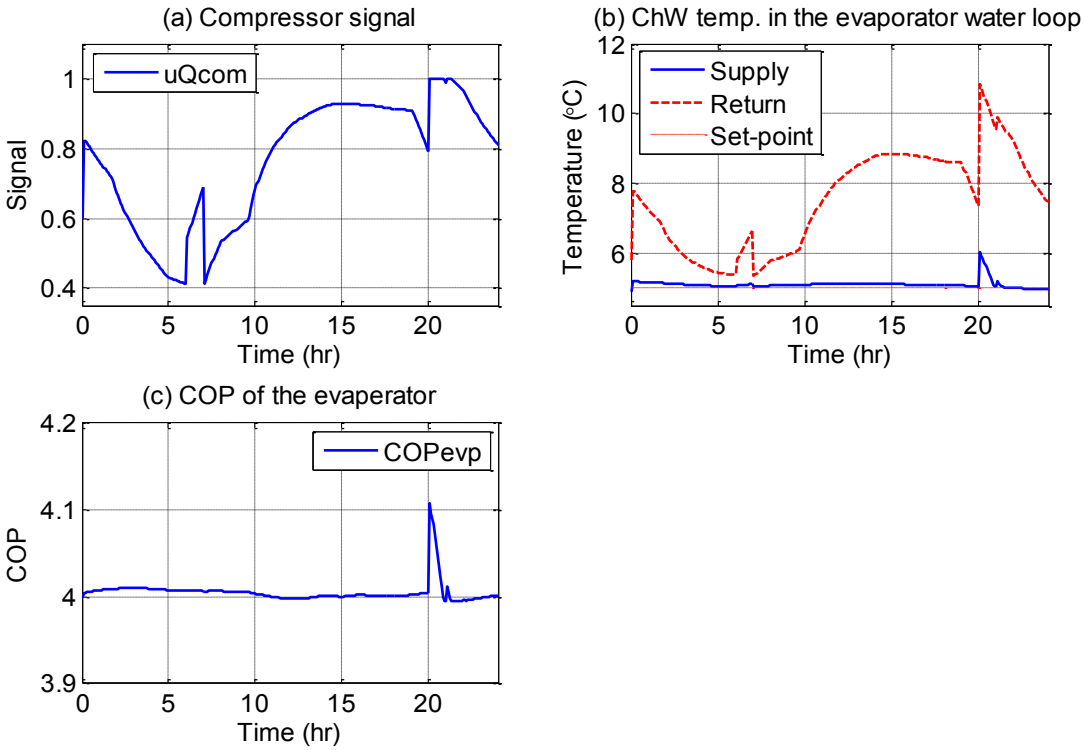

Figure 4.6.9 Simulation results of using the GS controller for the chiller (PLR 100).

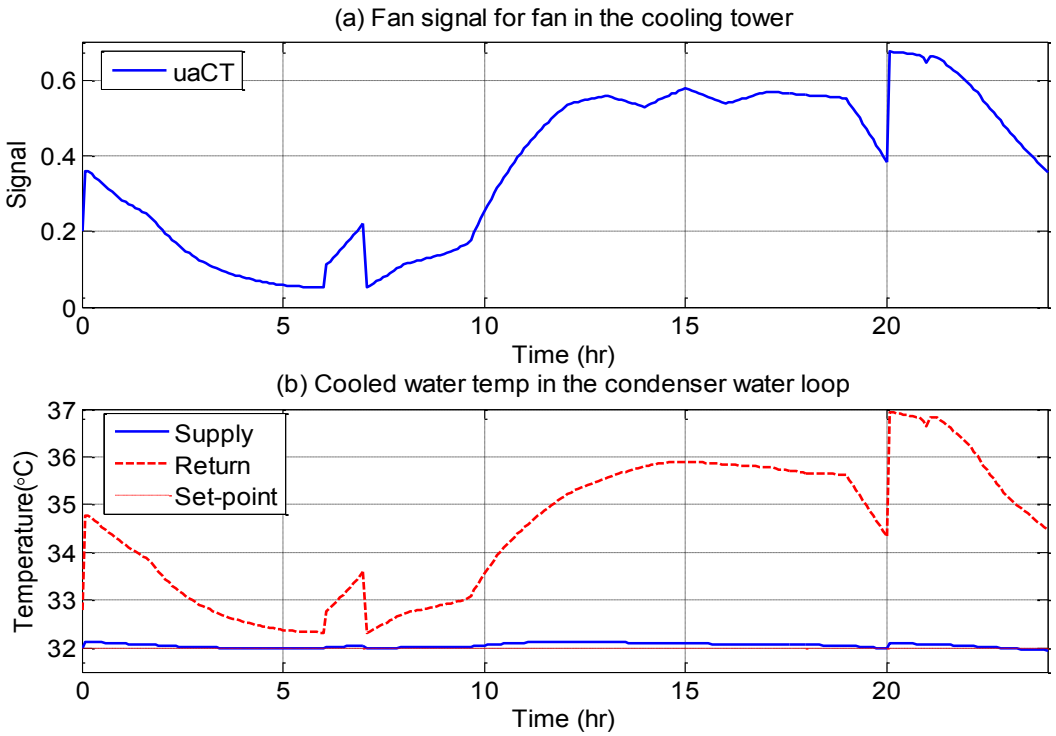

Figure 4.6.10 Simulation results of using the GS controller for the CT (PLR 100).

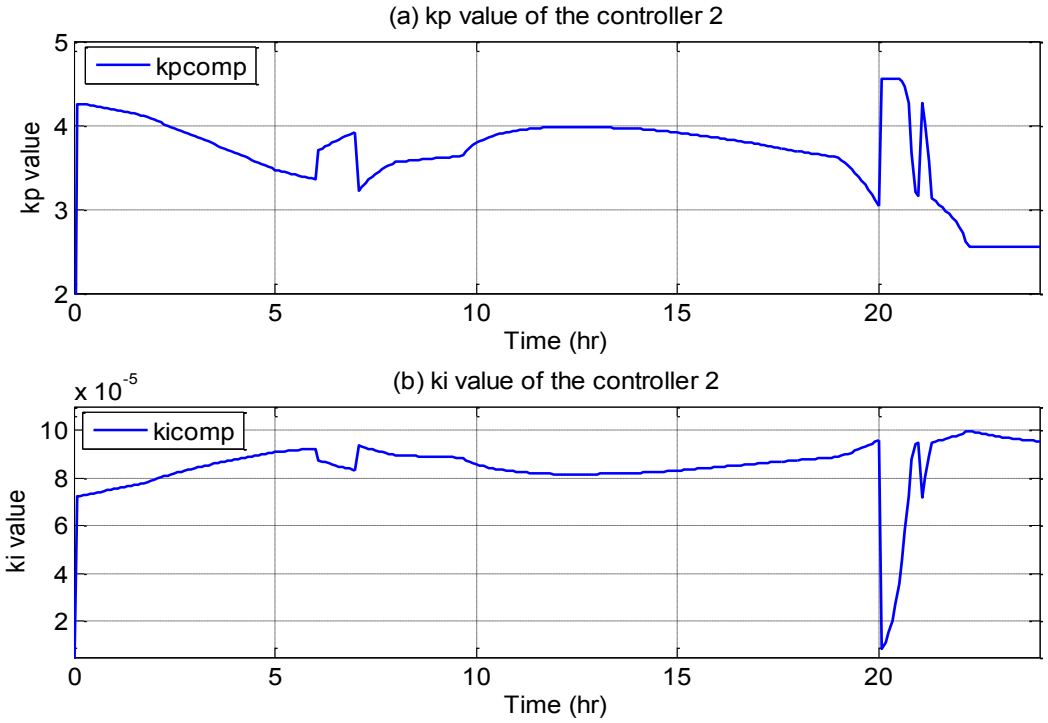

Figure 4.6.11 kp and ki values of the GS controller for the chiller (PLR 100).

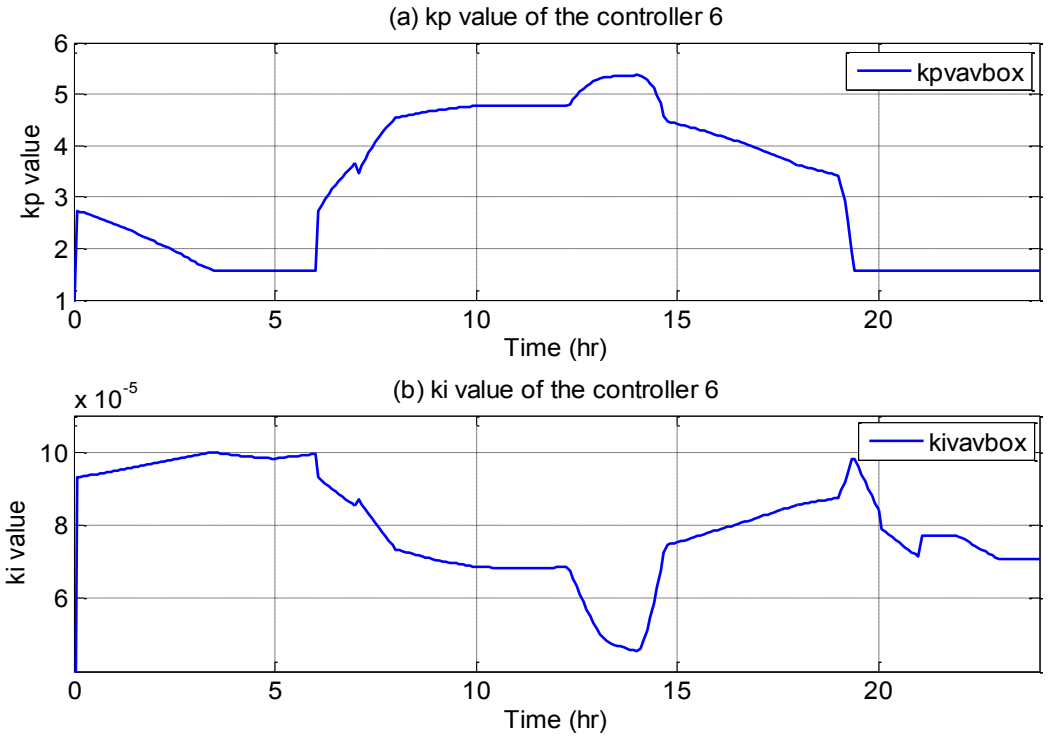

Figure 4.6.12 kp and ki values of the GS controller for the VAV box (PLR 100).

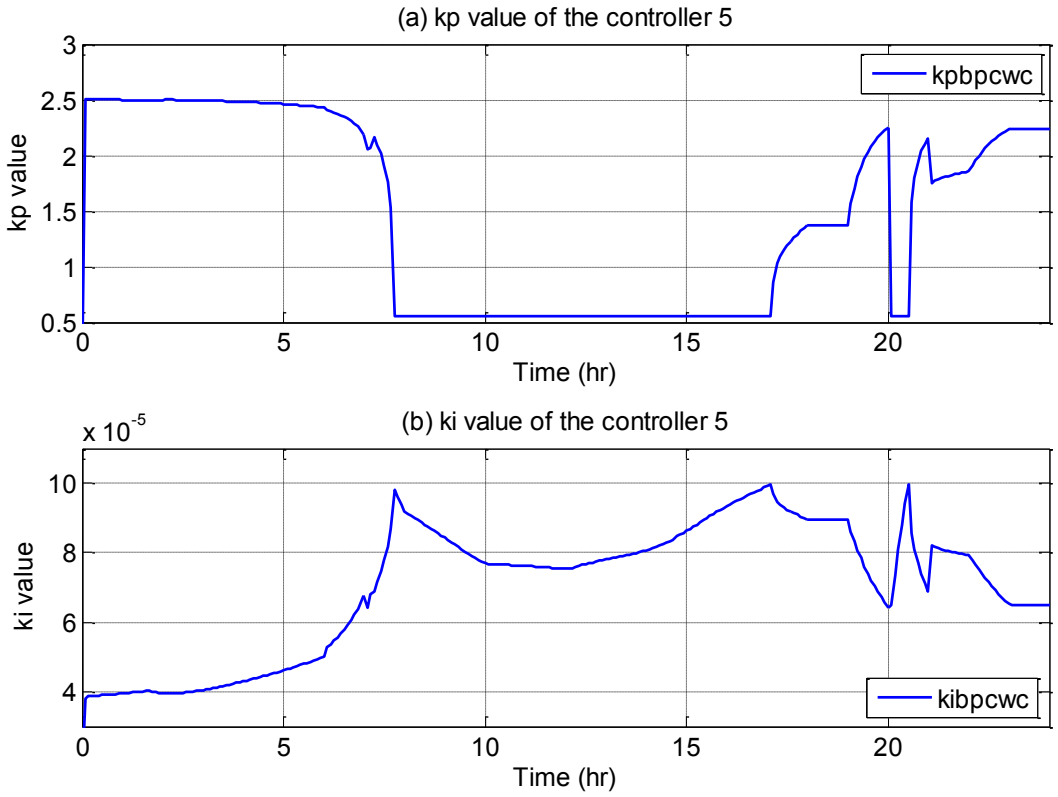

Figure 4.6.13 kp and ki values of the GS controller for the cooling coil (PLR 100).

Also it is worth noting that the GS controllers are self-tuning by increasing the proportional gain and decreasing the integral gain when the setpoint change occurs; and vice versa when the system reaches target setpoint and stable conditions.

Simulation results for the conventional PI controller (PLR 50)

The typical day simulations were repeated with system load at 50% of the design day loads. The impact of partial load on the performance of conventional PI control and GS control were examined. The results depicted in figures 4.6.14 – 4.6.17 show that constant gain PI control undergoes oscillation much more under partial load condition compared to full load condition.

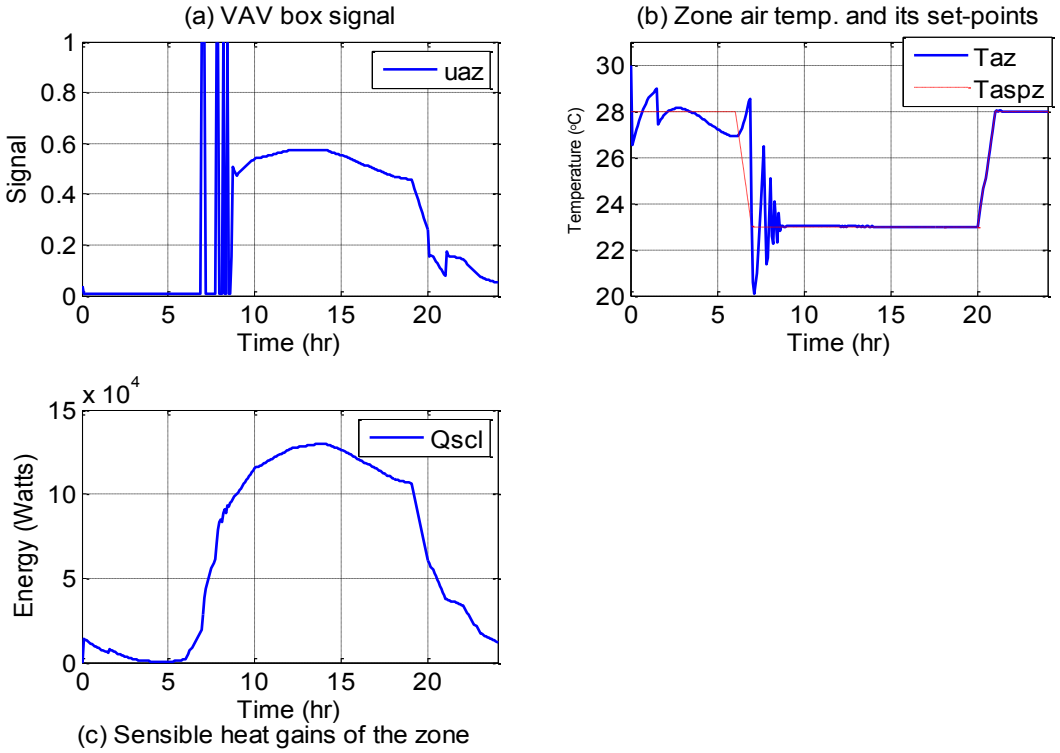

Figure 4.6.14 Simulation results of conventional PI controller for the VAV box (PRL 50).

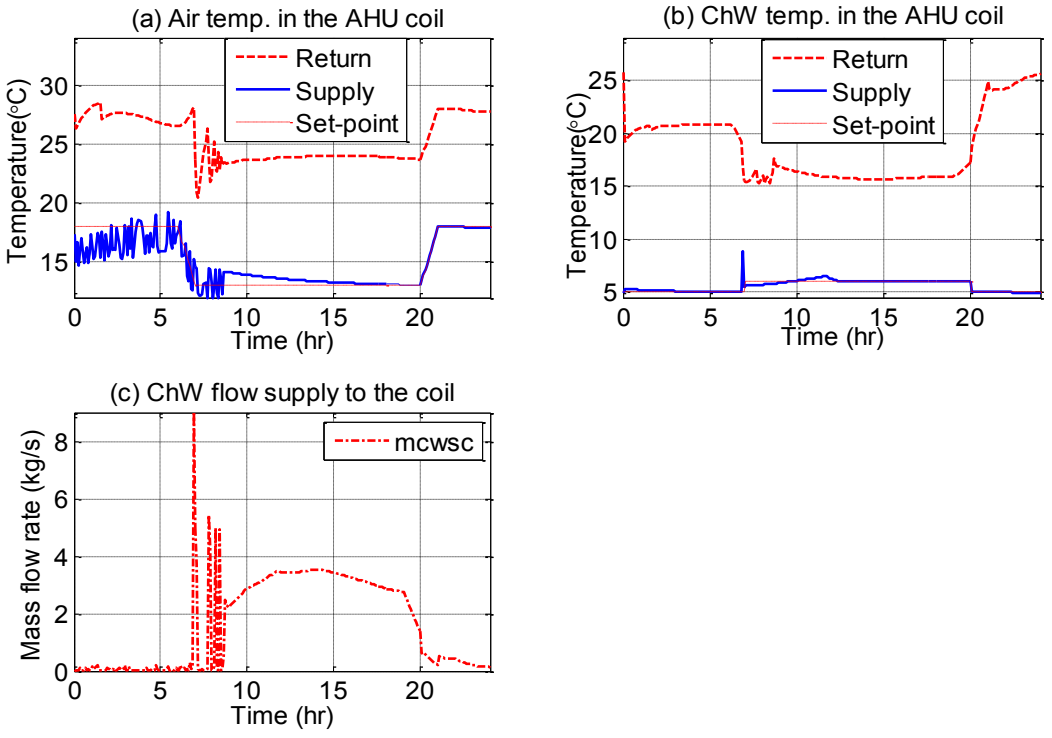

Figure 4.6.15 Simulation results of conventional PI controller for the cooling coil (PRL 50).

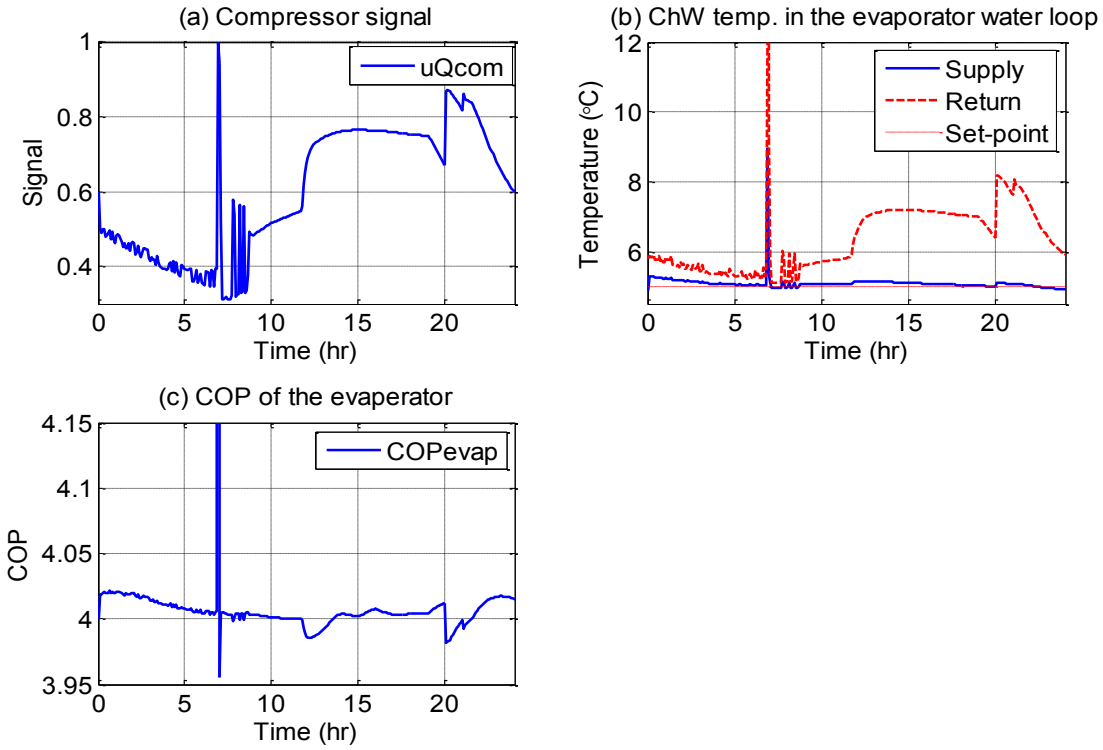

Figure 4.6.16 Simulation results of conventional PI controller for the chiller (PRL 50).

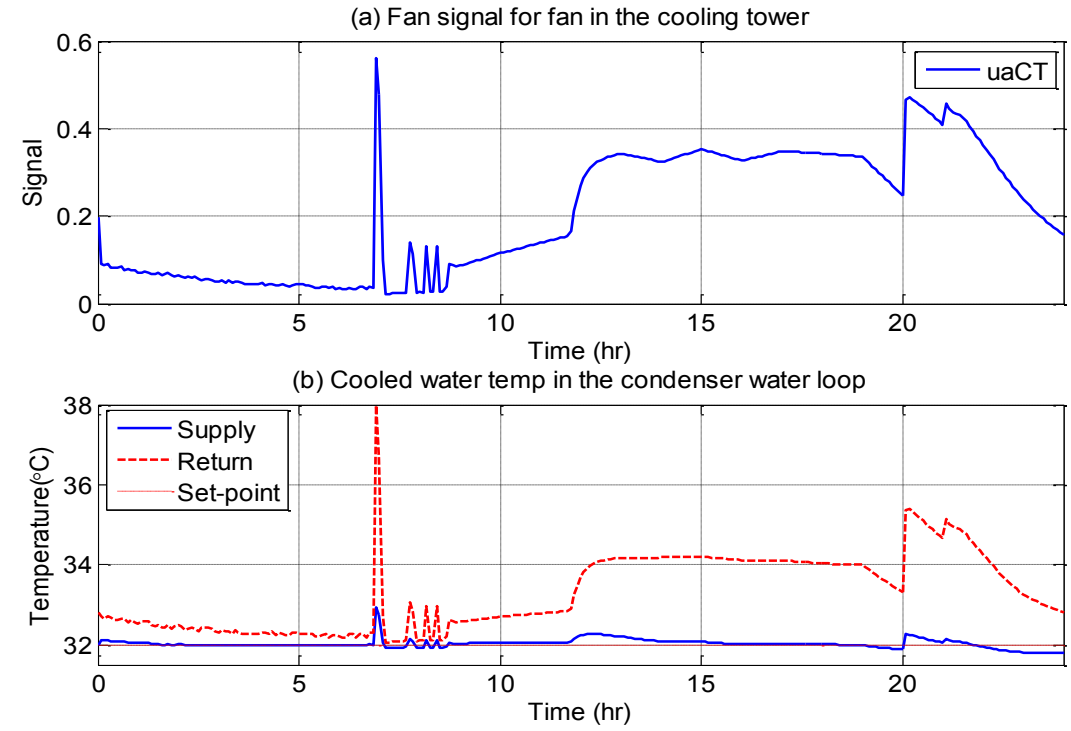

Figure 4.6.17 Simulation results of conventional PI controller for the cooling tower (PLR 50).

Simulation results for the GS controller (PLR 50)

On the other hand, the GS control performance remains good both under partial load (figures 4.6.18 – 4.6.21) and full load conditions (figures 4.6.7 – 4.6.10).

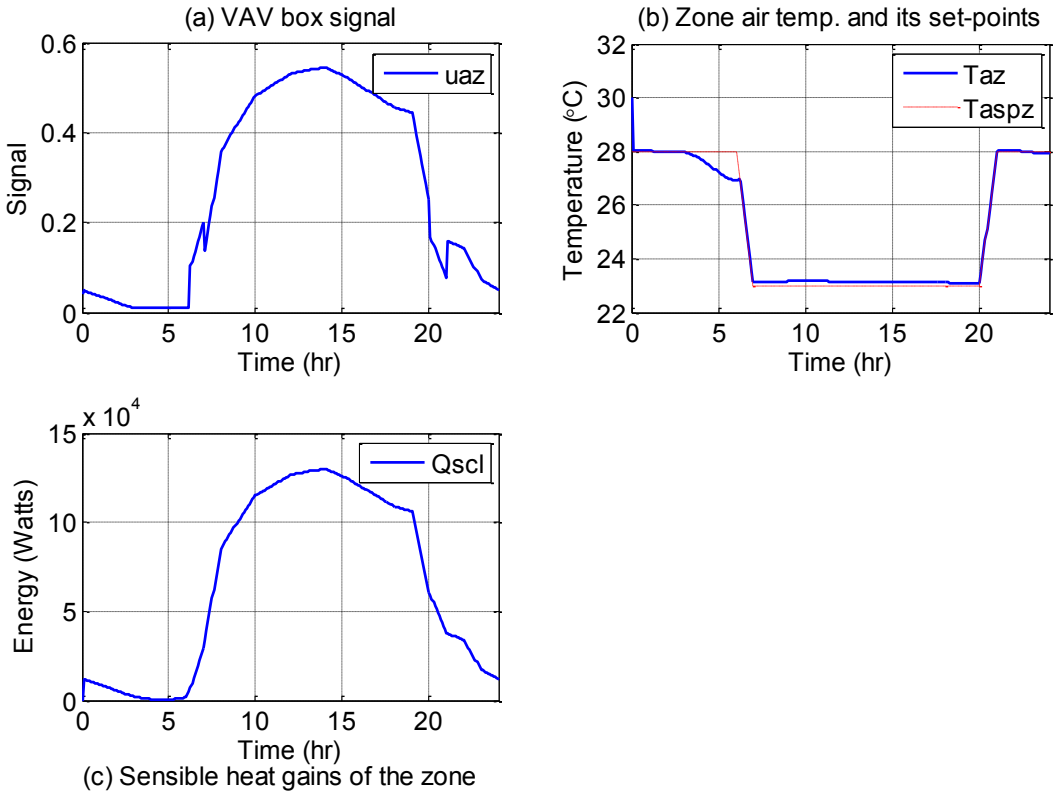

Figure 4.6.18 Simulation results of the GS controller for the VAV box (PLR50 – one day).

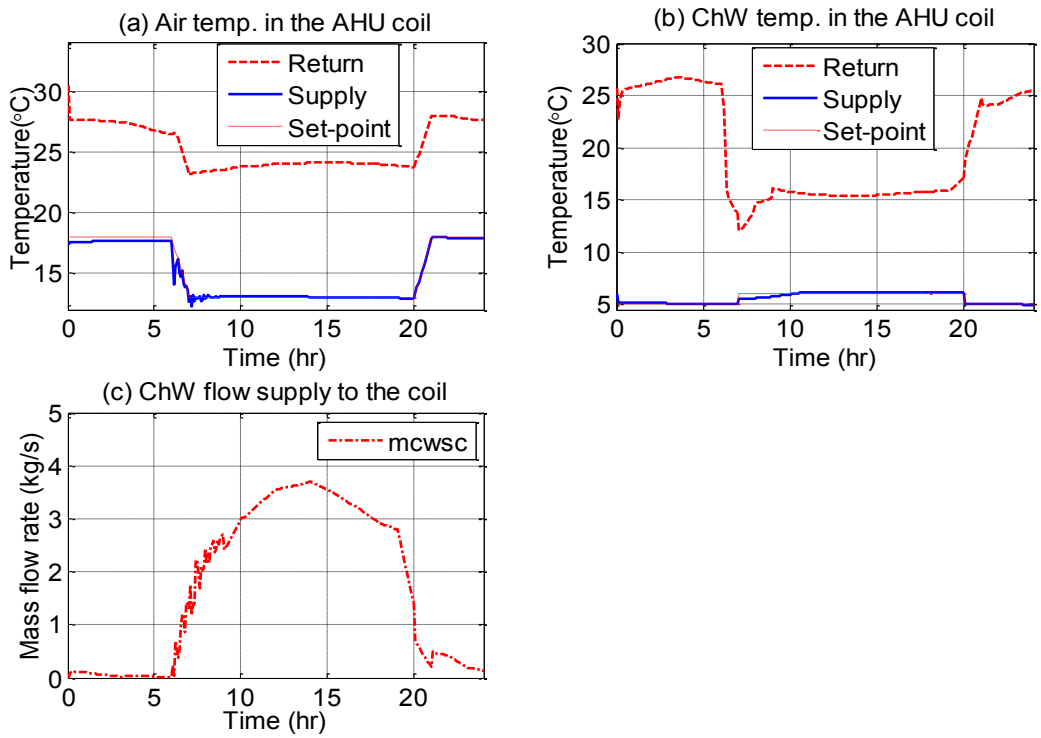

Figure 4.6.19 Simulation results of the GS controller for the coil (PLR50 – one day).

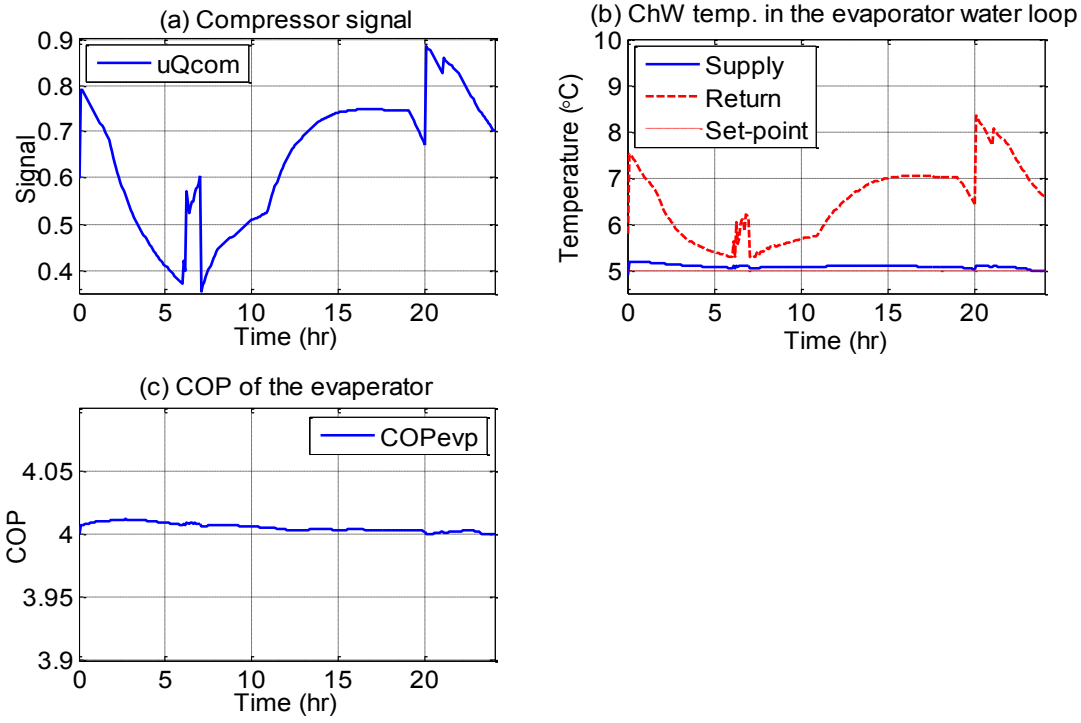

Figure 4.6.20 Simulation results of the GS controller for the chiller (PLR50 – one day).

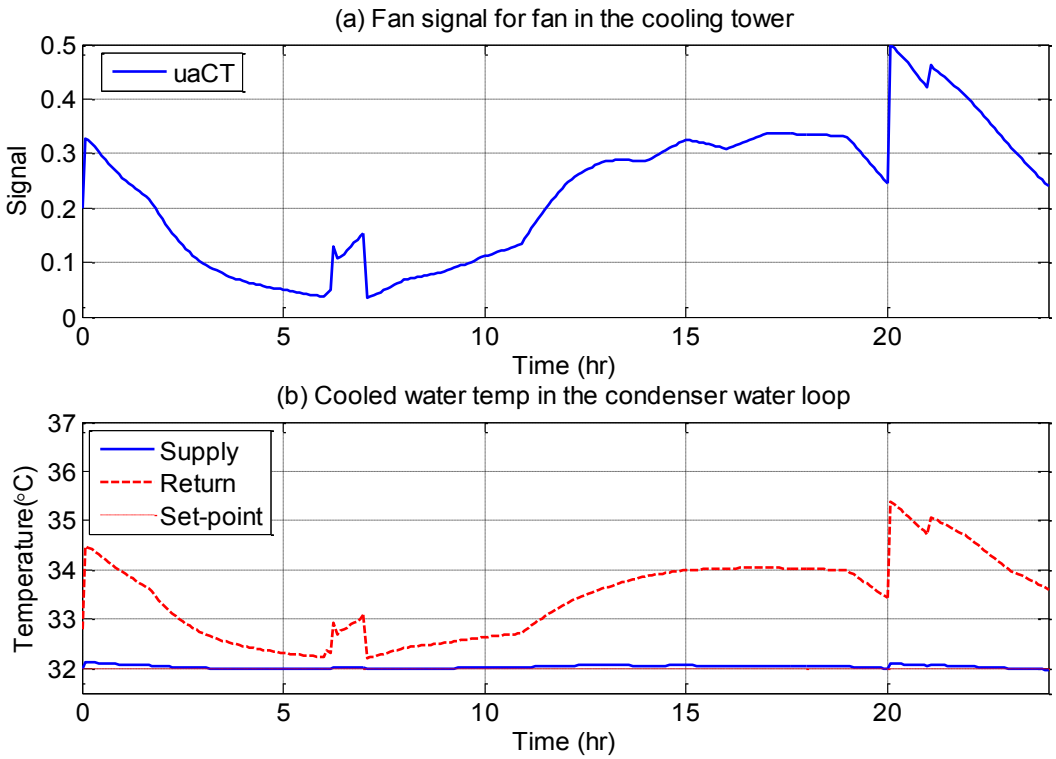

Figure 4.6.21 Simulation results of the GS controller for the cooling tower (PLR50 – one day).

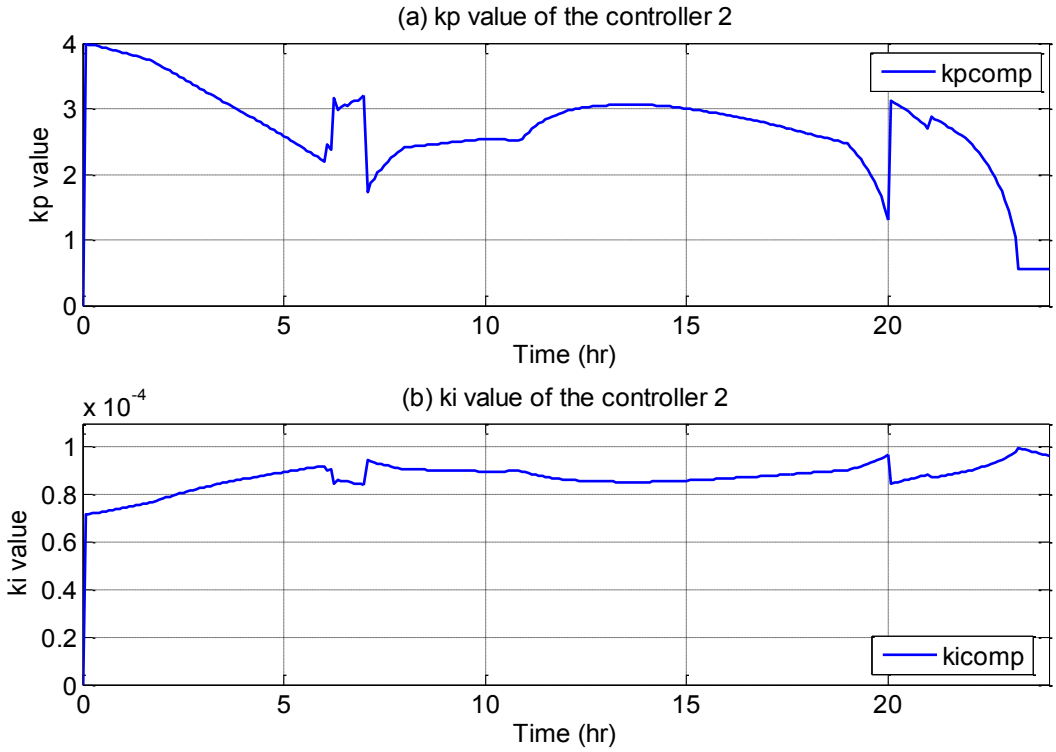

Figure 4.6.22 The k_p and k_i values of the controller 2 for the compressor (PLR50 – one day).

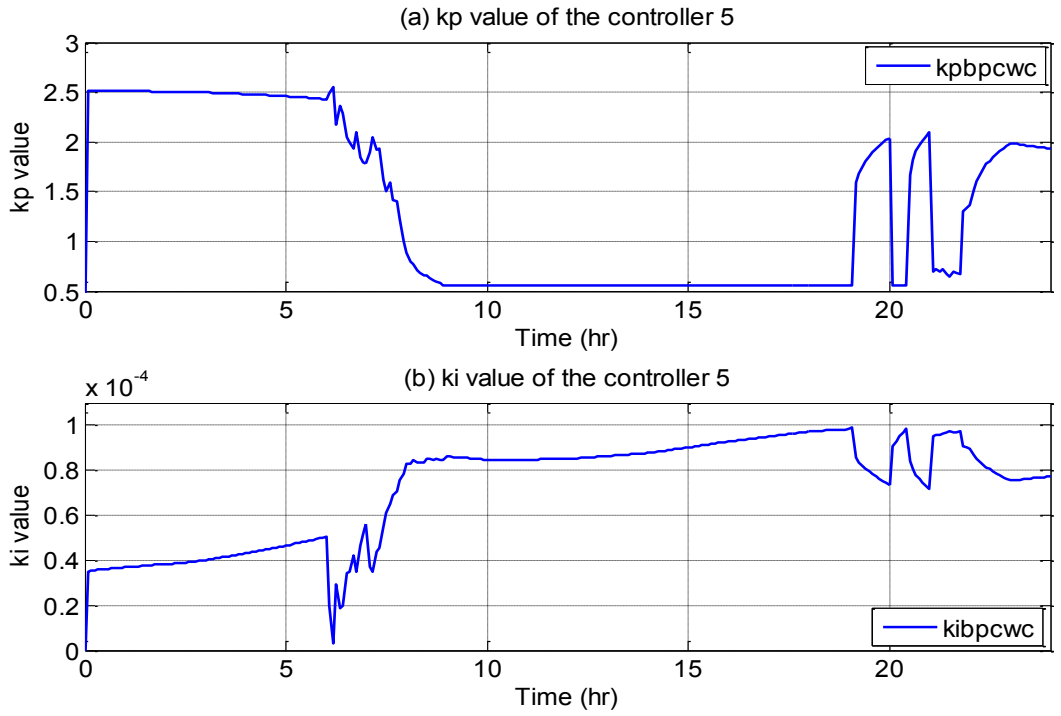

Figure 4.6.23 The k_p and k_i values of the controller 5 for the cooling coil (PLR50 – one day).

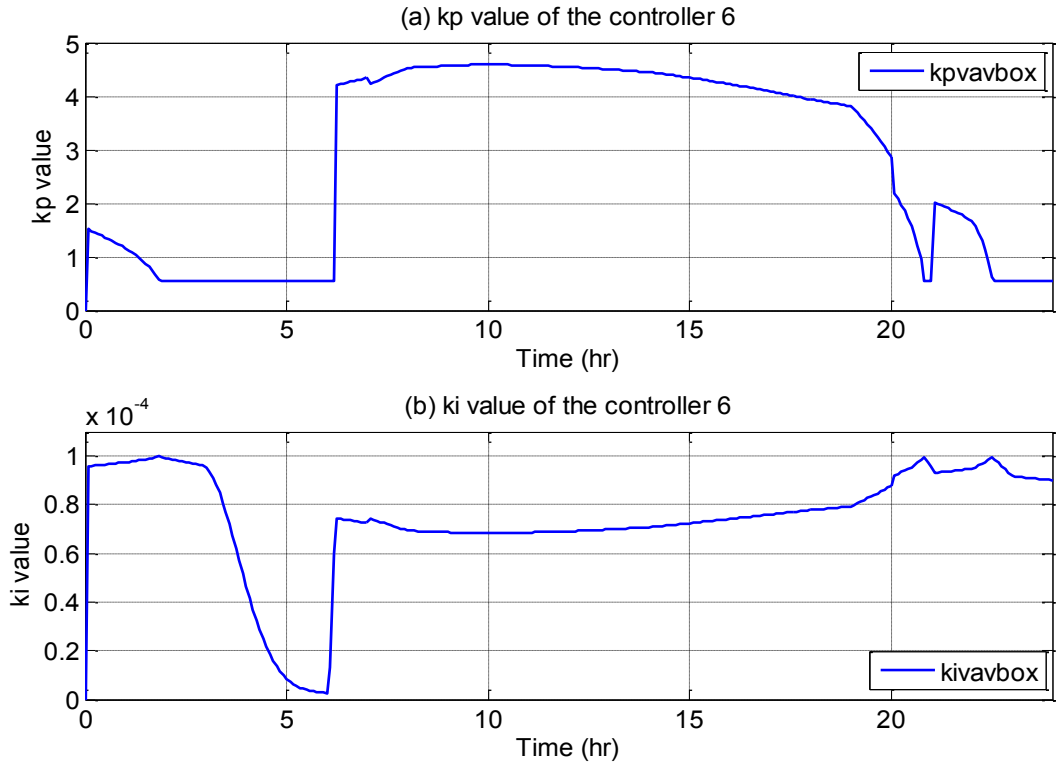

Figure 4.6.24 The k_p and k_i values of the controller 6 for the VAV box (PLR50 – one day).

Figure 4.6.18 shows the zone temperature results of one day simulation. The zone air temperature is controlled very well at its setpoint of 28 ºC during the charge cycle of the system and 23 ºC of the discharge cycle of the system.

Figure 4.6.19 shows the cooling coil system responses. The supply air temperature to the zone is controlled much better than the case with using PI controller, with few oscillation during the setpoint changing period. The supply ChW temperature is maintained at its setpoint of 5 ºC during the charge cycle and 6 ºC during the discharge cycle.

Figure 4.6.20 represents the results of chiller control. The COP of the chiller is very stable at around of 4.02. The compressor signal increases up to 0.85 during the peak-load condition and reaches up to 0.97 at the beginning of the charge cycle. The supply ChW temperature to the coil is always controlled at 5 ºC.

Therefore, it can be concluded that GS control gives smooth and stable responses and it is a good candidate control scheme for chilled water systems.

CHAPTER 5 ENERGY CONSUMPTION AND COST

5.1 Introduction

In this chapter, energy consumption and cost comparison between different control strategies are compared. The price of energy was chosen arbitrarily at $ 0.1/ kWh during night time (18:00 – 7:00) and at rate of $ 0.3/kWh during the day time (7:00 – 18:00). The simulations were run until the system reaches steady periodic conditions and the next day's results were used to compare the results. The GS controllers were used in these simulations.

5.2 Energy consumption

Several different operating strategies were simulated and energy consumption levels for each were determined. These are identified as operating strategy 1 (OS – 1), OS – 2 etc.

Basic cooling system without chilled water (ChW) tank (OS – 1)

In this case, the cooling system is simulated without the ChW tank. The setpoints for the controller in each control loop are selected based on the design day condition; and the values are shown in the following table – the day time simulation is from 7:00 – 20:00 and the night time period is the remaining hours of the day.

Table 5.2.1 Setpoints in the control loops of the cooling system.

Symbol	Item	Day time	Night time	Unit
$T_{sp\_a\_z}$	Setpoint of zone air temperature	23	28	ºC
$T_{sp\_sa\_c}$	Setpoint of supply air temperature to the zone	13	18	ºC
$T_{spcw\_s\_c}$	Setpoint of supply ChW temperature to the coil	7	7	ºC
$T_{spcw\_s\_chi}$	Setpoint of ChW temperature leaving evaporator	7	7	ºC

$T_{spcow\_s\_cond}$	Setpoint of cooled water temp. leaving the CT	32	32	ºC

Cooling system with ChW tank (OS – 2)

In this operating strategy the ChW tank is used to store cool energy and use it during the peak cooling period. The ChW tank is charged by the chiller at the setpoint of 5.5 ºC during the off-peak period and discharge cycle is initiated during peak period.

Optimized cooling system with ChW tank (OS – 3)

In this case, the operation of the cooling system is locally optimized by applying the following logic:

1. A supply air temperature profile as function of outdoor air temperature was assumed as shown in figure 5.2.1:

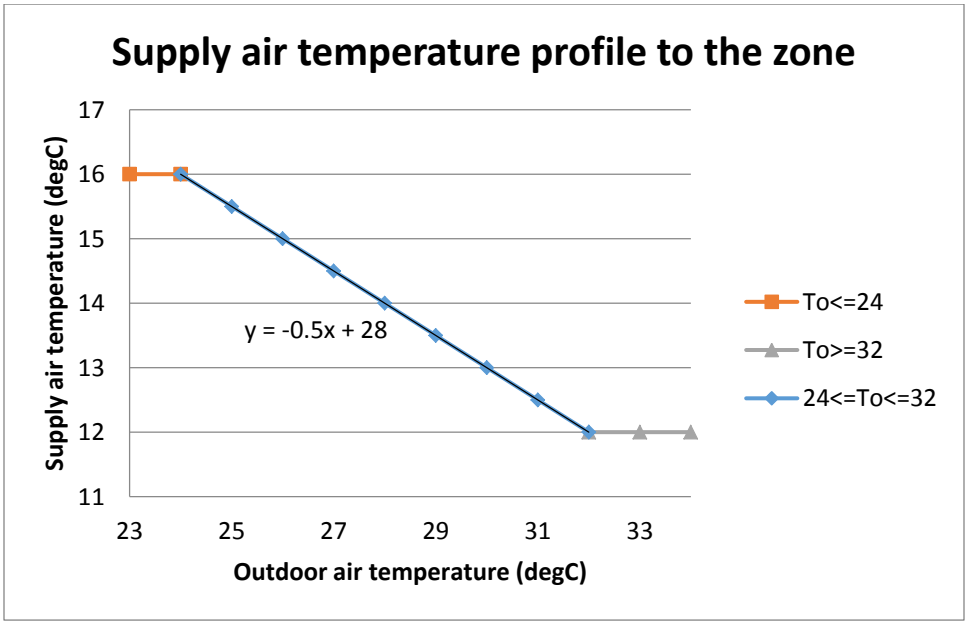

Figure 5.2.1 Supply air temperature profile to the zone.

2. With the assumed value of supply air temperature, the maximum supply ChW temperature to the coil was determined using MATLAB optimization routine fmin.

3. The supply ChW temperature to the coil could be calculated by using following equation:

$$T_{cws_c} = \frac{m_{cws_{chi}} T_{cws_{chi}} + m_{cws_{tank}} T_{cws_{tank}}}{m_{cws_{chi}} + m_{cws_{tank}}} \quad (5.2.1)$$

The setpoint of the ChW temperature leaving the evaporator could be calculated as followes:

$$T_{sp_{cws_{chi}}} = \frac{(m_{cws_{chi}} + m_{cws_{tank}}) T_{sp_{cws_c}} - m_{cws_{tank}} T_{cws_{tank}}}{m_{cws_{chi}}} \quad (5.2.2)$$

4. In the energy consumption simulations, the mass flow rate of the ChW from tank to the coil was set at maximum of 80% of the ChW flow rate to the coil in order not to deplete the tank at a faster rate.

Cooling system with ChW tank at 50% load (OS – 4)

In this operating strategy, the cooling system with chilled water tank is operated at partial load 50% of full load conditions.

Optimized cooling system with ChW tank at 50% load (OS – 5)

The cooling system is operated under the same optimized control logic as OS – 2's and undergoes the partial load 50% of full load conditions.

5.3 Energy consumption and cost

The daily energy consumption of the coil-fan, compressor, and cooling tower fan and the cost in each of the five operating strategies were determined under full load and partial load conditions. The results are summarized in the following tables.

Basic case without chilled water (ChW) tank – PRL 100 (OS – 1)

The following table shows the results of energy consumption and cost in of OS – 1.

Table 5.4.1 Energy consumption and cost of OS – 1.

Periods	Energy consumptions (OS – 1)		
	Coil – fan	Compressor	Fan
7:00 – 18:00	129.039	588.512	8.194
18:00 - 7:00	15.007	174.059	0.929
Discharge cycle	129.039	588.512	8.194
Charge cycle	15.007	174.059	0.929
Total	144.046	762.571	9.122
Periods	Cost due to energy consumptions (OS – 1)		
	Coil – fan	Compressor	Fan
7:00 – 18:00	38.712	176.554	2.458
18:00 - 7:00	1.501	17.406	0.093
Discharge cycle	38.712	176.554	2.458
Charge cycle	1.501	17.406	0.093
Total	40.212	193.960	2.551

The total energy consumption of the system was 915.739 kWh. The fan consumes the smallest portion of the total energy and the compressor takes the highest portion. Therefore the cost of the compressor is much higher than the other two components in the system. The total cost is about $ 236.72/day when the system is operated under full load conditions without the storage tank.

Cooling system with ChW tank – PLR 100 (OS – 2)

The system operation with OS – 2 resulted in the total energy consumption of the system is 973.72 kWh which is 58 kWh higher than the result from OS – 1. However the cost of $ 206.89

is 12.6% less than the one in previous case. This is due to the differential energy prices which help in reducing the cost.

The detail information of the results is shown in table 5.4.2.

Table 5.4.2 Energy consumption and cost of the components in case 2.

Periods	Energy consumptions (OS – 2)		
	Coil – fan	Compressor	Fan
20:00 – 7:00	1.443	314.352	2.487
7:00 - 18:00	135.557	408.380	3.652
18:00 – 20:00	15.775	91.239	0.835
Discharge cycle	151.332	499.619	4.487
Charge cycle	1.443	314.352	2.487
Total	152.775	813.971	6.974
Periods	Cost due to energy consumptions (OS – 2)		
	Coil – fan	Compressor	Fan
7:00 – 18:00	0.144	31.435	0.249
18:00 - 7:00	40.667	122.514	1.095
18:00 – 20:00	1.577	9.124	0.084
Discharge cycle	42.245	131.638	1.179
Charge cycle	0.144	31.435	0.249
Total	42.389	163.073	1.428

Optimized case with ChW tank – PLR 100 (OS – 3)

The following table shows the results from OS – 3.

Table 5.4.3 Energy consumption and cost of the OS – 3.

Periods	Energy consumptions in (OS – 3)		
	Coil – fan	Compressor	Fan
20:00 – 7:00	1.124	455.635	19.549
7:00 - 18:00	147.340	208.228	4.892
18:00 – 20:00	20.004	46.456	0.818
Discharge cycle	167.344	254.684	8.434
Charge cycle	1.124	455.635	19.549
Total	168.467	710.319	25.259
Periods	Cost due to energy consumptions (OS – 3)		
	Coil – fan	Compressor	Fan
7:00 – 18:00	0.112	45.564	1.955
18:00 - 7:00	44.202	62.468	1.468
18:00 – 20:00	2.000	4.646	0.082
Discharge cycle	46.202	67.114	1.549
Charge cycle	0.112	45.564	1.955
Total	46.315	112.677	3.504

Optimized operating strategy resulted in the total energy consumption of 904.046 kWh and the cost was $162.5. The percentages of the energy consumption and system operation cost savings compared to the OS – 2 are 7.16% and 21.46%, respectively. The savings in energy consumption is mainly due to lower energy consumed by the compressor in the optimized case.

Cooling system with ChW tank – PLR 50 (OS – 4)

Table 5.4.4 shows the energy consumption and cost of OS – 4 operating strategy. The percent savings are expected to be higher due to the fact that the system is operating under partial load conditions.

Table 5.4.4 Energy consumption and cost of OS – 4.

Periods	Energy consumptions (OS – 4)		
	Coil – fan	Compressor	Fan
20:00 – 7:00	0.160	187.100	0.739
7:00 - 18:00	21.653	194.645	0.518
18:00 – 20:00	2.440	50.901	0.169
Discharge cycle	24.094	245.546	0.687
Charge cycle	0.160	187.100	0.739
Total	24.254	432.646	1.426
Periods	Cost due to energy consumptions (OS – 4)		
	Coil – fan	Compressor	Fan
7:00 – 18:00	0.016	18.710	0.074
18:00 - 7:00	6.496	58.394	0.155
18:00 – 20:00	0.244	5.090	0.017
Discharge cycle	6.740	63.484	0.172
Charge cycle	0.016	18.710	0.074
Total	6.756	82.194	0.246

In this case, 458.326 kWh of total energy was consumed and the cost of energy was $ 89.20.

Compared to the full load case, this represents a cost reduction of more than 50%.

Optimized case with ChW tank under PLR 50% (OS – 5)

Table 5.4.5 depicts the energy consumption and cost resulting from OS – 5.

Table 5.4.5 Energy consumption and cost of OS – 5.

Periods	Energy consumptions (OS – 5)		
	Coil – fan	Compressor	Fan
20:00 – 7:00	0.143	321.150	13.226
7:00 - 18:00	22.673	52.848	0.100
18:00 – 20:00	2.591	6.734	0.004
Discharge cycle	25.263	59.582	0.104
Charge cycle	0.143	321.150	13.226
Total	25.407	380.732	13.330
Periods	Cost due to energy consumptions (OS – 5)		
	Coil – fan	Compressor	Fan
7:00 – 18:00	0.014	32.115	1.323
18:00 - 7:00	6.802	15.854	0.030
18:00 – 20:00	0.259	0.673	0.000
Discharge cycle	7.061	16.528	0.031
Charge cycle	0.014	32.115	1.323
Total	7.075	48.643	1.353

The total energy consumption in this case is 419.469 kWh which is 8.48% less compared with the OS – 4. However the cost $ 57.07 is about 36.02 % of the cost in OS – 4. The savings are higher under partial load conditions. Also the cost saving is mainly due to the load demand shifting from day time to low-cost period in the night. The following figure shows the comparison of total energy consumption for each operating strategy and the associated cost due to the energy consumption.

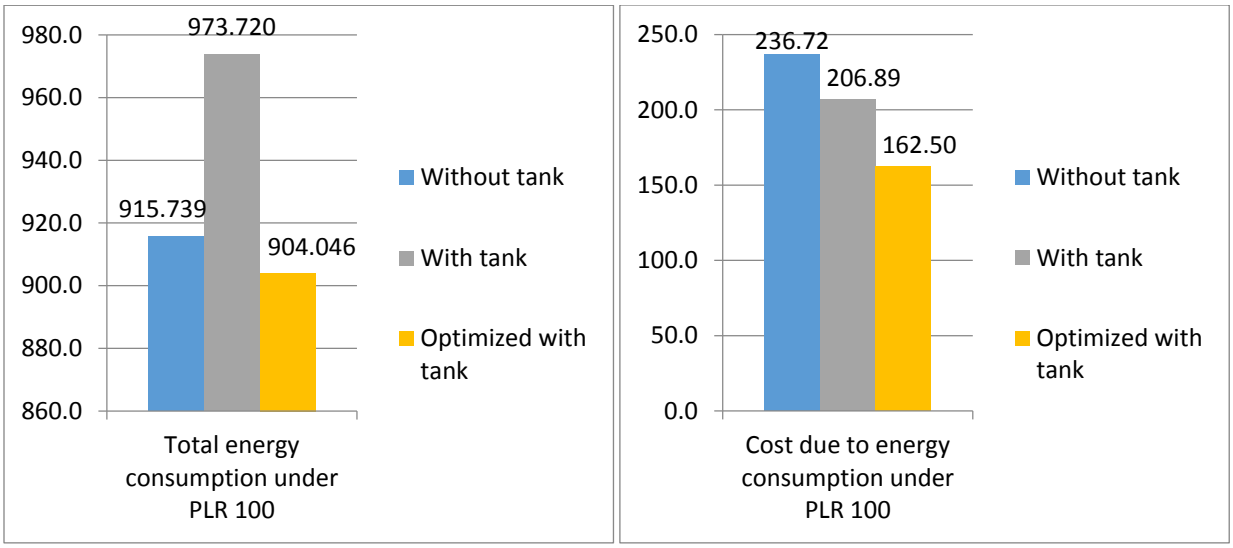

Figure 5.4.1 & 2. Total energy consumption and cost for OS – 1, OS – 2, and OS – 3.

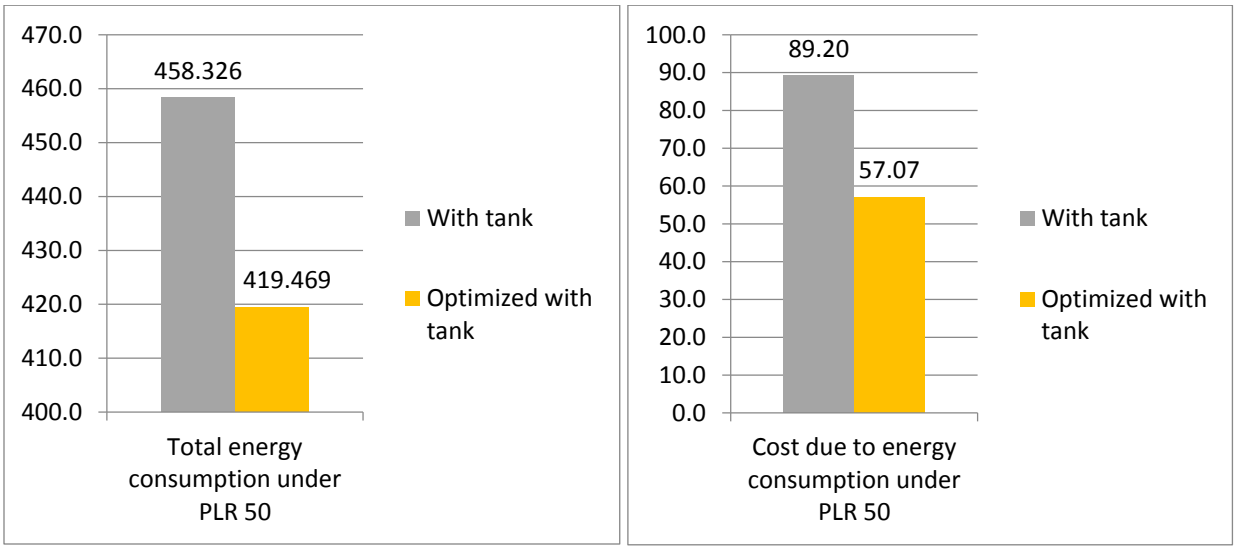

Figure 5.4.3 & 4 Total energy consumption and cost for OS – 4 and OS – 5.

5.4 Stratified ChW tank Performance Evaluation

In the previous section, the performance of cooling system with chilled water storage tank was assessed in terms of energy consumption and cost savings. Apart from the above, other indicators

are also used to assess the performance. These are defined in references (Bahnfleth, 1994, 1998 & 1999). The following three indicators were used to evaluate the ChW tank performance.

The cycle thermal efficiency

The cycle thermal efficiency measures the capacity loss from the tank to its surroundings, but without considering the loss of availability due to mixing of warm and cool water in the tank. The equation for this parameter is shown below:

$$\eta = \frac{[\sum \dot{m}c(T_{in}-T_{out})\Delta t]_{Discharge}}{[\sum \dot{m}c(T_{in}-T_{out})\Delta t]_{Charge}} \quad (5.4.1)$$

where m = mass flow rate over a time increment

c = specific heat, J/ (kg ºC)

T_{in} = inlet temperature, ºC

T_{out} = outlet temperature, ºC

Δt = time increment, sec or hr.

Figure-of-merit (FOM)

The FOM not only include the capacity loss to the surroundings of the tank, but also considers the losses due to mixing and conduction within the tank. Therefore the value of FOM should always be less than the η_{tank}. The equation to calculate the FOM is shown below:

$$FOM = \frac{[\sum \dot{m}c(T_{in}-T_{out})\Delta t]_{Discharge}}{Mc(T_{h^*}-T_{c^*})} \quad (5.4.2)$$

where M = the total mass contained in the tank, kg;

T_{h^*} = mass averaged discharge inlet temperature, ºC

T_{c^*} = mass averaged inlet temperature during previous charge cycle, ºC

Percentage tank utilization

This parameter is used to describe the portion of the energy consumption from the tank for meeting the total energy consumption required for the system operation. The total energy consumption includes the energy consumption from chiller, from tank, and capacity loss of the tank. Therefore this parameter is only used for evaluating the performance of the tank during the discharge cycle. The percent tank energy consumption ratio is calculated as follow:

$$Ptg_{tank} = \left(1 - \frac{\int Q_{loss_{tank}} dt + \int Q_{chiller} dt}{\int Q_{coil} dt}\right) 100\% \qquad (5.4.4)$$

where Ptg_{tank} = tank energy consumption ratio, %;

$Q_{loss_{tank}}$= capacity loss of the tank due to surroundings and internal mixing and heat transfer, watt.

$Q_{chiller}$ = energy consumption of the chiller, watt.

Q_{coil} = energy consumption in the coil at water side, watt.

These performance indicators were calculated for the operating strategies OS – 2 to OS – 5 for the system with storage tank. These are given in table 5.4.7.

Table 5.4.7 Stratified tank performance evaluation.

Case	η_{tank} (%)	FOM (%)	Ptg_{tank} (%)
OS – 2 (PLR 100)	97.60	76.40	30.10
OS – 3	98.94	95.00	59.09

(PLR 100)			
OS – 4 (PLR 50)	96.15	75.93	35.49
OS – 5 (PLR 50)	98.43	96.17	81.04

Tank cycle thermal efficiency

The tank cycle thermal efficiency of the optimized operation OS – 5 is higher than the tank cycle thermal efficiency obtained from OS – 2. Also, it can be noted that the losses from the tank are less than 3%.

Full cycle FOM of the tank

The FOM was computed for the operating strategies OS – 2 through OS – 5. The results depicted in table 5.4.7 show that FOM increased in the optimized operating strategy OS – 3 compared to non optimal conventional strategy OS – 2. The results show that FOM increased under full load and partial load conditions when optimized operating strategies (OS – 3 and OS – 5) were used.

Percentage tank utilization

According to the results presented in table 5.4.7, the percentage tank utilization increased from full load to partial load operating condition. Also the tank utilization efficiency increased in optimized operating strategy (OS – 3) compared to non optimal strategy OS – 2 under full load conditions. The same trend holds under partial load conditions. The highest tank utilization efficiency of 81% occurred under partial load conditions.

CHAPTER 6 CONCLUSIONS, CONTRIBUTIONS, and RECOMMENDATIONS FOR FUTURE RESEARCH

A dynamic model of a chilled water cooling system with a chilled water storage tank for air conditioning of a 4000 m^2 commercial-office building located in Montreal, Quebec was developed. The chilled water cooling system consists of a chiller, a cooling tower, an air handling unit, and a storage tank. Gain scheduling and optimal control strategies were designed. Simulation runs were made to evaluate the performance of the system. The conclusion, contributions, and recommendations for future research are given below.

6.1 Conclusions

The conclusions of the thesis are summarized below:

1. A dynamic model of a chilled water cooling system with a chilled water storage tank was developed to study dynamic responses of the system subject to variable cooling loads.
2. Open loop simulation results show that temperature responses of the zone, chilled water, supply air temperature reach steady state in about one hour when the chilled water storage tank is not used.
3. When the chilled water storage tank is added to the system, the thermal capacity of the overall system increases as such the temperature responses were much slower. The steady state time was more than 3 hours.
4. It was found that during the discharge cycle, the rate of increase in the chilled water temperature was about 1 ºC/hour.
5. The heat loss from the tank due to internal heat transfer and conduction with surroundings was very small.

6. A gain scheduling controller was designed. It was shown that by scheduling the gains the control performance of the system can be significantly improved compared with constant gain controller.
7. The temperature responses with GS controller had less overshoot and the system performance was stable and smooth throughout the operating range.
8. A near-optimal algorithm for operating the stratified ChW tank with the chiller plant was developed. The results showed that the system operation cost decreased by shifting large proportion of energy consumption into off-peak period when the utility rate structure is in effect. The energy consumption was also reduced due to optimal operation.
9. The efficiency of the tank was as high as 98%. The percent energy supplied by the tank ranged between 30 to 80% depending on the cooling loads.
10. The figure of merit of the storage tank is the ratio of discharge capacity to ideal capacity was found to be between 75% to 97%.
11. The energy consumption was determined under various operating conditions. The results showed that energy savings ranging from 21% to 36% can be achieved by using the optimal control strategy.

6.2 Contributions

The contributions of this study are summarized as flow:

1. An overall dynamic model of a chilled water cooling system with a storage tank was developed by applying fundamental principles of energy and mass balances.
2. PI-based gain-scheduling controller was designed and implemented on the VAV box, a three-way valve for controlling the ChW mass flow rate to the cooling coil, and

compressor to improve the thermal performance of the system during charge and discharge cycles.

3. A near-optimal algorithm for the ChW tank was developed. Energy savings of more than 36% were achieved.

6.3 Recommendations for future research

There are several improvements that can be made in this thesis. These are:

1. An improved chiller model would be useful to predict COP more accurately.
2. The steady-state model of the cooling tower can be replaced with a simplified detailed mass- and heat- transfer cooling tower model.
3. The PI-based gain scheduling controller can be made more adaptive to large changes in cooling loads. This aspect needs to be studied.

REFERENCES

Andrepont, J.S., 2006, Practical Development in Sensible Heat Diurnal Cool Thermal Energy Storage (TES): Large Applications, Low Temps, Energy Efficiency, and Operating Plus Capital Savings. ECOSTOCK 2006 Conference Proceedings, *TES systems*.

Antienitis, A.K. and Santamouris, M., Thermal Analysis and Design of Passive Solar Buildings, *Chapter 1 Introduction and basic concepts*, 2002, 9 – 16.

ASHREA, 1979, Cooling and Heating Load Manual (GRP-158), *The cooling load factor cooling load calculation method*.

Bahnfleth, W.P. and Joyce, W.S., 1994, Energy use in a district cooling system with stratified chilled-water storage, *ASHRAE Transactions*, 100(1), 1767-1778.

Bahnfleth, W.P. and Musser, A., 1999, Field-measured performance of Four Full-Scale Cylindrical Stratified Chilled-Water Thermal Storage Tanks, *ASHRAE Transaction,* Vol 105 Part 2*,* 218-230.

Bai, J.B. and Zhang, X.S., 2006, A new adaptive PI controller and its application in HVAC systems, *ScienceDirect*, Energy Conversion and Management 48, 1043 – 1054

Braun, J. E., 1992, A comparison of chiller-priority, storage-priority, and optimal control of an ice system, *ASHRAE Transactions,* Vol. 98 part 1: 893-902.

Braun, J. E., 2007a, A near-optimal control strategy for cool storage systems with dynamic electric rates. *HVAC&R* Research. Vol. 13 number 4, 557-580.

Braun, J.E., 2007b. Impact of control on operating costs for cool storage systems with dynamic electric rates, *ASHRAE Transactions* Vol. 113 part 2, 343-354.

Bryan, P.R., 2000, Control-Oriented Modeling of Transcritical Vapor Compression Systems, *Thesis for the degree of Master of Science*, Graduate College ,University of Illinois at Urbana-Champaign.

Caldwell, J.S. and Bahnfleth, W.P., September 1997, Chilled water thermal energy storage without electric rate incentives or rebates, *Journal of Architectural Engineering*, Vol. 3 No 3, 133-140.

Cypress Ltd, Stratified chilled water storage (SCHWS), *Shift & Save*, reference available in the link (http://cyp-res.com/stratified-chilled-water-storage-schws/).

Hajiah, A.E.H., 2000, Development and implementation of an optimal controller of a central cooling plant using ice storage system and building thermal mass, *Ph.D. Dissertation*,

Department of Civil Engineering, and Architecture Engineering, University of Colorado at Boulder.

Guan, Y. and Zaheer-uddin, M., 2005, Dynamic Modeling and Capacity Control of Multiple Chiller System, A thesis in Department of Building, Civil, and Environmental Engineering, Concordia University at Montreal.

Henze, G. P., Dodier, R.H., and Krarti, M., 1997, Development of a predictive optimal controller for thermal energy storage systems, *Energy and Buildings*, Vol. 35 number 3, 313-325.

Henze, G. P. and Schoenmann, J., 2003, Evaluation of reinforcement learning control for thermal energy storage systems. *HVAC&R* Research Vol. 9 number 3, 259-276.

Henze, G. P., Biffar, B., Kohn, D., and Becker, M.P., 2008, Optimal design and operation of a thermal storage system for a chilled water plant serving pharmaceutical buildings. *Energy and Buildings* Vol. 40 number 6, 1004-4019.

Homan, K.O., Chang, W.S., and Soo, S.L., April 1996, Thermal Performance of Stratified Chilled Water Storage Tanks, *HVAC&R Research*, Vol. 2, No 2. 158-169

Hydeman, M., Sreedharan, P., and Webb, N,, 2002, Development and Testing of a Reformulated Regression-Based Electric Chiller Model, *ASHRAE Transactions*, Vol 108 Part 2.

Khan, J. and Zubair, S.M., August 2001, An Improved Design and Rating Analyses of Counter Flow Wet Cooling Tower, *The Transactions of the ASME*, Vol 123.

Khan, J., Qureshi, B.A., and Zubair, S.M., April 2004, A Comprehensive Design And Performance Evaluation Study of Counter Flow Wet Cooling Towers, *International Journal of Refrigeration*, Vol. 27, 914-923.

Krarti, M., Brandemuehl, M. J., and Henze, G. P., 1995, RP-809 – Evaluation of Optimal Control for Ice Storage Systems, Atlanta, GA: American Society of Heating, Refrigerating and Air-Conditioning Engineers, Inc.

Kreith, F. and Bohn, M.S., 2001, Principles of Heat Transfer, *Chapter 8 Heat* Exchangers, six edition, 485 – 523.

Kuehn, T.H., Ramsey, J.W., and Threlkeld, J.L.,1998, Thermal Environmental Engineering, 3rd edition, *Part 4 Heat- and Mass- Transfer Processes and Applications*, 268 – 280.

Lee, T.S. and Lu, W.C., 2010, An Evaluation of Empirically-Based Models for Predicting Energy Performance of Vapor-Compression Water Chiller, *Applied Energy*, Vol 87, 3486-3493.

Li, B. and Alleyne, A.G., 2009, A Full Dynamic Model of a HVAC Vapor Compression Cycle Interacting with a Dynamic Environment, *2009 American Control Conference*. 3662 – 3668

Li, Z.F. and Sumathy, K., February 2002, Performance Study of a Partitioned Thermally Stratified Storage Tank in a Solar Powered Absorption Air Conditioning System, *Applied Thermal Enegineering*, Vol. 22, 1207-1216.

Long, J.Y., 2013, Steady State Model of Cooling Tower Used in Air Conditionning, *Proceedings of the 2nd International Conference on Computer Science and Electronics Engineering*, Atlantis Press, Paris, France.

Massie, D.D., 2002, Optimization of a building's cooling plant for operating cost and energy use. *International Journal of Thermal* Sciences, Vol. 41 issue 12: 1121-1129.

McQuiston, F.C., Parker, J.D., and Spitler, J.D., Heating, Ventilating, and Air conditioning Analysis and Desgin, *Chapter 14 Extended Surface Heat Exchangers*, 6 edition, 2005, 483 – 513.

Napps, Application Manual, *Scroll liquid chillers*, NWC 410A chillers, reference available in the link (http://www.nappstech.com/uploads/05-25-11_NTC_App_Manual_NCC-NWC_Rev_4.pdf)

Roth, K., Zogg, R., and Brodrick, J., September 2006, Cool Thermal energy Storage, ASHRAE Journal, Vol. 48. 94-96.

Sedaghati, A., 2006, A PI Controller Based on Gain-Scheduling For Synchronous Generator, *Turk J Elec Engin*, Vol 14, number 2, 241-251.

Wang, S.W. and Jin, X.Q., Model-based optimal control of VAV air-conditioning system using genetic algorithm, *Building and Environment*, issue 35, 471 – 487.

Swider, D.J., 2002, A comparison of empirically based steady-state models for vapor compression liquid chillers, *Applied Thermal Engineering*, Vol 23, 539-556.

Tashtoush, B., Molhim, M., and AI-Rousan, M., April 27, 2004, Dynamic Model of an HVAC System for control analysis, *Energy*, Vol. 30 issue 10, 1729-1746.

Teeter, J. and Chow, M.Y., 1998, Application of Functional Link Nerual Network to HVAC Thermal Dynamic System Identification, *IEEE Transactions* Vol 45, No. 1, 170 – 176.

Tran, N. and Kreider, J.F., 1989, Field Measurement of Chilled Water Storage Thermal Performance, *ASHRAE Transactions,* Vol. 95 part 1, 1106-1112.

Wildin, M.W., and Truman, C.R., 1985, A Summary of Experience With Stratified Chilled Water tanks, *ASHRAE Transaction,* Vol. 91 part 1B, 956-976.

Yoshida, H. and Gotou., Y., 1999. Development of optimal operation of thermal storage tank and the validation by simulation tool, Kyoto, Japan: Building Simulation 1999.

Yoshida, H. and Yamaguti, H., 2001, Optimal operation of a HVAC systm with a thermal storage water tank, Rio de Janeiro, Brazil: Seventh International IBPSAConference.

Zaky, M.S. and Ismaeil, E.M., December 2008, Gain Scheduling Adaptive PI Control of Hybrid Stepper Motor Drives, *Proceedings of the 14th International Middle East Power Systems Conference,* Cairo University, Egypt, 160-167.

Zhang, Z.Q., May 2010, Methodology for determining the opimal operating strategies for a chilled water storage system, *PhD. Dissertation*, Office of Graduate Studies of Texas, A&M University.

Zheng, G.R., 1997, Dynamic Modeling and Global Optimal Operation of Multizone Variable Air Volume HVAC System, *PhD. Dissertation*, Concordia University.

APPENDIX - A

Steady state design method was used to size the system components. The major design parameters of the chilled water cooling system are shown in the following table. These parameters corresponds to the design day load conditions.

Parameter [unit]	Description	Magnitude
Cooling Load Estimation		
T_o [ºC]	Outdoor air temperature	33
RH[%]	Relative humidity ratio	34
$T_{z_{set}}$ [ºC]	Setpoint of zone air temperature	23
ACH	Air change per hour	0.25
A_{win}/A_w	Ratio of window area to wall area	0.3
A_{we} [m^2]	Gross East wall area	150
A_{ws} [m^2]	Gross South wall area	240
A_f [m^2]	Floor area	4000
w_{light} [W/m^2]	Energy density for using the light in the building	13
Fu	Fraction factor for using w_{light}	0.85
Fs	Ballast allowance factor for fluorescent fixtures	1.2
N_{ocp}	Numbers of occupants in the building	100
q_{opt_s} [W/person]	Sensible heat gain per person	125
w_{equip} [W/m^2]	Energy density for using the equipment in the building	30
G_e[W/m^2]	Intensity of solar radiation hitting on the wall facing East	102.7
G_w[W/m^2]	Intensity of solar radiation hitting on the wall facing West	469.3
G_n[W/m^2]	Intensity of solar radiation hitting on the wall facing North	102.7
G_s[W/m^2]	Intensity of solar radiation hitting on the wall facing South	438.3
G_r[W/m^2]	Intensity of solar radiation hitting on the roof	709.8
Q_{solar} [W]	Heat gain due to solar radiation	42779.6

Q_{cond_w} [W]	Heat gain due to heat conduction through wall	2882.2
Q_{cond_r} [W]	Heat gain due to heat conduction through roof	22943.4
$Q_{cond_{win}}$ [W]	Heat gain due to heat conduction through windows	3514.3
Q_{inf} [W]	Heat gain due to air infiltration	7000
Q_{light} [W]	Heat gain due to light	47466.7
Q_{equip} [W]	Heat gain due to equipments	114820
Q_{opt} [W]	Heat gain due to occupants	10777.5
$Q_{h_{s_z}}$[W]	Total sensible heat gain of the zone	252184
Cooling Coil (Ɛ – NTU method)		
$Q_{c_{coil}}$[W]	Design coil load for cooling (1.12*$Q_{h_{s_z}}$)	282446.1
$T_{a_{s_c}}$ [ºC]	Supply air temperature	13
$T_{a_{r_c}}$ [ºC]	Return air temperature	25
$T_{cw_{s_c}}$ [ºC]	ChW temperature entering the cooling coil	7
$T_{cw_{r_c}}$ [ºC]	ChW temperature leaving the cooling coil	12
$m_{cw_{s_c}}$ [kg/s]	Mass flow rate of supply ChW to the zone	13.44
$m_{a_{s_c}}$ [kg/s]	Mass flow rate of supply air to the coil	23.27
v_{a_c} [m/s]	Velocity of air in the cooling coil	3
v_{cw_c} [m/s]	Velocity of ChW in the cooling coil	$\frac{4 \times m_{cw_{s_c}}}{\pi {D_{i_c}}^2 N_{tb_c} \rho_{cw}}$
ReD_{a_c} [-]	Reynolds number of the air	$\frac{v_{a_c} \times D_{o_c}}{v_a}$
ReD_{cw_c} [-]	Reynolds number of the ChW	$\frac{v_{cw_c} \times D_{i_c}}{v_{cw}}$
Pr_c [-]	Prandtl number of air	0.7367
Pr_{c_s} [-]	Prandtl number of air (surface)	0.7387

Pr_{cw_c} [-]	Prandtl number of ChW	11.0179
Eff_{fin_c} [-]	Fin efficiency	0.85
B_c [-]	Ratio of outside area to inside area of the tube	30
NTU_c	Number of transfer units	1.4
U_{t_c}[W/(m^2 ºC)]	Total heat transfer coefficient of the tubes	$\frac{1}{\frac{1}{Eff_{fin_c} h_{o_c}} + \frac{B_c}{h_{i_c}}}$
Cooling coil fan		
$Q_{c_{fan}}$[W]	Power of the fan in cooling coil	15000
Chiller		
COP	COP of the evaporator	4.3
Q_{comp} [W]	Power of the compressor	66000
Cooling Tower		
$T_{cow_{s_{cond}}}$ [ºC]	Cooled water temperature leaving the cooling tower	29
$T_{cow_{r_{cond}}}$ [ºC]	Cooled water temperature entering the cooling tower	34
$Q_{ct_{req}}$ [W]	Required capacity of the cooling tower	$Q_{c_{coil}} + COP \times Q_{comp}$
Cooling Tower Fan		
$Q_{fan_{ct}}$ [W]	Power of the fan in the cooling tower	2627.4
Stratified ChW tank		
$R_{w_{tank}}$ [(m^2 ºC)/W]	Thermal resistance of the tank wall	2.4
D_{tank}	Tank inside diameter	8
$H_{cw_{tank}}$ [m]	Water height in the tank	4.2
$A_{cr_{tank}}$ [m^2]	Cross section area of the tank	$\frac{\pi {D_{tank}}^2}{4}$